ENZYMATIC PRODUCTION OF CYCLODEXTRIN USING CYCLODEXTRIN GLYCOSYLTRANSFERASE IMMOBILIZED IN METAL ORGANIC FRAMEWORKS (MOFS)

Babatunde Azeez Ogunbadejo

UAEU

جامعة الإمارات العربية المتحدة
United Arab Emirates University

DOCTORATE DISSERTATION NO. 2024: 13

College of Engineering

ENZYMATIC PRODUCTION OF CYCLODEXTRIN USING CYCLODEXTRIN GLYCOSYLTRANSFERASE IMMOBILIZED IN METAL ORGANIC FRAMEWORKS (MOFS)

Babatunde Azeez Ogunbadejo

Starch
α-1,4-glycosidic bonds

Immobilized CGTase

Apolar Cavity — Secondary side
Primary Side
Cyclodextrins
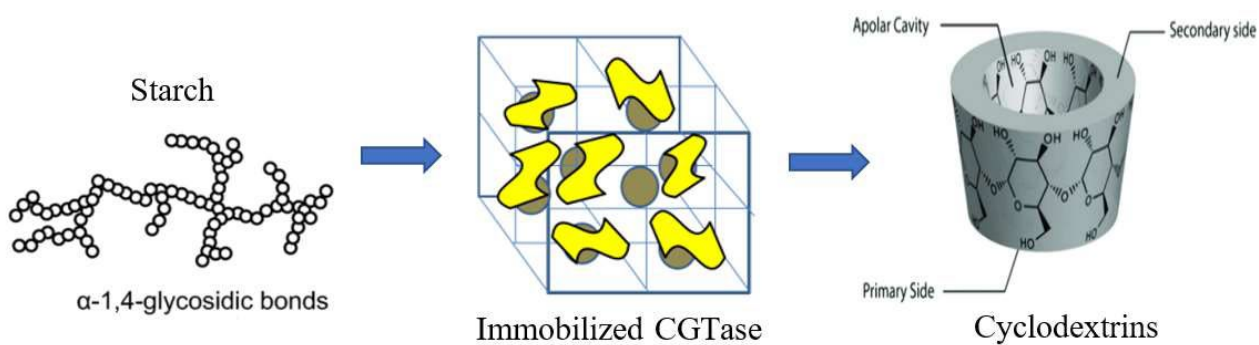
April 2024

United Arab Emirates University

College of Engineering

ENZYMATIC PRODUCTION OF CYCLODEXTRIN USING CYCLODEXTRIN GLYCOSYLTRANSFERASE IMMOBILIZED IN METAL ORGANIC FRAMEWORKS (MOFS)

Babatunde Azeez Ogunbadejo

This dissertation is submitted in partial fulfilment of the requirements for the degree of Doctor of Philosophy in Chemical Engineering

April 2024

Cover: Immobilized enzyme within a porous support

(Photo: By Babatunde Azeez Ogunbadejo)

Declaration of Original Work

I, Babatunde Azeez Ogunbadejo, the undersigned, a graduate student at the United Arab Emirates University (UAEU), and the author of this dissertation entitled "*Enzymatic Production of Cyclodextrin Using Cyclodextrin Glycosyltransferase Immobilized in Metal Organic Frameworks (MOFs)*", hereby, solemnly declare this is the original research work done by me under the supervision of Prof. Sulaiman Al-Zuhair, in the College of Engineering at UAEU. This work has not previously formed the basis for the award of any academic degree, diploma or a similar title at this or any other university. Any materials borrowed from other sources (whether published or unpublished) and relied upon or included in my dissertation have been properly cited and acknowledged in accordance with appropriate academic conventions. I further declare that there is no potential conflict of interest with respect to the research, data collection, authorship, presentation and/or publication of this dissertation.

Student's Signature: _____

Date: _____21/05/2024_____

Advisory Committee

1) Advisor: Sulaiman Al-Zuhair

Title: Professor

Department of Chemical and Petroleum Engineering

College of Engineering

2) Member: Basim Abujdayil

Title: Professor

Department of Chemical and Petroleum Engineering

College of Engineering

3) Member: Mohamednoor Al Tarawneh

Title: Professor

Department of Chemical and Petroleum Engineering

College of Engineering

Approval of the Doctorate Dissertation

This Doctorate Dissertation is approved by the following Examining Committee Members:

1) Advisor (Committee Chair): Sulaiman Al-Zuhair
   Title: Professor
   Department of Chemical Engineering
   College of Engineering

   Signature _S.Al-Zuhair_   Date _07/05/2024_

2) Member: Joy Tannous
   Title: Assistant Professor

   Department of Chemical and Petroleum Engineering

   College of Engineering

   Signature _____   Date _07/05/2024_

3) Member: Emad Elnajjar
   Title: Professor

   Department of Mechanical and Aerospace Engineering

   College of Engineering

   Signature _____   Date _07/05/2024_

4) Member (External Examiner): Ali Demirci
   Title: Professor

   Department of Agricultural and Biological Engineering
   Institution: Pennsylvania State University, USA

   Signature _Ali Demir_ Date _07/05/2024_

This Doctorate Dissertation is accepted by:

Dean of the College of Engineering: Professor Mohamed Al Marzooqi

Signature _Mohamed AlMarzouqi_

Date _May 31, 2024_

Dean of the College of Graduate Studies: Professor Ali Al-Marzouqi

Signature _Ali Hassan_

Date _31/05/2024_

Abstract

Cyclodextrins (CDs) and their derivatives have attracted significant attention in the pharmaceutical, food, and textile industries, which has led to an increased demand for their production. CDs are typically produced by the action of cyclodextrin glycosyltransferase (CGTase) on starch. Owing to the relatively high cost of enzymes, the economic feasibility of the entire process strongly depends on the effective retention and recycling of CGTase in the reaction system, while maintaining the enzyme's activity and stability. Previous supports used for this purpose such as silica and hydrogels, have numerous drawbacks, including enzyme leaching, activity loss and significant mass transfer limitations. The aim of this dissertation was to improve performance of immobilized CGTase by using metal–organic frameworks (MOFs), possessing better properties than conventional supports, as immobilization support. CGTase was immobilized on different synthesized MOFs, namely MIL-101, Cu-BTC, using either surface, covalent attachment or entrapment and compared to conventional support, namely Zeolite Y as well as Graphene nano-particles (GNP). The use of a calcium-based two-dimensional MOF, namely Ca-TMA, and modified Cu-BTC using N.N- dimethylcyclohexylamine to produce hierarchical H-Cu-BTC were also tested for enhanced enzyme capacity and reduced diffusional limitations of the large starch molecules. The adsorption capacity, the effect of immobilization on the secondary structures of CGTase and on the characterization of the support as well as the kinetic parameters of the free CGTase were assessed. The adsorption isotherms of CGTase on the tested MOFs were best represented by the Langmuir isotherm, with maximum adsorption capacities reaching 21, 30.6, 37.5, and 40 mg/g over Ca-TMA, Cu-BTC, microporous MIL-101 and GNP, respectively. The adsorption capacity was improved to 49.5 mg/g over H-Cu-BTC. These capacities were significantly higher than that observed using conventional Zeolite-Y, which did not exceed 6.1 mg/g, as well as other supports reported in previous literature. Characterization of the free supports using combination of X-ray Diffraction (XRD), Scanning Electron Microscopy (SEM), Thermal Gravimetric Analysis (TGA) revealed that the structures of the MOFs remained intact post-CGTase immobilization. The deconvolution of the amide I band of the Fourier Transform Infrared spectra indicated that free CGTase molecules predominantly contain β-sheets (56% β-sheets, 38.5% α-helix and 5.5 % β-turns), with its composition changing over MIL-101

(84.1% β-sheets, no α-helix and 15.9 % β-turns), Ca-TMA (51.3% β-sheets, 37.5% α-helix and 11.2 % β-turns), and GNP (41.9% β-sheets, 18,1% α-helix and 40% β-turns. Lesser conformational changes were also observed using Cu-BTC (44% β-sheets, 37.5% α-helix and 11.2% β-turns) and H-Cu-BTC (76.1% β-sheets, 23.9% α-helix and no β-turns) supports. The immobilized CGTase on the different MOFs were tested for CDs production from starch, and the relative activity, reusability and mass-transfer limitations were investigated. The specific activity of the free CGTase used was 167 U/mg, which dropped upon immobilization to 28, 38, 65.2 and 98.5 U/mg protein on GNP, Ca-TMA, Cu-BTC, and H-CU-BTC, respectively. Reusability studies revealed that based on α-CD, MIL-101 showed 29% residual enzyme activity, which improved with covalent attachment via glutaraldehyde to 40%, Ca-TMA gave 33%, and GNP showed 74% relative activity after eight reaction cycles. Entrapment of CGTase within H-Cu-BTC led to residual CGTase activity of 87% after ten reaction cycles, compared to microporous Cu-BTC which gave 70% and presence of macropores and mesopores enhanced substrate mass transfer from 0.68 min^{-1} over microporous MOFs to 0.89 min^{-1} on macroporous H-Cu-BTC, thus, improved cyclodextrin production. This dissertation provides information on the effect of MOFs properties on immobilized CGTase performance, which can be used in developing robust CGTase-based biocatalysts for industrial application.

Keywords: Biocatalysis, Metal–organic framework, Enzymes, Cyclodextrin glycosyltransferase, biomaterials, Enzyme immobilization, Food waste.

Title and Abstract (in Arabic)

الإنتاج الأنزيمي للسايكلودكسترين باستخدام ناقلة الغليكوزيل السيكلوديكسترين المثبت في الأطر المعدنية العضوية (MOFs)

الملخص

لقد اجتذبت مركبات السيكلودكسترين (CDs) ومشتقاتها اهتمامًا كبيرًا في الصناعات الدوائية والغذائية والنسيجية، مما أدى إلى زيادة الطلب على إنتاجها. يتم إنتاج السيكلودكسترين عادة عن طريق عمل سيكلوديكسترين جليكوزيل ترانسفيراز (CGTase) على النشا. ونظرًا للتكلفة المرتفعة نسبيًا للإنزيمات، فإن الجدوى الاقتصادية للعملية برمتها تعتمد بشدة على الاحتفاظ الفعال وإعادة تدوير CGTase في نظام التفاعل، مع الحفاظ على نشاط الإنزيم واستقراره. الدعامات السابقة المستخدمة لهذا الغرض لها عيوب عديدة، بما في ذلك ترشيح الإنزيم، وفقدان النشاط الأنزيمي، وقيود كبيرة على نقل الكتله. كان الهدف من هذه الأطروحة هو تحسين أداء CGTase المثبت عن طريق استخدام الأطر المعدنية العضوية (MOFs)، التي تمتلك خصائص أفضل من الدعامات التقليدية، كدعائم للتثبيت. تم تثبيت CGTase على مختلف من إطارات MOF المُصنَّعة، وهي MIL-101 وCu-BTC، باستخدام إما السطح أو المرفق التساهمي أو الانحباس، ومن ثم مقارنته بالدعامة التقليدية، أي الزيوليت Y وكذلك جزيئات الجرافين النانوية (GNP). تم أيضًا اختبار استخدام MOF ثنائي الأبعاد القائمة على الكالسيوم، وهي Ca-TMA، وCu-BTC المعدلة باستخدام ثنائي ميثيل سيكلوهيكسيلامين لإنتاج H-Cu-BTC الهرمي لتعزيز قدرة الإنزيم وتقليل قيود الانتشار لجزيئات النشا الكبيرة. تم تقييم قدرة الامتصاص وتأثير التثبيت على الهياكل الثانوية لـ CGTase وعلى توصيف الدعم بالإضافة إلى القيم الحركية لـ CGTase الحر. لقد وجد أن الامتصاص متساوي الحرارة لـ CGTase على الأطر العضوية المعدنية التي تم اختبارها تتمثل بشكل أفضل باستخدام متساوي الحرارة Langmuir، حيث وجدت أن سعات الامتصاص القصوى تصل إلى 21، 30.6، 37.5، 40 ملغم/جم على Ca-TMA، Cu-BTC، MIL-101 الصغيرة المسامية وGNP، على التوالي. تم تحسين قدرة الامتصاص إلى 49.5 مجم / جم على H-Cu-BTC. وكانت هذه القدرة أعلى بكثير من تلك التي لوحظت باستخدام الزيوليت-Y التقليدي، والتي لم تتجاوز 6.1 ملغم/جم، بالإضافة إلى وسائل الدعم الأخرى المذكورة في الأدبيات السابقة. كشف توصيف الدعامات الفارغة باستخدام مزيج من حيود الأشعة السينية (XRD)، والمجهر الإلكتروني الماسح (SEM)، وتحليل الجاذبية الحرارية (TGA) أن هياكل الأطر المعدنية العضوية ظلت سليمة بعد تجميد CGTase. وأشار تفكك نطاق الأميد I في مطيافية الأشعة الحمراء باستخدام تحويل فورييه إلى أن جزيئات CGTase الحرة تحتوي في الغالب على صفائح β (56% صفائح β، و38.5% α-helix و5.5% β-turns)، مع تغير تركيبها على MIL-101 (84.1 % صفائح β، ولم توجد أي α-helix، 15.9 % β-turns)، Ca-TMA(51.3 % صفائح β، و37.5% α-helix و11.2 % β-turns)، و GNP (41.9 % صفائح β، و18.1% α-helix و40 % β-turns). وقد لوحظت أيضًا تغييرات شكلية أقل باستخدام دعائم Cu-BTC (44 % صفائح β، و37.5% α-helix و11.2 % β-turns)، و H-Cu-BTC (76.1 % صفائح β، و23.9 % α-helix ولم توجد أي β-turns). تم اختبار CGTase المثبت على الأطر العضوية المعدنية المختلفة لإنتاج CDs من النشا، وتم التحقيق في النشاط النسبي وقابلية إعادة الاستخدام وقيود نقل الكتلة. كان النشاط المحدد لـ CGTase الحر المستخدم هو 167 وحدة / ملغ، والذي انخفض عند التثبيت إلى 28 و38 و65.2 و98.5 وحدة / ملغ من البروتين على GNP وCa-TMA وCu-BTC وH-CU-BTC على التوالي. كشفت دراسات قابلية إعادة الاستخدام أنه بناءً على α-CD، أظهر MIL-101 نشاط إنزيم متبقي بنسبة 29%، والذي تحسن مع الارتباط التساهمي عبر الجلوتارالدهيد إلى

40%، وأعطى Ca-TMA نشاط بنسبة 33%، و GNP أما فقد أعطى نشاط بنسبة 74% بعد ثماني دورات تفاعل. أدى انحباس CGTase داخل H-Cu-BTC إلى نشاط CGTase المتبقي بنسبة 87% بعد عشر دورات تفاعل، مقارنة بـ 70% على Cu-BTC الصغيرة المسامية، ووجود المسام الكبيرة والمسام المتوسطة أدت إلى تعزيز نقل الكتلة من 0.68 في الدقيقة عبر MOFs ذات المسامية الصغيرة إلى 0.89 في الدقيقة على H-Cu-BTC كبير المسام، وبالتالي تحسين إنتاج CDs. تقدم هذه الأطروحة معلومات عن تأثير خصائص الـ MOFs على أداء CGTase، والتي يمكن استخدامها في تطوير محفزات حيوية قوية تعتمد على CGTase للتطبيقات الصناعية.

مفاهيم البحث الرئيسية: التحفيز الحيوي؛ الإطار المعدني العضوي؛ الانزيمات؛ سيكلوديكسترين غليكوزيل ترانسفيراز؛ المواد الحيوية؛ تثبيت الانزيم؛ مخلفات طعام.

List of Publications

This dissertation is based on the work presented in the following three papers, referred to by Roman numerals.

I. B. A. Ogunbadejo and S. Al-Zuhair, "Bioconversion of starch to Cyclodextrin using Cyclodextrin glycosyltransferase immobilized on metal organic framework," *Biocatal. Agric. Biotechnol.,* vol. 53, p. 102878, Oct. 2023.

II. B. A. Ogunbadejo, K. A. Aljahoushi, A. Alzamly, Y. E. Greish, and S. Al-Zuhair, "Immobilization of Cyclodextrin glycosyltransferase onto three dimensional-hydrophobic and two dimensional-hydrophilic supports: A comparative study," *Biotechnol. J.,* vol. 19, no. 1, p. 2300195, Dec. 2023.

III. B. Ogunbadejo, S. Al-Zuhair, "Enhanced performance of cyclodextrin glycosyltransferase by immobilization on amine-induced macroporous metal organic framework," *Food Sci. Technol.,* vol. 200, p. 116221, May 2024.

Author's Contribution

The contribution of Babatunde Azeez Ogunbadejo to the papers included in this dissertation was as follows:

I. Participated in conceptualizing the work, had main responsibility for the methodology, data collection and processing, evaluation of results and manuscript writing.

II. Participated in planning of the work, had main responsibility for the experimental work, data collection and processing, evaluation of results and manuscript writing.

III. Sole responsibility for planning the research, conducting the experiments, data collection and processing and writing the manuscript.

Author Profile

Babatunde Azeez Ogunbadejo is a young talented researcher and tutor whose zeal for knowledge acquisition and dissemination have taken him far and wide. He received his MSc degree in 2015 from King Fahd University of Petroleum and Minerals, Saudi Arabia under a full scholarship award, after obtaining his BEng degree as the best graduating student in the Chemical Engineering department of Federal University of Technology, Minna, Nigeria. Babatunde has over 7 years teaching, research and industrial experience. He is presently a tutor at the UAE University tutorial center (at the time of printing this dissertation), where he guides undergraduate students in understanding various courses ranging from mathematics to core chemical engineering courses. As a young researcher with interests in waste valorization, biochemical processes, catalysis and reaction modelling, he has published six articles in highly ranked peer-reviewed journals with over 80 citations. He has received several awards in recognition of his academic prowess, some are; Nigerian Society of Engineers (Minna Branch) prize for the best graduating student in Chemical Engineering 2010/2011 session, national merit award by the Federal Government of Nigeria in 2010 and post-secondary merit award by Total Exploration and Production Company, Nigeria. Babatunde is also a member of the Canadian Society of Chemical Engineers and Nigeria Society of Engineers.

Acknowledgements

Dedication

To my late mum, beloved family and all those who are under oppression

Table of Contents

List of Tables

List of Figures

List of Abbreviations

BSA	Bovine Serum Albumin
CD	Cyclodextrin
CGTase	Cyclodextrin glycosyltransferase
FTIR	Fourier Transform Infrared Spectroscopy
GNP	Graphene Nanoplatelets
HPLC	High Performance Liquid Chromatography
MIL	Materials of Institute Lavoisier
MOF	Metal Organic Framework
PDA	Polydopamine
PVDF	Polyvinylidene Fluoride
SEM	Scanning Electron Microscopy
TGA	Thermal Gravimetric Analysis
XRD	X-Ray Diffractogram

Chapter 1: Introduction

1.1 Overview

Cyclodextrins (CDs) are valuable compounds, which have found applications in numerous fields, including the pharmaceutical, medical, food, and cosmetic industries. They are cyclic oligosaccharides consisting of 6 (α-CD), 7 (β-CD), or 8 (γ-CD) D-glucose units joined by glycosidic bonds to form a hollow truncated cone shape [1]. The importance of CDs stems from the amphibious nature of their structure, which exhibits a hydrophilic exterior that confers solubility in water and a hydrophobic interior cavity that forms inclusion complexes with various hydrophobic compounds [2]. Also, the ease of manipulating the hydroxyl groups in cyclodextrins to enhance the host-guest behavior.

CDs are produced by cyclization of dextrins or its derivatives obtained during degradation of starch by cyclodextrin glycosyltransferase (CGTase). The product is a mixture of different major types of CDs (i.e., α, β, and γ) and negligible quantities of CDs with more than eight D-glucose units. The application of natural enzymes in biochemical reactions faces several limitations, such as recycling difficulty and denaturing as a result of harsh operating conditions [3]. To overcome these disadvantages, enzymes are usually immobilized on solid support. The support should be a porous material with large surface area, void volume and the immobilization method should cause minimal loss in enzyme activity. The properties of the support play an important role in determining the success of the immobilization process; therefore, significant attention is paid to selecting a suitable support for the desired enzyme. Nevertheless, despite numerous advantages over soluble enzymes, the use of immobilized biocatalysts is associated with mass transfer limitations. Thus, the support should preferably be a porous material with a large surface area and void volume.

Materials that have been used for this purpose include mesoporous silica, hydrogels, sol-gel matrices. Sol-gels have been used for CGTase immobilization but they possess low immobilization efficiency and the bulkiness of the starch molecules limits access into the pores [4, 5]. Also, the immobilization takes place during sol-gel synthesis leading to loss of enzyme activity due to the harsh conditions. In hydrogels, the immobilized enzymes are bound to leach once the matrix swells [6]. Mesoporous silica

displays a large surface area, theoretically making it an ideal immobilization material. Nonetheless, the presence of surface charges often leads to enzyme deactivation. Moreover, mesoporous silica also suffers from significant enzyme leaching [7]. In recent years, metal–organic frameworks (MOFs) have found use as immobilization support for several enzymes and we also hypothesize that it can be attractive alternatives to the aforementioned supports for CGTase. Compared to other immobilizing matrices, MOFs have shown to possess great promise due to their ease of pore size tuning and functionalization, some possess favourable synthesis conditions with enzymes amongst other physico-chemical properties [8].

1.2 Statement of the Problem

Cyclodextrins are gaining wide use as agents of drug delivery systems in pharmaceutical companies since they can form inclusion complexes with therapeutic substances which allows them to be suitable for time-controlled dosage. The use of CD in the pharmaceutical industry has been limited due to the cost of production with a significant part of it being accounted for by CD glycosyltransferase used in the process, as appreciable amount of it are usually lost. In response to this challenge, this dissertation investigated how CGTase can be immobilized on MOFs to offer the needed stability and the factors that affect CGTase-MOFs' functionality in the production of CD.

1.3 Research Objectives

The objectives of this research work are to;

1. Identify and synthesize suitable MOFs for CGTase immobilization based on functional groups and pore size.

2. Modify and optimize the immobilization yield of CGTase on the MOFs

3. Compare the performance of immobilized CGTase on MOFs to those of previously reported supports.

4. Develop an understanding of the effect of immobilization on the secondary structures of CGTase by evaluation them before and after immobilization.

2

5. Investigate the kinetics of the immobilized CGTase and other thermodynamic variables that can be used to improve CD production from immobilized CGTase.

1.4 Research Motivation

This dissertation seeks to develop a MOF-CGTase matrix for production of CD. Several other supports have been used for CGTase but existence of significant mass transfer limitations and limited reusability have not made them desirous especially for industrial applications. This dissertation will explore usage of suitable two-dimensional and three-dimensional MOFs with a view to reduce activity loss and improve diffusional restraints in the products formed. The drive behind this research work is the need to retain and reuse CGTase during CD production while ensuring that it can withstand industrial conditions.

Chapter 2: Literature Review

2.1 Background

Highly useful substances known as cyclodextrins (CDs) have found use in a wide range of sectors, including food, medicine, cosmetics, and pharmaceuticals. These are glycosidic-bonded cyclic oligosaccharides that have a hollow, truncated cone shape and are made up of six (α-CD), seven (β-CD), or eight (γ-CD) D-glucose units [1]. The chemical structures of CDs are shown in Figure 1. The structure of CDs is amphibious, with a hydrophilic surface that allows for solubility in water and a hydrophobic internal cavity that forms inclusion complexes with a variety of hydrophobic chemicals. This amphibious nature accounts for the significance of CDs [2].
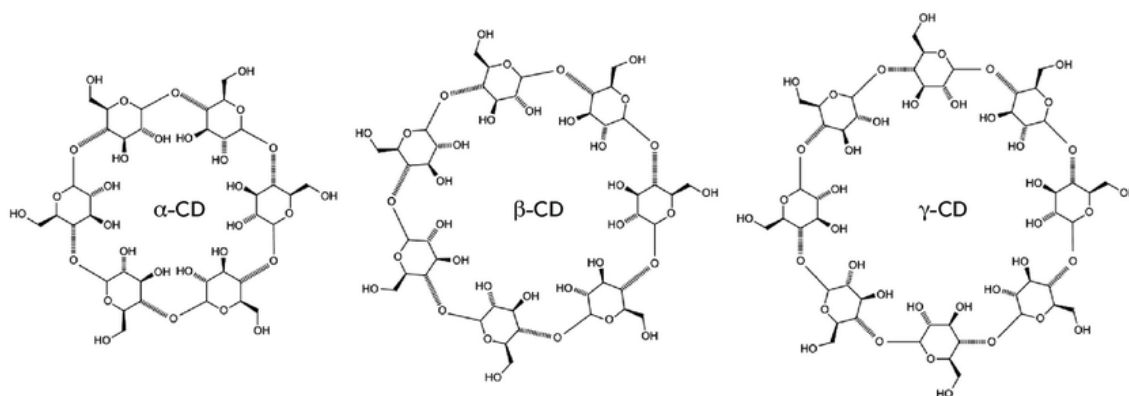
Figure 1: Structures of Cyclodextrins [9]

CDs are produced by cyclization of dextrins or its derivatives obtained during degradation of starch by cyclodextrin glycosyltransferase (CGTase). The product is a mixture of different major types of CDs (i.e., α, β, and γ) and negligible quantities of CDs with more than eight D-glucose units. However, the involvement of enzymes limits the production of CDs. One of the biggest challenges is the economic viability of the production process and the high cost of CGTase. To solve this issue, the biocatalyst must be effectively recovered and reused. Immobilization is the most common approach to achieve this, while maintaining the activity and enhancing the stability of the enzyme [10]. Notably, immobilization refers to physical confinement of the enzyme in a defined space [11]. In addition to increasing the enzyme recovery and reuse, immobilization of

biocatalysts on suitable supports may also enhance their thermal and shear stability. Furthermore, immobilization enables efficient handling of the enzyme, adequate control of the reaction, and prevents contamination of the products.

The effectiveness of the immobilization procedure is largely dependent on the characteristics of the support, therefore choosing the best support for the target enzyme receives a lot of consideration. Immobilized biocatalysts provide a number of benefits over soluble enzymes, however there are mass transfer restrictions when using them. As a result, a porous material with a big surface area and void volume should ideally serve as the support. Enzymes can adhere to these porous materials by chemical or physical adsorption. Physical adsorption is the most common immobilization technique owing to its simplicity and maintenance of the enzyme activity. Nevertheless, leaching occurs often with enzymes adsorbed by such methods, which over time reduces the immobilized biocatalysts' activity. Furthermore, the chemical bonds that are established between the enzyme and the support have an impact on the biocatalyst's activity, even though chemical adsorption leads to a stronger attachment to the support and resistance to leaching. Other immobilization matrices, such as sol-gel, hydrogels, and mesoporous silica, have recently been suggested to overcome the leaching problem without affecting the enzyme activity [4-7]. Nonetheless, the above materials exhibit low immobilization efficiency and high mass transfer. In addition, they cannot be used for bulky substrates due to the restricted access to the pores [4, 5]. It is also noteworthy that immobilization in sol-gel takes place during the sol-gel synthesis and subjecting the enzyme to harsh curing conditions results in reduced activity. These issues have been overcome by utilizing hydrogels instead of sol-gel; however, enzymes immobilized in hydrogels are prone to leaching upon swelling of the matrix [6]. Mesoporous silica displays a large surface area, theoretically making it an ideal immobilization material. Nonetheless, the presence of surface charges often leads to enzyme deactivation. Moreover, mesoporous silica also suffers from enzyme leaching [7]. In recent years, metal–organic frameworks (MOFs) have found use as immobilization support for several enzymes and it can as well be proposed as attractive alternatives to the aforementioned supports for CGTase. Compared to other immobilizing matrices, MOFs have been considered as promising materials due to the possibility of easy pore size modification, mild synthesis conditions, and desirable physico-chemical properties [8].

This dissertation looks at the use of immobilized CGTase for enhanced cyclodextrin production, and highlights the potential of MOFs as new immobilization supports. Despite the clear evidence of the favorable characteristics of MOFs, to the best of our knowledge; there is no report in the literature before commencement of this study showing MOFs usage for CGTase immobilization, thus, this dissertation paves the way for researchers to investigate the effectiveness of using MOF in this very important application.

2.2 Cyclodextrin Glycosyltransferase

Based on their functions, enzymes are often divided into six groups: ligases, transferases, hydrolases, lyases, isomerases, and oxidoreductases. The transfer of functional groups between molecules is facilitated by transferases. This group includes CGTases (EC 2.4.1.19), which are capable of catalyzing four distinct kinds of reactions: cyclization, coupling, hydrolysis, and disproportionation [12]. Extracellular enzymes known as CGTases are exclusively found in bacterial cells. Similar to amylases, which hydrolyze starch or starch derivatives into linear products, they have several functional characteristics. Therefore, CGTases that are thermally stable can be used to dissolve starch [13]. These biocatalysts are classified into α-, β-, and γ-CGTases based on the major CD produced in the initial phase of the reaction between the enzyme and starch [14].

2.2.1 Sources and Properties

Examples of the many sources of enzymes and optimal cultivation conditions are shown in Table 1. The desired type of CD is taken into consideration while choosing the bacteria that will produce CGTase for CD synthesis. For example, it has been reported that CGTase derived from *Bacillus pseudalcaliphilus* 8SB has no α-activity, strong β-activity, and low γ-activity [15].

Table 1: CGTase Sources and Optimum Growth Conditions

Bacteria	Type of CGTase	Optimum condition	Reference
Bacillus licheniformis	α-CGTase	40°C, pH 6.0–8.0	[16]
Bacillus circulans	β-CGTase	56°C, pH 6.4	[1]
Bacillus sp.	β-CGTase	55°C, pH 5.0	[17]
Bacillus agaradhaerens	β-CGTase	55°C, pH 9.0	[18]
Bacillus megaterium	β-CGTase	60°C, pH 7.2	[19]
Bacillus subtilis	γ-CGTase	65°C, pH 8.0	[20]
Bacillus firmus strain 290-3	β/γ-CGTase	60°C, pH 6–8	[21]
Paenibacillus macerans	α-CGTase	45°C, pH 6.0–10	[22]
Thermoanaerobacterium thermosulfurigenes	α-CGTase	80–85°C, pH 4.5–7.0	[23]
Geobacillus thermoglucosidans	β-CGTase	65-70°C, pH 5.5	[12]
Brevibacillus brevis strain CD162	β/γ-CGTase	55°C, pH 8.0	[24]
B. macorous strain WSH02–06	γ-CGTase	50°C, pH 6.5	[25]
Brevibacterium sp. strain 9605	γ-CGTase	45°C, pH 10	[26]

Based on the study of Uitdehaag et al. [27], the molecular weight of CGTase may be assumed to be 77.24 kDa. This yields an estimated size of 5.62 nm based on the equation created by Erickson [28]. The choice of matrix or immobilization technique must take into account the sizes of both the substrate and CGTase. Making appropriate judgments about the kinds of MOFs that might enhance CGTase immobilization can be aided by identifying the inefficiencies found in the matrices that have been utilized thus far.

2.2.2 Production

The aerobic alkalophilic strains of *Bacillus* sp. are the main producers of CGTases. It has been found that other mesophilic, thermophilic, psychrophilic may also manufacture CGTase enzymes, some are *Klebsiella pneumonia,* microorganisms, including *Brevibacterium* sp., hyper thermophilic archaea-bacteria, and *Bacillus stearothermophilus* [26, 29, 30].

The process of producing CGTase entails a number of processes, such as choosing an appropriate microbial source, growing the microorganism under ideal circumstances, and extracting the enzyme from the fermentation broth. The chosen microbe must be cultivated in an appropriate growth medium in order to start the synthesis of CGTase. The carbon, nitrogen, vitamin, and mineral sources that are essential for microbial development and enzyme synthesis are usually present in the growth medium. In order to stimulate the synthesis of CGTase, carbon sources such as starch or starch-containing substrates, such

as corn syrup or malt extract, are frequently used. In a typical medium, 2% (w/v) soluble starch, 5% (w/v) yeast extract, 5% (w/v) peptone, 0.1% (w/v) K_2HPO_4, 0.02% (w/v) $MgSO_4 \cdot 7H_2O$, and 1% (w/v) Na_2CO_3 can be used [31]. To maximize the production of CGTase, the culture conditions—pH, temperature, agitation, and aeration—are tuned. These variables change based on the particular microbe and fermentation technique being utilized. For instance, mesophilic *Bacillus* strains may grow best at lower temperatures, whereas thermophilic *Bacillus* strains usually produce CGTase at higher temperatures (e.g., 50–65°C) [31, 32].

The bacterium is cultivated in a fermenter or bioreactor under carefully monitored circumstances. Depending on the particular needs of producing CGTase, the fermentation process can be carried out in a batch, fed-batch, or continuous manner [33-35]. The microbe creates and secretes CGTase into the fermentation broth during fermentation, where it catalyzes the transformation of starch into cyclodextrins. To retrieve the enzyme, the fermentation broth is harvested when CGTase production reaches its maximum. Usually, the broth is separated using methods like centrifugation or filtering to take out solid particles and microorganisms, leaving behind the filtrate or supernatant that contains enzymes. Next, contaminants are eliminated from the recovered enzyme to provide a homogenous and highly concentrated formulation of CGTase using precipitation, chromatography (such as affinity and ion exchange chromatography), ultrafiltration.

2.3 CGTase Immobilization

The necessity for appropriate enzyme handling, storage, and reuse is driving research concerning immobilization of biocatalysts on different supports. For economic viability of any biochemical process, the cost of enzymes should not be more than a few percent of the total cost of the production; thus, the possibility of biocatalyst reuse is important [6]. Traditionally, enzymes are lyophilized, i.e., freeze-dried; however, this may lead to significant distortion of the enzyme structure [36]. Immobilization of enzymes on supports enables better access for the substrates, as the biocatalysts are dispersed, thus increases the available surface area. The support should preferably be inert to the enzyme and possesses microbial resistance. Additionally, it should not pose diffusional problems

to the enzyme's substrate. The desired properties for the enzyme and support are summarized in Figure 2.
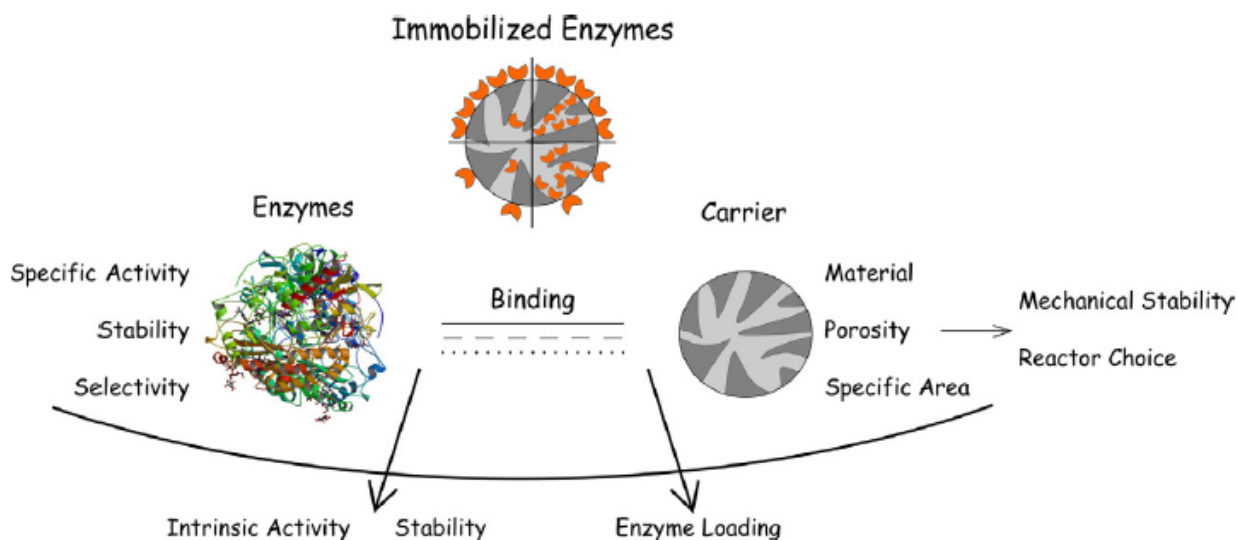
Figure 2: Summary of Enzyme Immobilization and the Desired Enzyme and Support Properties [37]

To efficiently utilize CGTase for the production of CD, different supports have been used for its immobilization in literature. Table 2 summarizes the previously reported supports for CGTase immobilization.

Table 2: Properties of CGTases Immobilized on Different Supports for CD Production

Support	Source of CGTase	Optimum pH	Optimum Temperature (°C)	Activity of immobilized enzyme (U/g-support)	Max. yield of CD (%)	Reusability (%)	Ref.
Physical Adsorption							
Polyvinylidene difluoride hollow fiber	*Bacillus lincheniformis*	7.0	25	n.r	69.37	n.r	[38]
Covalent attachment							
Cellulose nanofiber		n.r.	70	159.34	69 (α)	68% after 10 cycles	[39]
Trisoperl (activated porous glass)	*Bacillus macerans*	5.1	48	3.0	~85 (β)	68% after 20 cycles	[40]
Aminated polyvinylchloride (PVC)		6	75	121	15.6	85% after 14 cycles	[41]
Fe₃O₄@PEI-PDA	*Bacillus pseudalcaliphilus*	6.0	55	300	88.9 (β)	19% after 9 cycles	[15]
Resin (FE 4611)		6-8	~58	≤ 2	14	n.r.	[42]
Glutaraldehyde-pre-activated Silica	*Thermoanaerobacter sp.*	4.0-8.0	n.r.	101.73	n.r.	n.r.	[43]
Glyoxyl-agarose		6.0	85	27.38	85.4(β)		[44]
Functionalized Magnetic double mesoporous core-shell silica	*Amphibacillus sp.*	8.5	55	n.r.	n.r.	56% after 10 cycles	[45]
Entrapment							
Calcium alginate beads	*Bacillus maceran*	7.5	60	n.r.	n.r.	75% after 7 cycles	[46]
	Aspergillus oryzae	4.0	40	2760.4 U/mL	n.r.	57% after 12 cycles	[47]

2.3.1 Supports Used for CGTase Immobilization

Nanomaterials have been employed as support for CGTase. For example, cellulose nanofibers (CNF) made from kenaf bast fiber was used for immobilization of CGTase using chemical coupling with 1,12-diaminododecane as coupling agent [48]. The immobilized enzyme was added to a 50 g/L soluble starch solution and incubated at an optimum temperature of 70°C. HPLC analysis of the product revealed a gradual increase in the yield of α-CD, which reached a maximum yield of 69%. The performance of the immobilized CGTase prepared at higher microwave power levels led to CNF with smaller diameter (higher surface area) resulting into better interaction between the coupling agent and the –OH group present on the cellulose, observed at 3400-3200 cm⁻¹. The covalent

attachment of CGTase to the ligand ensures that the enzymes gain rigidity by reducing the chances of conformational changes, thus resulting in better stability. This could be observed in the thermal stability, which shifted from 60°C for free CGTase to 70°C for immobilized CGTase and the retained activity after 10 cycles was 68% [48]. The maximum binding efficiency, after several modifications both on the process and CNF synthesis parameters, was 72%.

In another study, Fe_3O_4 nanoparticles functionalized with polydopamine (PDA) was used [15]. It has been reported that PDA contains various surface functional groups such as amino and catechol which influences enzyme immobilization [49, 50]. The immobilized biocatalyst was mixed with 3 mL of a 1% potato starch solution. The reaction was conducted at 55 °C and maximum yield of β-CD was 88.9%. It is noteworthy that the immobilized enzyme retained 19% of its initial activity after nine cycles which showed that the attachment of CGTase to the functional groups present on PDA might not be enough for use in industrial set-up.

Commercially available Eupergit C and Eupergit C 250L, which are epoxy-activated acrylic beads, with difference in their pore sizes and oxirane groups was used for CGTase immobilization [51]. The average pore size in Eupergit C is 10 nm, making it mesoporous based on the classification of IUPAC and it has oxirane density of 600 µmol/g. Eupergit C 250L on the other hand is macroporous (average pore size 100 nm) but with lesser oxirane density of 300 µmol/g [52]. The immobilization mechanism of enzymes on Eupergit beads have been proposed to follow two steps [53], firstly, there is physisorption on the support by hydrophobic interaction which brings the amino and thiol groups present on the enzyme's surface close to the oxirane group. Lastly, these groups then react with the oxirane group via nucleophilic attack to form very stable C-S and C-N bonds. Therefore, it is expected that Eupergit beads should offer minimum enzyme loss when used as immobilization support. The bound protein for Eupergit C 250L was 72% compared to 81% observed on Eupergit C [51]. As Eupergit C contains more oxirane groups, this leads to better retainment of CGTase and can also promote multipoint attachment, to produce a more stable enzyme/support matrix. The reusability studies showed that 40% of the initial CGTase activity was retained after 10 cycles of 24 h each. Despite these advantages of Eupergit C over Eupergit C 250L, its mesopores will pose

diffusional limitations, especially for bulky substrate e.g. starch, in the production of CD using CGTase.

In addition, Schoffer et al. described immobilization of β-CGTase on glutaraldehyde pre-activated silica, functionalized with 3-aminopropyltrimethoxysilane (APT) [43]. Although the immobilization yield was high (above 96%) as a result of functionalization, the efficiencies were very low, between 3-5%. The possible cause of this could be the mesoporous nature of the silica used, preventing the substrate from accessing the active sites. At an optimal temperature, pH, and reaction time, the immobilized enzyme resulted in the production of 4.9 mgmL^{-1} of α-CD, 3.6 mgmL^{-1} of β-CD, and 3.5 mgmL^{-1} of γ-CD. Moreover, porous glass beads (e.g., Trisoperl) functionalized with APT has also been employed in the presence of glutaraldehyde as the cross-linker. The catalytic activity of the immobilized enzyme was studied in the reaction involving a 2.5% (w/v) starch solution. A maximum CD yield of 85% was obtained at a temperature of 37 °C and pH of 6.0 [40]. A lag phase of 10 min was observed before the reaction started using the immobilized CGTase, supporting the earlier assertion that diffusional barriers exist.

Furthermore, CGTase was previously also immobilized by covalent attachment on polyvinylchloride aminated with three different diakylamines using glutaraldehyde. The enzymatic activity reached 121 U/g in the reaction involving a 5% (w/v) starch solution. Stability studies showed that immobilized CGTase retained 85% of activity after 14 cycles of batch operation. It was demonstrated that the amount of retained activity depended on the length of the spacer, i.e., the dialkylamine group, and glutaraldehyde [41].

On the other hand, on a macroreticular hydrophilic resin (e.g., FE 4611) containing a primary amine, the optimum pH of the immobilized enzyme was shown to range between pH 6.0 and 8.0, with a maximum β-CD yield of 14% [42]. CGTase was also successfully immobilized on calcium alginate beads [47]. Under optimized conditions, 43% immobilization efficiency was achieved using starch concentration of 3.5% (w/v). The immobilized enzyme exhibited good activity of 2760.4 U/mL. Notably, the CGTase immobilization yield reached nearly 100% after 5 h at 25 °C when glyoxyl-agarose was utilized as the support at pH 10. Using immobilized CGTase on a 1% soluble starch

solution at 85 °C, a β-CD yield of 85.4% was obtained at a 2-fold higher rate than that observed for the free enzyme [44].

Since CGTase from different bacterial sources display various optimum temperature as shown in Table 1, a number of ionic interactions and disulphide bonds present in the structures of different sources of CGTase were examined [54]. All of the studies exhibited a similar number of disulphide bonds; however, the thermally stable enzymes displayed more ionic interactions. Hence, disulphide bonds are not responsible for the thermal stability of CGTases [55]. The attachment of the CGTase to the support, depending on the functional group on the support, could be responsible for this observed phenomenon.

From the supports used in the literature for CGTase immobilization, it is evident that apart from the differences in their physical characteristics, such as the pore diameter, particle size, and mechanical strength, the performances of the CGTase/support depend on the type and density of the functional group used, the length of the coupling agent (for covalent bonding) and the pore network of the support. The surface area of the support, which depends on the pore diameter and particle size, significantly affects the capacity for CGTase binding. It is noteworthy that porous supports, such as agarose or Trisoperl, displayed better immobilization yield (thus increased CD yield), particularly in the presence of hydrophilic moieties. For example, utilizing agarose, a highly porous matrix with hydrophilic properties, resulted in an 85.4% yield of β-CD, which was comparable to that, achieved using Trisoperl and Fe_3O_4@PEI-PDA (Table 2). For more optimal utilization of porous supports, better control of the pore size distribution, such as utilizing supports with hierarchical pore networks, will likely give better results. This would improve the diffusional limitation and enhance the production of CD.

2.3.2 Immobilization Techniques

The most commonly used enzyme immobilization approaches include surface adsorption, covalent binding, encapsulation, and cross-linking. The selection of the method depends on the properties of the enzyme and support as well as on the potential application of the immobilized biocatalyst.

Surface adsorption occurs through a physical interaction between the enzyme and support. It is achieved by soaking the support in a buffered solution of the enzyme for a suitable incubation time. Alternatively, the biocatalyst solution can be allowed to dry on the support surface before washing away unattached enzymes [56, 57]. The reversible nature of physical adsorption enables the removal of immobilized enzymes from the supports under mild conditions upon the deterioration of the enzymatic activity [58]. Nevertheless, the weak forces holding the enzymes make them susceptible to leaching from the support when subjected to industrial conditions.

Ionic and covalent binding of the enzyme to the support is stronger than the physical adsorption described above. It offers enhanced enzyme stability; however, the presence of chemical bonds may affect the activity of the attached biocatalyst, which is a major disadvantage of this approach [6]. Generally, compared with a free enzyme, a reduction in activity is observed when an enzyme is immobilized on a support due to several factors, including protein crowding, biocatalyst inactivation, stearic hindrance, and enzyme orientation.

Enzyme encapsulation is a method of immobilization whereby the enzyme is confined within a porous support. The entrapped enzyme is not actually physically attached to the support; however, its ability to diffuse out is restricted [59]. Enzyme entrapment is fast and involves mild conditions. Moreover, the enzyme is not chemically interacting with the support and the possibility of denaturing is lower. Nonetheless, this approach suffers from mass transfer limitations, as the access of the substrate to all active sites might be restricted [60].

More recent immobilization techniques include Cross-linked Enzyme Aggregates (CLEAs) and Cross-linked Enzyme Crystals (CLECs). These methods are typically called carrier-free immobilization approaches, as there is no requirement for any supports [6]. As described above, immobilization of enzymes on supports involves attachment of biocatalysts on the surface of suitable materials. On the other hand, in the case of cross-linking, the enzyme exhibits greater stability because it is stabilized by links in a 3D structure [61]. Consequently, cross-linked enzymes usually display enhanced mechanical stability, ability to withstand shear stress, and improved high temperature tolerance

compared to other immobilized enzymes.

The formation of CLEAs involves the generation of enzyme aggregates in the presence of salts, non-ionic polymers, or organic solvents, followed by cross-linking using bi-functional (e.g., glutaraldehyde) or poly-functional (e.g., aldehyde–pectin, aldehyde–dextran, or aldehyde–starch) chemical agents without the need for a support [62]. This approach offers various advantages over other immobilization methods, including simplicity as well as thermal and operational stability of the aggregates. Importantly, it can easily be applied to more than one enzyme at a time. The effects of cross-linking agents on the activity of CGTase CLEAs have been previously investigated [63]. Nevertheless, the cross-linking technique is also associated with several limitations. Even at an optimum concentration of the cross-linking agent, i.e., glutaraldehyde, the activity of the recovered enzyme was determined at < 10%, while the aggregate activity loss was established at > 80%. The observed low activity recovery was attributed to diffusional resistance of the bulky starch substrate or inadequate enzyme cross-linking, leading to increased loss of the enzyme, thus resulting in low activity recovery.

On the other hand, CLECs are solid crystalline particles, which are insoluble in organic solvents and water. They are prepared by precipitating enzymes into microcrystals, which is followed by a cross-linking step. The lattice interactions in the microcrystals provide additional stability for the biocatalysts. The advantages and disadvantages of various immobilization techniques are summarized in Table 3. From the various methods used for CGTase immobilization, covalent attachment has shown to offer the best immobilization yield with relatively higher activity retainment.

Table 3: Summary of Conventional Immobilization Techniques

Immobilization method	Binding characteristics	Advantages	Disadvantages	References
Physical adsorption	Weak bonds by either van der Waals or ionic interactions	• Simple/cheap • Little or no conformational change in the enzyme • Ease of regeneration • Wider selection of support	• High enzyme desorption/leaching	[64, 65]
Covalent binding	Chemical attachment between functional groups on support and enzyme	• Low enzyme leaching • Enhanced enzyme stabilization	• Difficulty in regenerating enzyme/support • Reduced enzyme activity	[66]
Entrapment/ Encapsulation	Inclusion of enzyme within the supports structure	• High enzyme loading • Low enzyme leaching • Little or no conformational change in the enzyme	• High mass transfer limitation • Inactivation of enzyme during encapsulation	[67, 68]
Cross-linking	Aggregate/cluster of enzyme cross-linked by a functional reactant	• Enzyme stabilization without support	• High mass transfer limitations • Loss of enzyme activity • Less useful in packed bed reactors	[69, 70]

2.4 Metal–Organic Frameworks (MOFs)

In recent years, MOFs have been utilized in various fields; therefore, their application as supports for enzyme immobilization has attracted significant attention. MOFs are formed by linking metal ions and organic linkers into well-defined three-dimensional porous solids [71]. The surface area of these materials ranges from 1000 to 10000 m^2/g, surpassing those of other known porous structures [72]. The stability of MOFs depends on the strength of the metal–organic linker coordination bond [73, 74]. Notably, nearly all metal atoms in their stable oxidation states can be used for the synthesis of

MOFs. The coordination number of employed metals defines the possible molecular geometry, e.g., linear, planar, pyramidal, or octahedral [75].

The commonly used organic linkers include carboxylates, sulfonates, imidazolate, amines, and their derivatives. The functional groups on the organic linkers in MOFs must be carefully selected as they provide the necessary interaction sites for the enzyme. Appropriate functionalities minimize leaching and improve stability [76]. To investigate this in more detail, the interactions between microperoxidase 11 (MP-11) and mesoporous Tb-MOF were studied using Raman spectroscopy. The presence of a π-π interaction between the organic component of the examined MOF and the heme unit of MP-11 was established. However, this interaction was missing when mesoporous silica was used instead of Tb-MOF [77]. Generally, a ligand is said to be flexible if it can rotate around a single bond. It is noteworthy that during the selection of organic linkers, rigid organic molecules are preferred over flexible ones. Rigid molecules aid the formation of crystalline MOFs exhibiting good thermal and mechanical stability and specific topology [78, 79]. Moreover, both charged and neutral compounds can be used as ligands for the MOF synthesis; however, positively charged molecules are used less frequently. This is predominantly due to the low affinity of positively charged moieties for the formation of bonds with metal cations, i.e., the required charge balance cannot be achieved [80]. The metal centers in the coordination spheres created by the metal ions in MOF structures are usually protected from the reactants by bulkier organic linkers [81].

The availability of different metal ions and organic linkers results in the formation of MOFs with different physicochemical properties. Examples of typical MOF structures are demonstrated in Figure 3. A more recent subclass of MOFs is the biological MOFs (bio-MOFs), which introduces biomolecules in the formation of the porous material. Apart from the general properties offered by MOFs, bio-MOFs offer the much needed properties, especially in biological application, where toxicity [82], efficacy and stability must be critically controlled [83]. Most bio-MOFs are constructed using a biomolecule as the ligand, such as proteins, amino acids, peptides and cyclodextrins or any other bio relevant organic linker, which can bind to bioactive metal nodes[83-85]. Examples of successfully synthesized bio-MOFs include Co-Cys, made from cobalt and cystine [86] and silver-

based phosphadamantane (Ag-PTA) [87]. Silver is very useful in bio-MOFs synthesis due to its recognized antimicrobial action.
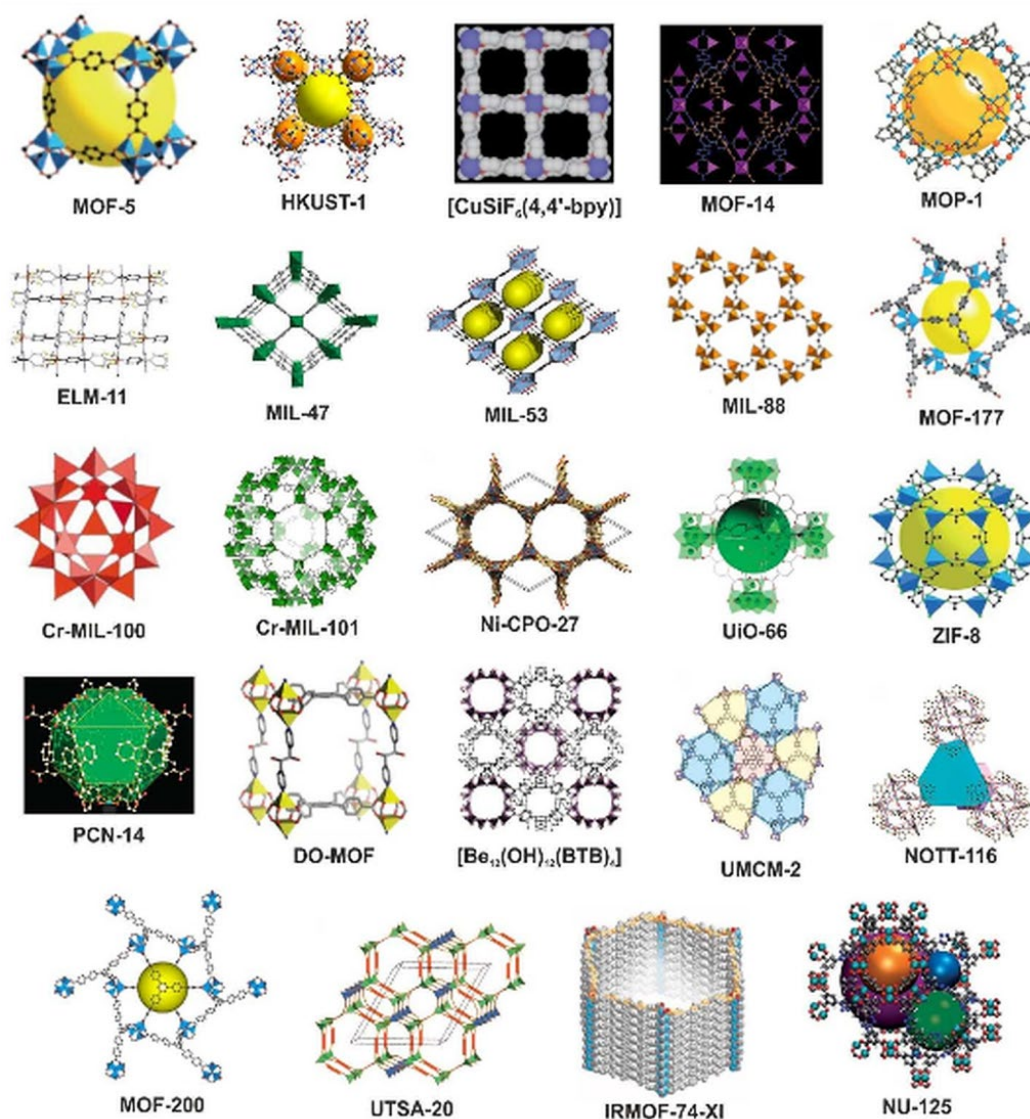
Figure 3: Examples of typical MOF structures

2.4.1 Types and Properties

Various types of MOFs have been synthesized for application in enzyme immobilization. The majority of the investigated MOFs can be synthesized at ambient conditions. These include zeolite imidazolate frameworks (ZIFs), terbium benzene-1,4-dicarboxylate (Tb-BDC), Materials of Institute Lavoisier (MILs), and Hong Kong University of Science and Technology MOFs (HKUST). Synthesis at ambient conditions

enables in-situ encapsulation of the enzyme, also known as co-precipitation. During the process, the biocatalysts are not subjected to harsh conditions; therefore, their activity is not affected.

Synthesis of MOFs is often conducted in liquid phase by mixing different solutions containing the chosen metal and organic linkers, e.g., at room temperature. The available synthesis methods include solvothermal [88], microwave-assisted [89], sonochemical [90], mechanochemical [91], electrochemical [92, 93], and direct evaporation (also known as slow diffusion) approaches [94-96]. A summary of different MOF preparation methods as well as their advantages and disadvantages are demonstrated in Table 4.

Table 4: Summary of MOF Synthesis Methods

Synthesis method	Advantages	Disadvantages	Examples of MOFs
Solvothermal	• Ease of technology transfer to the industry • Crystal growth can be controlled • Wide temperature range	• High operating cost • Long synthesis time	ZIF- 95 [97] ZIF- 78 [98]
Microwave-assisted	• Reduced crystallization time • Energy efficient • Ease of controlling reaction conditions • Particle size can be controlled from precursor concentration	• Difficult to implement in the industry • Isolation of single crystals is nearly impossible	VSB-1, VSB-5 [99] IRMOF-1, IRMOF-2, IRMOF-3 [100] Zr-UiO-66 [101] Hf-UiO-66
Sonochemical/ Ultrasonic	• Can achieve homogenous crystal size and morphology • Can be used to isolate pure phase	• Breakage of large single crystals needed for diffraction studies	TMU-46, TMU-47, TMU-48 [102]
Mechanochemical	• Only mechanical forces are needed • Extreme operating conditions are avoided • Solvent-free	• Difficulty in obtaining single crystals for diffraction studies • Secondary phases usually present in product	Copper isonicotinate $Cu(INA)_2$ [103] Copper benzenetricarboxylate $Cu_3(BTC)_2$ [104] Cd(II)-based MOFs [91]
Electrochemical	• Ease of industrial application • Short synthesis time • Uses current and voltage to control morphology	• Few MOFs have been synthesized till date	UiO-66 [105] $Cu_3(BTC)_2$ [106]
Slow diffusion	• Preparation of large single crystals • Ambient or low temperature required	• Synthesis could take several days • Minute quantity of product	$Zn_3(BDC)_3.6CH_3OH$ [107]

Solvothermal approaches are the most commonly employed methods for the production of MOFs. In solvothermal synthesis, the reactants are subjected to temperatures in the range of 100–240°C and pressures up to 105 kPa. In addition, polar solvents with high boiling points are typically utilized and the reaction time ranges from 6 h to several days. Sealed vessels or Teflon-lined autoclaves are used for the reaction [108]. Hydrothermal synthesis can be taken as a special class of solvothermal technique, involving the use of aqueous solvents, usually water, at elevated temperature and pressure [109]. Its advantages in MOFs synthesis include growth of microcrystalline phases during

MOFs synthesis, utilization of a water, considered as a green solvent and high reactivity of the reacting species [110, 111]. The hydrothermal route can also be used to obtain MOFs with extended channel systems [112]. Due to the elevated synthesis conditions, encapsulation of CGTase within the pores of MOFs in one-pot synthesis might not be feasible as the harsh conditions might cause structural damage to the enzyme. A post-synthesis modification of the MOFs remains the best immobilization route for these synthesis approaches.

To accelerate the process, microwaves or ultrasound waves are utilized in microwave-assisted and sonochemical methods, respectively. In microwave synthesis, the reaction medium heats up due to the effect of the applied oscillating electric field on the permanent dipole moment of the molecules present in the medium, resulting in molecular rotations and rapid heating [113]. The usefulness of microwave synthesis largely depends on the dipole moment of the solvent molecule. Solvents with large dipole moments, such as DMF (dipole moment = 3.86 D), are preferred [114]. On the other hand, in sonochemical synthesis, the increased heating rate is a consequence of acoustic cavitation, which is the formation and collapse of bubbles by ultrasound waves, typically between 20 kHz and 1 MHz. This phenomenon results in an increased heating rate (> 1010 K/s), temperature (as high as 5,000 K in gas-phase reaction zones), and pressure (up to 1000 bar) [115-117]. Nonetheless, both of the above accelerated methods lead to the formation of MOFs exhibiting small crystal sizes, which range between 10 nm and 50 μm. Unlike other approaches, mechano-chemical synthesis is characterized by the absence of solvents. In the process, the intramolecular bonds between the metal salts and organic linker molecules are subjected to mechanical breakage using a ball mill, which results in a chemical transformation and the formation of the desired MOFs [95, 118]. Furthermore, electrochemical synthesis is similar to the solvothermal method. However, instead of using metal salts, metal ions are supplied from the dissolution of the anode. The metal ions then react with the dissolved linker molecule present in the reaction medium [118]. Direct evaporation, or slow diffusion, is also comparable to the solvothermal approach. In this case, however, no external energy is needed. The metal salts and organic linkers are mixed and the solvent gradually evaporates from the reaction solution at room temperature [119]. When selecting a suitable method, considering the reaction time and the amount of solvent

needed for the synthesis of MOFs is necessary. In all approaches, the structural units self-assemble into ordered metal–organic coordination bonds to form the structural frameworks of MOFs. The simplest method reported to date is direct evaporation, which does not necessitate the use of any external energy sources. However, the approach requires long synthesis times, which range from a few hours to several days.

The rate of reaction can be significantly increased using microwave synthesis, which results in rapid achievement of high temperatures in localized zones. Examples of MOFs that have been synthesized employing this method include IRMOF-1 [100], HKUST-1 [120], and MIL-100-Cr [99]. To understand the mechanism of microwave synthesis, the rate enhancement was studied during the preparation of HKUST-1 [120]. It was found that the reaction rate enhancement was a result of an increase in the nucleation rate and not the crystal growth rate. In contrast, the outcomes of the investigation involving MIL-53 (Fe) demonstrated that both nucleation and growth rates contributed to the observed enhancement in the rate of reaction [121]. Despite the increased rate of reaction, using microwave-assisted heating results in significantly smaller crystals compared to other methods. For instance, the synthesis of MOF-5 utilizing direct evaporation and microwave-assisted methods resulted in similar cubic-shaped MOFs; however, the crystal size of the microwave-heated material was approximately 20 times smaller (Figure 4) [122].
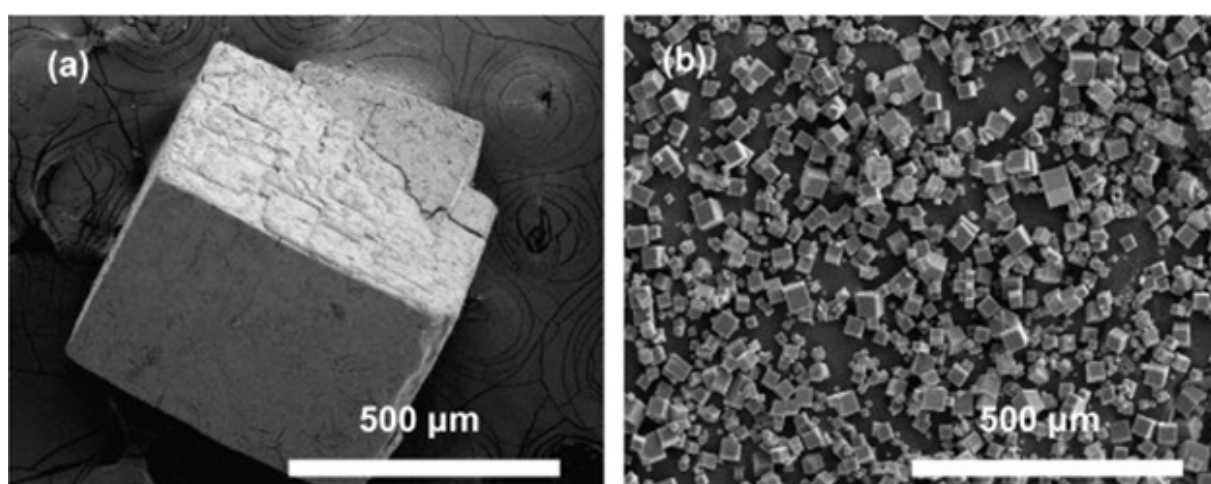
Figure 4: Scanning Electron Microscopy (SEM) Images of MOF-5 Crystals Obtained Using (a) Conventional and (b) Microwave-Assisted Approaches [122]

Consequently, based on the promising results obtained by immobilizing CGTases on functionalized supports as highlighted in Section 2.3.1, improvement in CGTase immobilization is expected using MOFs based on the numerous advantages that have been highlighted. The presence of both organic (i.e., the linker) and inorganic (i.e., metal nodes) components in MOFs could promote several interactions between the support and various functional groups in CGTase. The organic linker can be modified to generate interaction sites for CGTase, thereby minimizing leaching and enhancing stability. In addition, the ordered, crystalline, and multi-dimensional structure of MOFs could ensure a protective environment for CGTase and prevent the activity loss due to denaturing factors. This would further reduce the leaching of the biocatalyst and limit mass transfer problems. Nevertheless, careful selection of appropriate MOFs is essential to ensure the presence of suitable cavities capable of accommodating CGTase [123]. In this regard, MOFs exhibiting hierarchical structures are promising. The large channels in these materials could be used for immobilization of CGTase, while the smaller channels would remain available for substrate and product diffusion, minimizing diffusional problems [123].

Different MOFs with hierarchical pore networks have already been synthesized by various researchers that could be adapted for limiting the effect of diffusion in CGTase immobilization. Mondloch et. al. [124] described the synthesis of hierarchical zirconium-based MOFs (NU-1000) which contains windows connecting 3.1 nm hexagonal channels with triangular channels having edge length of 1.5 nm. In making hierarchical MOFs, the nucleation and growth processes must be well controlled [125, 126].

The large surface areas of MOFs could result in higher CGTase loading capacity, providing more active sites for substrate transformation into CD. Lastly, the ability to tune the properties of the MOF, most importantly the hydrophilic or hydrophobic nature of its surface, would ensure that the free cysteine residue in the enzyme could be used for binding to the support, leading to better biocatalyst stability.

2.5 Summary

In this literature review, CGTase immobilization on various functionalized supports was discussed. Covalent attachment was identified as the best immobilization technique for CGTase, with density of the functional group, length of the coupling agent and type of

pores present in the support affecting the reusability of the matrix and diffusion of both reactant and product when used in CD production. MOFs have been shown as robust supports for enzyme immobilization, exhibiting enhanced biocatalytic properties compared to conventional supports. The increasing number of new MOF structures will undoubtedly lead to utilization of these materials in various fields. Although MOFs have been employed for immobilization of several different enzymes, their superior properties have not been applied for CGTase immobilization to produce CD. To achieve this, the interactions between CGTase and the MOF components must be investigated and understood. Better knowledge of such interactions could lead to enhancement in enzyme loading, stability, and reusability, particularly in industrial settings. As immobilized enzymes display different activity trends from those of free biocatalysts, more research is needed to determine the effects of CGTase immobilization on MOFs on the activity of the enzyme. Moreover, the affinity of MOFs for CGTase requires evaluation. Among the possible conventional immobilization techniques, covalent attachment of enzymes has been shown to result in more stable and reusable biocatalysts. Nevertheless, the high cost and difficult regeneration of the support currently limit the application of this technique. Thus, improvements are needed to utilize this approach for industrial production of CD.

2.6 Research Hypotheses

Thus, based on the findings from the literature, we hypothesize that;

1. Carefully selecting MOFs with functional groups such as –COOH or –NH$_2$ might create strong bonding with the amide groups in CGTase. This will lead to a MOF-CGTase matrix with higher enzyme uptake and reusability.

2. Protecting CGTase within the cavities of suitable MOFs might help reduce enzyme conformational changes post-immobilization. Supports to be used for this should possess mesopores/ macropores.

3. Due to the bulkiness of the substrate molecules i.e. starch, surface attachment of CGTase might limit diffusional restraints, reduce activity loss since there will be less stress on the active sites and result in better yield of cyclodextrins. Surface attachment should also result in minimal changes in the secondary structures of CGTase.

4. Using a non-porous support with high external surface area might improve CGTase uptake and eliminate diffusional limitations encountered by starch molecules and the products entirely.

Chapter 3: Materials and Methodology

3.1 Reagents and Chemicals

CGTase Toruzyme® 3.0 L (*Thermoanaerobacter* sp.) was provided by Novozymes A/S (Bagsvaerd, Denmark), containing 23.0 mg of protein/mL, with specific activity of 167 U/mg protein. α-CD, β-CD, γ-CD, chromium nitrate nonahydrate ($Cr(NO_3)_3.9H_2O$, 99%), methanol, 1,3,5-benzenetricarboxylic acid (H_3BTC or TMA), glutaraldehyde solution (25%), copper nitrate trihydrate ($Cu(NO_3)_2.3H_2O$), N, N-dimethylcyclohexylamine, acetonitrile, Bradford reagent were procured from Sigma-Aldrich (St Louis, MO, USA). Zeolite Y was obtained from TOSOH, Japan. Soluble starch (extra pure), methyl orange, phenolphthalein, sodium carbonate (Anhydrous, 99.9%) were purchased from Sisco research laboratory (Maharashtra, India). Graphene nanoplatelets (GNP) (purity: 99%, size: 3 nm, 530 m^2/g) was purchased from Nanografil Nano Technology (Ankara, Turkey). Ethanol was obtained from J.T. Baker (Deventer, Netherlands). Starch soluble (extrapure), phenolphthalein, methyl orange, bromocresol green, terephthalic acid, and sodium carbonate (anhydrous, 99.9%) were obtained from Sisco research laboratory (SRLCHEM), (Mumbai, India). Deionized water was purchased from Fisher Scientific (Loughborough, United Kingdom). The corn flour waste was collected domestically. All other used chemicals were of analytical grade and were utilized as purchased.

3.2 Experimental Section

3.2.1 Syntheses of Supports

3.2.1.1 MIL-101 Synthesis (Paper I)

MIL-101 was synthesized based on the process described elsewhere [127]. 2.0 g (5 mmol) of $Cr(NO_3)_3 \cdot 9H_2O$ and 0.83 g (5 mmol) of H_2BDC (terephthalic acid) were added to 20 mL of deionized water and sonicated to produce a dark blue suspension with pH of 1.4. The mixture was then put into a 50-mL hydrothermal Teflon-lined autoclave (Aoshi, China), which was heated in an oven (DAIHAN OF5, Korea) at 218°C without stirring. After 18 h, the suspension was left to equilibrate at ambient temperature and then centrifuged (OHAUS FC5816, USA) at 5,000 rpm for 10 min to separate the MOF

particles. The collected MOFs were washed with distilled water, methanol, and acetone respectively. The MOF particles were placed in *N*, *N*-dimethylformamide (DMF), sonicated for 10 min, and then kept overnight at 70°C. The solids were washed with methanol and acetone multiple times. Then, they were dried at 75°C for 12 h. The MOF was activated by vacuum drying (DAIHAN SOV-30, Korea) at 140ºC for two days.

3.2.1.2 Ca-TMA Synthesis (Paper II)

In a typical experiment, Ca-TMA was prepared using the following procedure. Two solutions (A and B) containing 100 mL of an H_2O: ethanol (1:1) mixed solvents were prepared and heated at 50ºC. A total of 7.875 g TMA was dissolved in solution A, and 5.9 g of calcium nitrate tetrahydrate was dissolved in solution B. The two homogeneous solutions were thoroughly mixed using a magnetic stirrer at 1000 rpm for three hours at 50ºC, then allowed to cool in air to room temperature for 12 hours. The mixed solution was centrifuged, and washed twice with the H_2O-ethanol mixed solvent. The Ca-TMA precipitate was filtered, dried in air to be used for the adsorption experiments and for characterization.

3.2.1.3 Synthesis of Hierarchical Copper-based Metal–Organic Framework (H-Cu-BTC) (Paper III)

The H-Cu-BTC was synthesized according to a previously described method, with some modifications [128]. Solution A was prepared by dissolving 2.5 mmol of 1,3,5-benzenetricarboxylic acid (H_3BTC) in 15 mL of anhydrous methanol. Solution B was prepared by dissolving 4.5 mmol of $Cu(NO_3)_2 \cdot 3H_2O$ in 15 mL of deionized water. To ensure homogeneity, solution B was mixed with solution A and stirred (150 rpm at 25°C) for 30 minutes. Subsequently, 6.75 mmol of N, N-dimethylcyclohexylamine was added to the mixture, with the immediate formation of glaucous floccules, showing that the organic amine expedited the synthesis of the MOFs. The glaucous suspension was stirred continuously for 24 h, after which it was filtered, rinsed twice with ethanol, and dried for 12 h at 120°C in a vacuum oven (DAIHAN SOV-30, Korea). The final product was designated as H-Cu-BTC. In contrast, conventional Cu-BTC (microporous) was prepared using the solvothermal method at 120°C described elsewhere [129]. Then, 15 mL of ethanol was mixed with 2.5 mmol of H_3BTC to obtain solution C, and 15 mL of deionized

water was mixed with 4.5 mmol of $Cu(NO_3)_2 \cdot 3H_2O$ to obtain solution D. Each solution was stirred for 30 min, and the two solutions were added together and mixed for an additional 30 min. The mixture was then placed in a 100 mL stainless-steel autoclave vessel, coated with Teflon, and heated in an oven (DAIHAN OF5, Korea) at 120°C for 12 h. The solid product was filtered, washed with ethanol, and dried at 120°C for 12 h.

3.2.2 Protein Assay

CGTase concentration was determined using the Bradford method by preparing various concentrations of bovine serum albumin (BSA) used as standard, ranging from 0 to 1.2 mg/mL [130]. To prepare the calibration curve, 20 μL of BSA solutions with different known concentrations was added to 180 μL of a Bradford solution and then left for 5 min for color development. The absorbance of each solution was then measured at 595 nm (SPECTROstar[nano] BMG LABTECH, Ortenberg, Germany) to produce a calibration curve. For the measurement of CGTase, the same procedure was followed, and the reading at 495 nm was compared with that of the calibration curve.

3.2.3 Support Characterization

3.2.3.1 Fourier Transform Infrared Spectroscopic (FTIR) Analysis

The FTIR analyses of the functional groups on the supports, when empty, with adsorbed enzyme and after the reaction were performed using a Fourier transform infrared spectrometer (Jasco Corporation FT/IR-6300, Japan). The samples were prepared prior to the analysis by mixing with potassium bromide (KBr; Sigma-Aldrich) and previously dried at 105°C to remove any interference by water molecules. The spectra were captured between 400 and 4000 cm^{-1}.

3.2.3.2 X-Ray Diffraction (XRD) Studies

XRD patterns for empty support and with the adsorbed enzyme were obtained using an X-ray diffractometer (PANalytical Instrument, X'Pert[3] Powder, Philips, Holland) equipped with Cu Kα with a wavelength λ = 1.540598 nm and operated at 40 mA. Scanning was performed within a 2θ range of 5°-80° with a step size of 0.026°/min.

3.2.3.3 Thermogravimetric Analysis (TGA)

To determine the thermal stability of the samples, thermogravimetric analysis (TGA) was conducted using a TGA Q50 V20.10 Build 36 analyzer (TA Instruments, Haan, Germany) in the temperature range of 0°C–700°C. The used heating rate was 20°C/min under a continuous flow of nitrogen.

3.2.3.4 Brunauer–Emmett–Teller (BET) Analysis

An N_2 adsorption–desorption experiment was conducted using Quantachrome Instruments (NOVAtouch NT 2LX-1, USA) to determine the supports' total pore volume, surface area, and average pore size. The analysis was performed for the empty support and with the adsorbed enzyme before the reaction. The immobilization supports were outgassed to remove moisture at 300°C. Then, liquid nitrogen (N_2) was used to obtain the surface area at a temperature of −196°C with a partial pressure (P/P_o) range of 0.05–0.35 [131]. The average pore size and its distribution were determined using the Barrett–Joyner–Halenda (BJH) technique [132].

3.2.3.5 Scanning Electron Microscopy (SEM) Analysis

The morphology of the supports, when empty, after enzyme adsorption and reuse were observed using a scanning electron microscope (JEOL JSM 6010 PLUS/LA) coupled with an energy-dispersive spectroscope to conduct surface characterization and elemental analysis. The samples were coated with gold particles before analysis.

3.2.3.6 Zeta Potential Measurement

Zeta potential is one of the fundamental characteristics that is known to determine stability. It measures the strength of the electrostatic or charge repulsion/attraction between particles. Zeta potentials were measured using a NanoPlus zeta/nanoparticle analyzer (NanoPlus, Japan). Here, 0.1 g of each solid sample or 1 mL of the enzyme solution was diluted in 5 mL of buffer solution (pH 7.4). Then, 1 mL of the resulting solution was injected into the high-concentration flow cell of the analyzer for measurement.

3.2.3.7 Fluorescence Spectroscopy

Fluorescence spectroscopy (FS) analysis of the free and immobilized CGTase were conducted to study changes in CGTase tertiary structure by measuring formation of N-formylkynurenine (N-FK), a photo-oxidation product of tryptophan, using Edinburgh Instruments' spectrofluorophotometer FS5 (United Kingdom) [133, 134]. The emission spectra were scanned between 400 – 650 nm, using an excitation wavelength of 375 nm.

3.2.4 CGTase Adsorption Isotherm

To obtain the adsorption isotherm, 1 mL of deionized water was combined with 0.1 g of activated MOFs (or 0.5 g of zeolite) and the mixture was sonicated for 5 min to create a well-dispersed suspension. Then, the suspension was added to 9 mL of phosphate buffer (0.05 M, pH 6.0), followed by the addition of 10 mL of CGTase solution with different concentrations (0 – 0.65 mg/mL). The resulting mixture was incubated for 24 h at 25°C in a water bath shaker (Labtech LSB-015S, KOREA) while stirring at 100 rpm to attain equilibrium. The immobilized enzyme was separated, thoroughly rinsed with phosphate buffer to remove the loosely attached enzyme, and immediately stored at 4°C. The protein amount in the remaining buffer solution and the washing solution were measured to evaluate protein uptake (q_e) using Equation 1 as follows:

$$q_e = \frac{(C_{initial} \cdot V_{initial}) - [(C_{final} \cdot V_{final}) + (C_{wash} \cdot V_{wash})]}{m} \qquad 1$$

where q_e (mg/g) is the equilibrium protein uptake, $C_{initial}$, C_{final}, and C_{wash} (mg/mL) are the protein concentrations in the initial CGTase solution, remaining buffer solution at the end of the adsorption test, and washing solution, respectively; $V_{initial}$, V_{final}, and V_{wash} (mL) are the volumes of the initial, remaining buffer, and washing solutions, respectively; and m (g) is the mass of the support. The data obtained were fitted to the Langmuir and Freundlich models, Equations (2) and (3), respectively

$$q_e = \frac{q_m b C_e}{1 + b C_e} \qquad 2$$

$$q_e = K_F C_e^{1/n} \qquad 3$$

where q_e is the protein uptake at equilibrium (mg/g), q_m is the maximum protein uptake (mg/g), C_e is the equilibrium concentration of CGTase (mg/mL), b is a parameter related to the interaction between protein and support surfaces (mL/mg), $1/n$ is the adsorption intensity, which indicates energy distribution on adsorbate surfaces, and K_F is the Freundlich adsorption capacity [135].

3.2.5 CGTase Adsorption kinetics

For the adsorption kinetics study, 0.02 g of MIL-101 (0.5 g of zeolite Y) was introduced into 5 mL of CGTase solution (0.57 mg/mL) at 25°C under stirring for different times (0-16 hrs.). After each time, the solids were separate by centrifuge (OHAUS FC5816, USA) at 5000 x g for 5 min and the protein concentration in the supernatant was measured, then used to determine the protein uptake at each time. Data from the adsorption kinetics study were fitted to the pseudo 1st and 2nd order, Elovich and intraparticle diffusion models, shown in Equations (4), (5), (6) and (7), respectively;

$$q_t = q_e(1 - e^{-kt}) \qquad\qquad 4$$

$$q_t = \frac{q_e^2 k_2 t}{1 + q_e k_2} \qquad\qquad 5$$

$$q_t = \frac{ln\,abt}{b} \qquad\qquad 6$$

$$q_t = k_d t^{0.5} + \theta \qquad\qquad 7$$

where q_t, q_e are the protein uptake (mg/g) at any time t and at equilibrium, k_1 (hr^{-1}), k_2 (gmg^{-1}hr^{-1}) are the pseudo first and second order kinetic constants, b (mgg^{-1}hr^{-1}) is the desorption rate constant, a (mgg^{-1}hr^{-1}) is the initial adsorption rate, k_d (mg/g.hr$^{-1/2}$) is the intra-particle rate constant, θ is the layer thickness [136, 137].

3.2.6 Kinetic Study for Free and Immobilized CGTase

The enzymatically produced CDs were spectrophotometrically determined using different indicators for each CD, as described by Vikmon (1982), with slight modifications [138]. The method is based on the change in the absorbance of the indicator solutions at certain wavelengths due to the formation of a colorless complex with CD, which was measured using a SPECTROstar Nano spectrophotometer (BMG Labtech, Germany). For

the free enzyme, 1 mL of the substrate solution, consisting of different starch concentrations (in the range of 1-10 g/L) in 0.01 M phosphate buffer at pH 7.4, was mixed with 100 μL enzyme solution (8.93 mg protein/mL) and incubated at 70°C while mixing at 100 rpm. For the immobilized CGTase, an equivalent mass containing the same protein amount as that of the free enzyme was used instead (0.893 mg protein) of the 100 μL enzyme solution. At regular intervals, the reaction was stopped by placing the mixture in boiling water and was centrifuged at 5000 ×g for 5 min to separate the precipitate. Then, the concentration of α-CD in the supernatant was measured by adding 1 mL of 0.01 M methyl orange to 0.5 mL of the reaction mixture, and absorbance was measured at 507 nm. α-CD was determined by comparing the absorbance against a calibration curve prepared using several dilutions of standard α-CD. For β-CD determination, 2 mL of phenolphthalein solution (0.04 mM phenolphthalein dissolved in 125 mM Na_2CO_3) was added to 0.5 mL of the reaction mixture, and absorbance was measured at 550 nm. γ-CD was measured by adding 1 mL of 0.005 M bromocresol green indicator to 0.5 mL of the reaction mixture, using 630 nm for absorbance determination. The concentrations measured for the CD at different substrate concentration was used to calculate the reaction rate. The resulting reaction rate versus starch concentration was used for kinetic parameter evaluation by non-linear fitting of the experimental data to the Michaelis-Menten model (Equation 8) using OriginPro® software.

$$V_o = \frac{V_{max}S}{K_M + S} \qquad\qquad 8$$

where V_o, V_{max} are the initial and maximum reaction rate (gL^{-1}min^{-1}) respectively, S is the substrate concentration (gL^{-1}) and K_M is the Michaelis-Menten constant (gL^{-1}).

3.2.7 Reusability Studies

For the reusability studies, the immobilized enzyme was separated from the reaction mixture before boiling, and the CD production steps described in Section 3.2.6 were repeated for 10 cycles. The reusability with the surface attachment as described under CGTase immobilization was compared with that of the covalent attachment via glutaraldehyde. The immobilization procedure was the same as the surface attachment but

with the addition of 0.5 mL glutaraldehyde before enzyme addition. The residual activity after each cycle was calculated using Equation (9),

$$Residual\ Activity(\%) = \frac{activitty\ at\ a\ cycle}{activity\ in\ cycle\ 1} \times 100\% \qquad\qquad 9$$

3.2.8 Data Analysis

All experiments were conducted in triplicates, with reported values being the mean, and standard deviation shown as error bars on the respective plots. The models used in this work were non-linearly fitted using Levenberg-Marquardt (L-M) method available on OriginPro 2021® software, using adjusted R^2 and reduced chi-square (χ_v^2) as validation parameters [139]. Statistical analysis was performed using the one-way analysis of variance (ANOVA) with Minitab 21 (Minitab LLC, Chicago, USA).

Chapter 4: Results and Discussion

4.1 Bioconversion of Starch to Cyclodextrin using Cyclodextrin glycosyltransferase Immobilized on Metal Organic Framework (Paper I)

The aims of this work are to investigate the enzymatic production of CD using CGTase immobilized on a 3-D MOF support, that is, MIL-101, and to compare this method with the use of a conventional support (zeolite). MOF was selected as a support because of its numerous favorable properties. To the best of our knowledge, there have not been any reports on CGTase immobilization on MOFs for CD production. The effect of the support properties on enzyme adsorption and the changes in the secondary structures after immobilization were investigated. Moreover, the catalytic performances of both free and immobilized CGTases were studied to understand how immobilization on MIL-101 affects the activity of CGTase. This study also examined the immobilized CGTase's kinetics and reusability, which are crucial components for industrial application.

4.1.1 Summary of the Main Findings

The superiority of a metal organic framework, namely, MIL-101 (Cr) over conventional support, zeolite Y, as immobilization support for *Cyclodextrin glycosyltransferase* (CGTase) was investigated. The adsorption capacity, stability, and secondary structures of CGTase upon immobilization were investigated. CGTase adsorption on MIL-101 and zeolite Y was best represented by the Langmuir isotherm with optimum adsorption capacities of 37.5 and 6.1 mg/g on two supports, respectively. The deconvolution of the amide I band of the FTIR spectrum indicated that free CGTase molecules predominantly contain β-sheets, which increased with the immobilization on MIL-101 and zeolite Y from 56% to 84.1% and 69.7%, respectively, suggesting the existence of CGTase agglomerates on the supports. The CGTase immobilized on MIL-101 showed relative activity of about 50% at a substrate concentration of up to 4 g/L (compared with free enzymes) and above 3 times higher selectivity towards the more valuable α-CD. A diffusion–reaction model was used to predict the behavior of the immobilized system, and reusability studies revealed that immobilized CGTase may be utilized for numerous reaction cycles, with possible improvements via covalent attachment using glutaraldehyde. Overall, the obtained results in this study provide insights into the

34

usefulness of MIL-101 as a suitable support for CGTase immobilization.

4.1.2 CGTase Adsorption Isotherms

Figure 5 shows the results of the CGTase adsorption on MIL-101 and zeolite Y. The equilibrium capacity for both supports increased with the increase in the CGTase concentration, which reached 31.6 and 1.3 mg/g for MIL-101 and zeolite Y, respectively. The experimental values taken at the same conditions for both supports show that MIL-101 has a greater adsorption capacity than zeolite Y. This result can be attributed to the combined effect of the larger surface area and more enzyme-compatible functional groups, mainly the –COOH groups offered by MIL-101 compared with zeolite Y. These results were fitted to the Langmuir and Freundlich models to identify the one that better correlates to the experimental results, as shown in Figure 5. Table 5 shows the fitting parameters of the supports under study. Both models provided good predictions of the experimental values for MIL-101 (Figure 5a). However, the Langmuir prediction appeared closer to the experimental data with the model having higher R^2 and lower reduced chi-square value, with maximum adsorption uptakes of 37.1 and 6.1 mg/g for MIL-101 and zeolite Y, respectively. The Langmuir isotherm also showed to be preferred for the adsorption of CGTase on zeolite. The Langmuir isotherm assumed that there was uniform adsorption of CGTase on the support surface with only monolayer coverage. The value of b in the Langmuir isotherm indicated a better interaction between CGTase and the surface, thus explaining the higher q_m observed for MIL-101. MIL-101 conferred high affinity for the enzymes, partly due to its high porosity and mainly due to the presence of functional carboxyl groups, and it has been identified as a good host for enzymes [140]. Under optimized conditions, 42 mg/g was reported as q_m in the CGTase immobilization via adsorption and crosslinking on a melamine–epoxy resin composite sponge [141], 8.1 mg/g over Eupergit C via covalent binding with glutaraldehyde [51], and 4.1 mg/g over activated silica using covalent binding [142]. The maximum adsorption uptake via the surface attachment on MIL-101 in this work (37.1 mg/g) stands comparably higher than that of most of the supports previously reported.
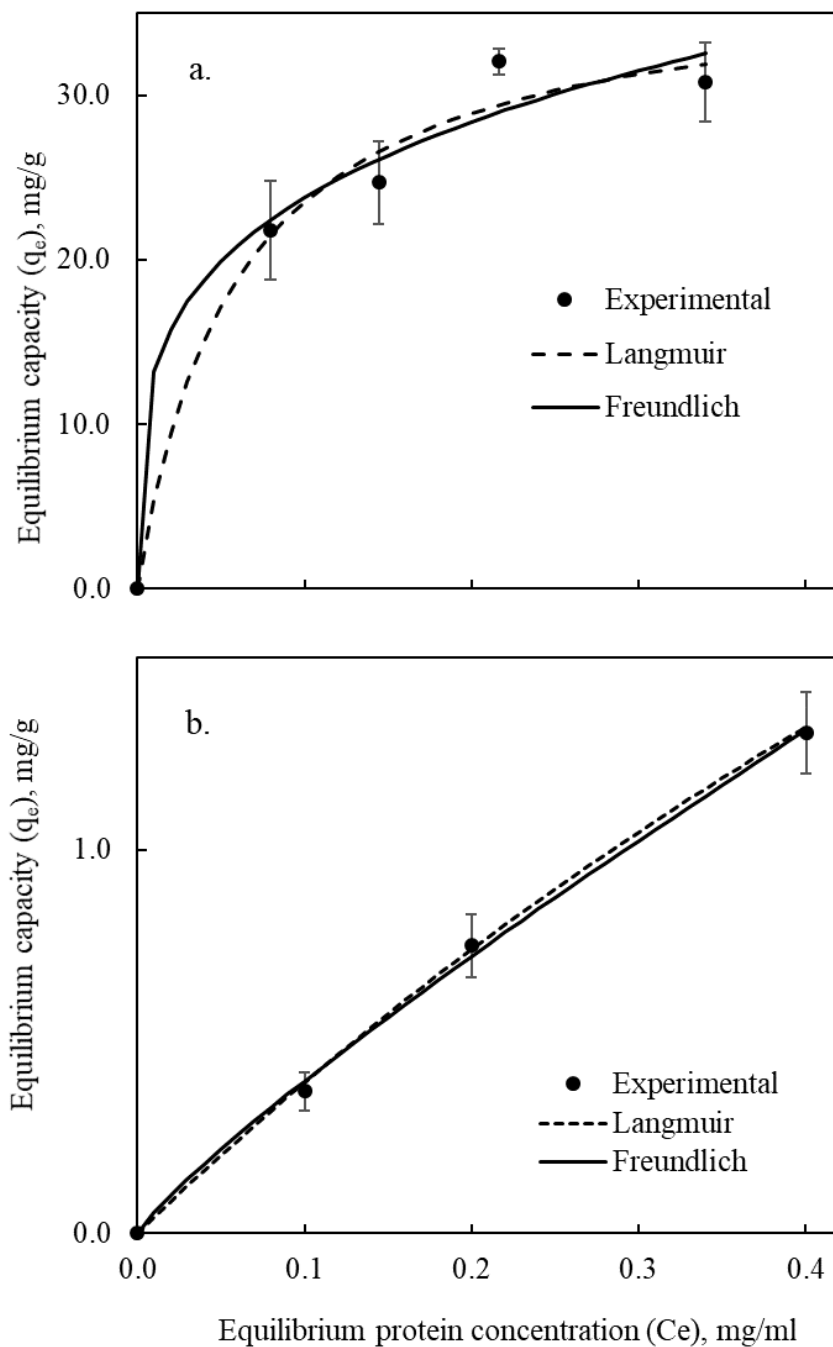
Figure 5: Langmuir and Freundlich Isotherms Fitting for the CGTase Adsorption at 25°C on (a) MIL-101 and (b) zeolite

Table 5: Adsorption Isotherm Parameters of CGTase on MIL-101 and Zeolite

Support	Langmuir model				Freundlich model			
	q_m (mg/g)	b (mL/mg)	R^2	χ_v^2	K_F (mg/g (mL/mg)^b)	n	R^2	χ_v^2
MIL-101	37.5	16.8	0.98	3.9	42.9	3.9	0.97	4.9
Zeolite Y	6.1	0.69	0.99	0.0003	2.89	1.16	0.99	0.0008

4.1.3 CGTase Adsorption Kinetics

Figures 6a and 6b show the adsorption kinetics of CGTase on MIL-101 and zeolite Y at 25°C, respectively. The amount of the adsorbed CGTase per gram of MIL-101 increased gradually from 0 to 28 mg/g with the increase in time up to 8 h. The gradual increment could be due to the high surface area offered by MIL-101. The CGTase uptake kinetics on zeolite showed an initial gradual uptake, followed by a sharp increase of up to 4 h and then by a less steep uptake as time increased. The initial lag in the uptake on zeolite could be a result of the bulkiness of CGTase, which needs time for adequate attachment to the zeolite surface. Once the attachment of CGTase occurred, the number of vacant sites decreased, resulting in a decrease in the uptake slope. This was not observed with MIL-101, indicating that it offers better attractive forces for CGTase molecules. This result was verified by conducting a zeta potential analysis on both surfaces. The zeta potentials of CGTase and the supports were measured at pH of 7.4. CGTase, MIL-101, and zeolite provided zeta potentials of −0.06, 0.53, and −0.47 mV, respectively. These results show that the surface of MIL-101 was positively charged at the operating condition. Hence, CGTase, which is negatively charged, showed more affinity toward MIL-101 because of the electrostatic attraction compared with the zeolite surface. Another possible reason can be the affinity of the carboxylic group on MIL-101 to the numerous amine groups found on the enzyme. Moreover, the adsorption rate of CGTase on MIL-101 was faster (up to 12 mg/g in 4 h) than that on zeolite (1.3 mg/g in 4 h) under the same conditions, which can be vital for CGTase stabilization during immobilization as enzymes might be inactivated if they remain in an unsuitable storage condition for a long time.

The pseudo-first-order, second order, Elovich and intraparticle diffusion models were used in fitting the results for the kinetics study, and the results are presented in Table 6. Using R^2 and χ_ν^2 for model discrimination, the pseudo-first-order model provided a better prediction for MIL-101 while Elovich model showed better performance for Zeolite-Y, especially at higher times, which is typical of multilayer adsorption, although, it does not allow for prediction at smaller time values due to the presence of a natural logarithmic function.
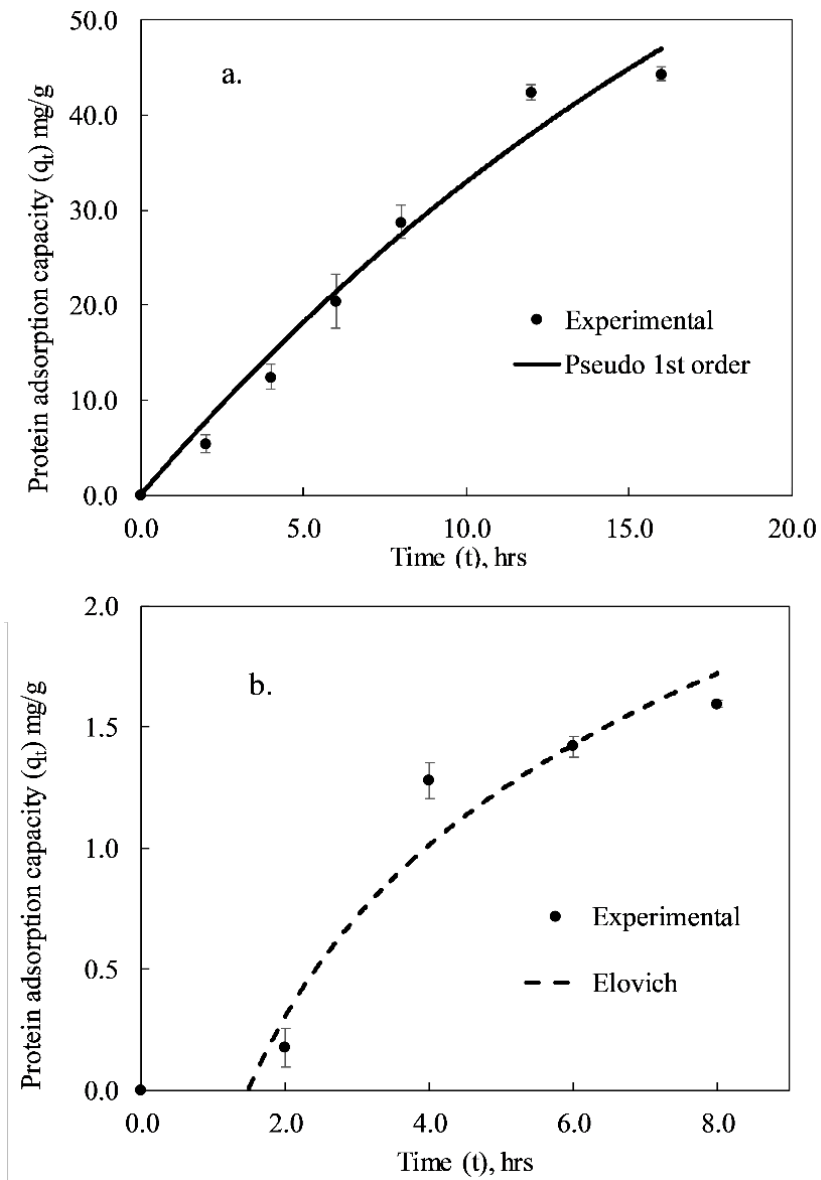
Figure 6: Adsorption Kinetics of CGTase at 25°C on (a) MIL-101 and (b) Zeolite-Y

Table 6: Adsorption Kinetic Parameters of CGTase on MIL-101 and Zeolite

Model/Support		MIL-101	Zeolite-Y
Pseudo 1st order	$q_e =$	95.72	3.19
	$k_1 =$	0.04	0.09
	$R^2 =$	0.97	0.90
	$\chi_v^2 =$	7.9	0.075
Pseudo 2nd order	$k_2 =$	1.34	0.0086
	$R^2 =$	0.97	0.90
	$\chi_v^2 =$	8.2	0.076
Elovich	$a =$	11.1	0.69
	$b =$	0.05	0.98
	$R^2 =$	0.96	0.94
	$\chi_v^2 =$	11.4	0.035
Intraparticle diffusion	$k_d =$	10.16	0.54
	$\theta =$	10.0	10.0
	$R^2 =$	0.97	0.82
	$\chi_v^2 =$	8.2	0.133

4.1.4 Secondary Structure Analysis

During immobilization, the forces involve in enzyme adsorption on surfaces are mostly due to the electrostatic attraction between charged amino acids on the enzyme and the surface of the support, which could lead to structural deformation or alteration of the arrangement of the polypeptide chain at the secondary structure level [143]. This structure can be identified using the amide bands on the FTIR spectra. Among the several amide bands, the amide I band (1600–1700 cm^{-1}), which originates from the C=O stretching vibration of the amide group, is widely used and accepted as a better predictor for the quantitation of protein secondary structures due to the correlation of its vibrational frequencies to secondary structure elements [144]. The peaks found at 1620–1641 cm^{-1} are generally assigned to β-sheets. This phenomenon can also occur below 1620 cm^{-1} in some proteins at 1600–1620 cm^{-1}, as in intermolecular β-sheets [145, 146]. The bands at 1648–1660 and 1665–1688 cm^{-1} are assigned to α-helices and β-turns, respectively [147].

The FTIR deconvolution of the amide I band in the free CGTase, CGTase@MIL-101, and CGTase@Zeolite-Y after baseline correction and the subtraction of the support FTIR spectrum from that of the immobilized enzyme is shown in Figure 7. The assignment

of the secondary structures, which were quantified using the corresponding areas as percentages of the total area in the amide I band, is shown in Table 7. The values show a maximum amide I vibration centered at 1626–1643 cm^{-1}, suggesting that CGTase had a signature of β-sheets before and after immobilization.
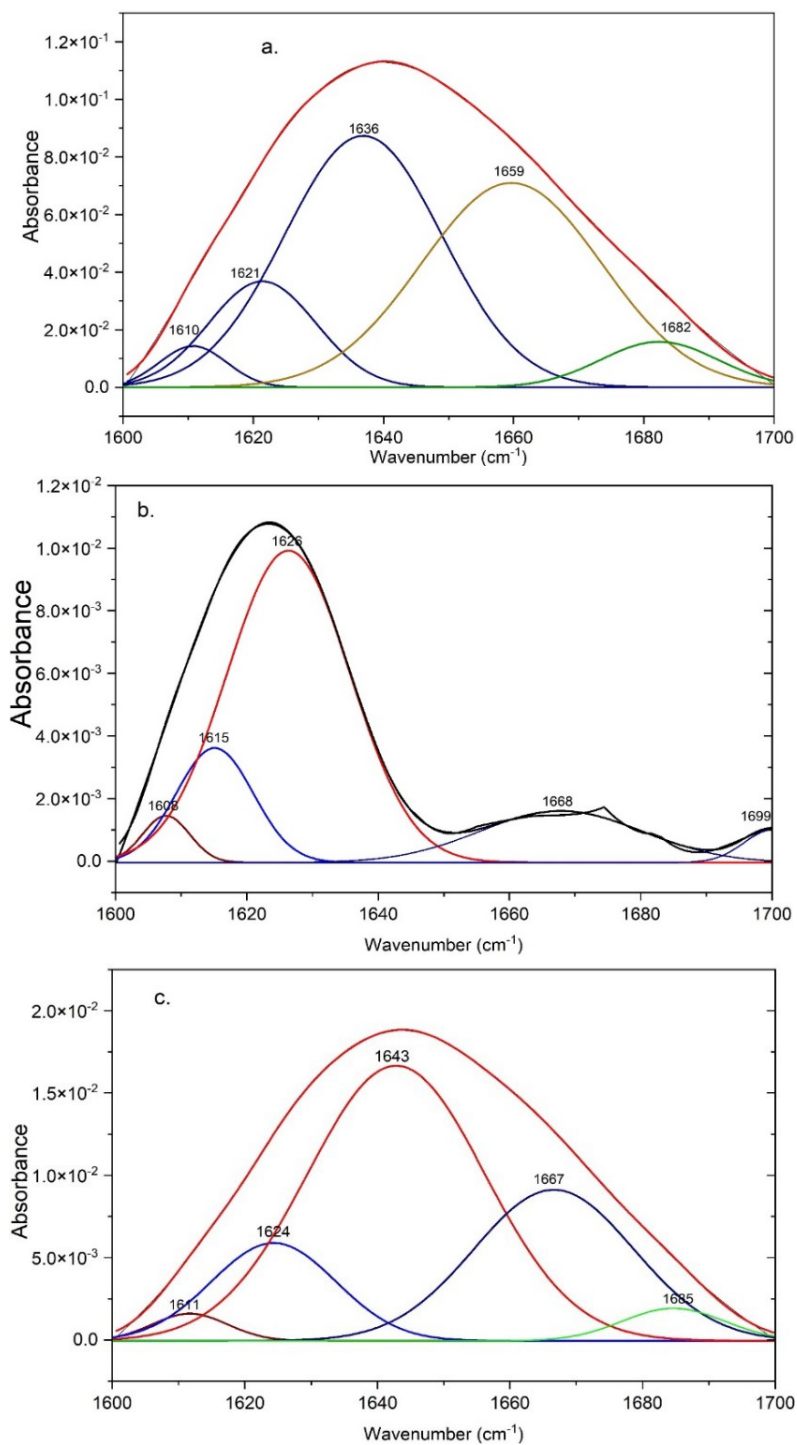
Figure 7: FTIR Deconvolution for the Secondary Structure Analysis of CGTase: (a) Free CGTase, (b) CGTase@MIL-101, and (c) CGTase@zeolite-Y

Table 7: Deconvolution of Amide I Band in FTIR Spectrum for Secondary Structure Analysis

	Wavenumber range[1] (cm^{-1})	Percentage (%)		
		Free CGTase	CGTase@MIL-101	CGTase@zeolite-Y
β-sheets	1620–1644	56.0	84.1	69.7
α-helix	1648–1660	38.5	-	-
β-turns	1660–1688	5.5	15.9	30.3

[1][144]

To determine the changes in the secondary structures in CGTase after immobilization on various supports, the peak deconvolution of the amide I band in the FTIR spectrum of the immobilized CGTase was conducted using the peak deconvolution app in Origin® 2021. The free CGTase predominantly contains β-sheets in phosphate buffer, which increased from 56% to 84.1% and 69.7% after immobilization on MIL-101 and zeolite, respectively. The increment in the observed β-sheets after immobilization suggests that CGTase tended to form aggregates on the surfaces of MIL-101 and zeolite, resulting in protein–protein interactions and in the increase in intermolecular β-sheet structures [148]. This finding is also strengthened by the SEM micrographs.

After immobilization, there was no observable peak for α-helix compared with the free CGTase, suggesting that there might have been an α-helix to β-sheet transition due to the interaction of nonspecific hydrogen bonds in the amino acid sequence of CGTase [149]. It could be observed that there was a decrease in the intensity of the amide I band for all immobilized CGTase when compared with the free CGTase, indicating that immobilization affected the secondary structure.

4.1.5 Kinetics of Enzymatic CD Production

To evaluate the performance of the free and immobilized CGTases, kinetic studies were conducted, with the displayed data being the mean values of triplicate experiments. Owing to the higher adsorption capacity of MIL-101 over that of zeolite Y, a reaction kinetics study was performed on CGTase@MIL-101, with the error bars providing evidence of the results' reproducibility. The initial analysis of the product showed a very minute quantity of γ-CD; hence, it was not considered in this study. Figure 8 shows the concentration–time profile of α-CD, which is the dominant product of the starch

conversion using free and immobilized CGTases at different substrate concentrations. To avoid congestion, only three concentrations were demonstrated, as shown in Figure 8. However, the experiment was conducted at smaller intervals of concentration changes. As time increased, the concentration of α-CD increased, reaching values of 6 and 3 g/L after 20 min for both free and immobilized CGTases, respectively, at a starch concentration of 10 g/L. The reduction in the CD production rate after 20 min might be attributed to the enzyme activity loss due to product inhibition. Because equivalent protein amounts were used for the free and immobilized CGTases, the lower production using the immobilized enzyme is attributed to the substrate diffusion limitation. The conformational changes in the CGTase secondary structure discussed in Section 4.1.4 could also contribute to the activity drop. A similar trend was also observed for β-CD (not shown here), but the amounts produced were smaller than those of α-CD. This observation agrees with that obtained for the CD production using Toruzyme [150], which showed that the buffer type can affect the ratio of CDs produced. Using phosphate buffer, as used in this study, α-CD production was slightly greater than that of β-CD.
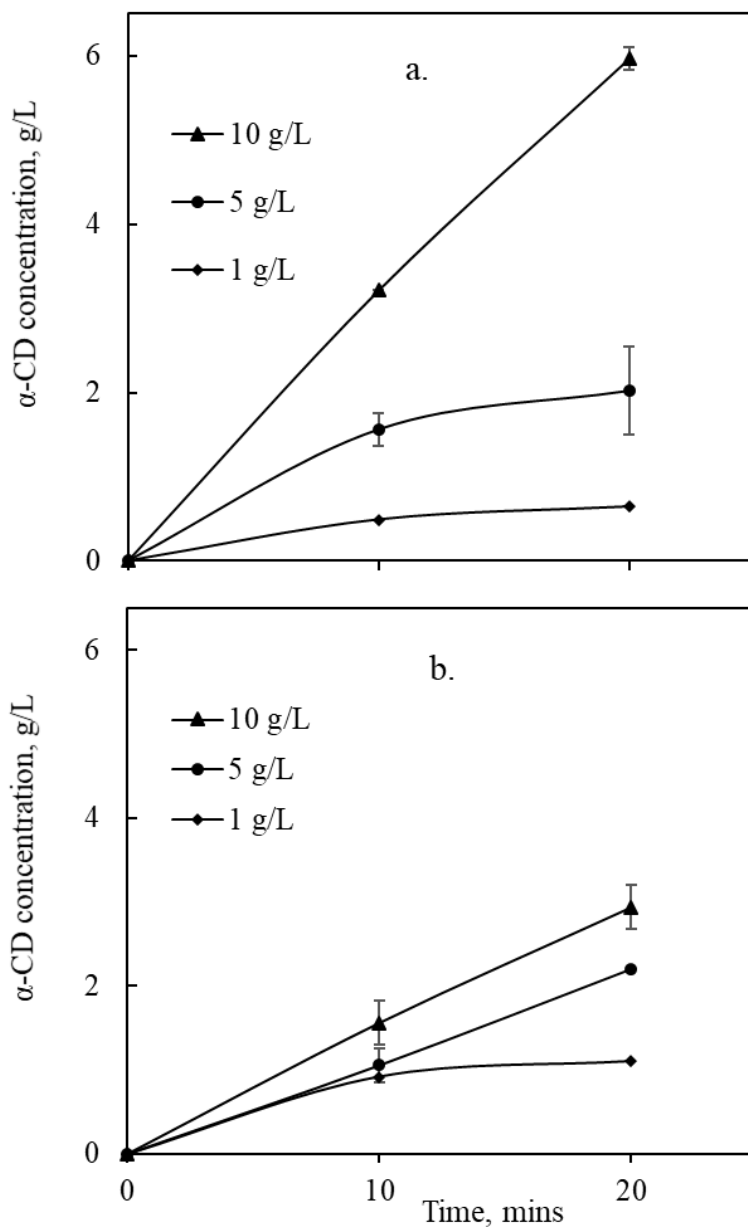
Figure 8: Time Effect on α-CD Production at Different Substrate Concentrations, pH 7.4, and 70°C for (a) Free CGTase and (b) CGTase@MIL-101

The initial reaction rate was determined for each substrate concentration based on the curves shown in Figure 9. This step was performed for all substrate concentrations and both α -CD and β -CD, and the results were demonstrated, as shown in Figure 9. The initial reaction rate gradually increased with the increase in the substrate concentration up to 10 gL^{-1}, with α -CD reaching a value of 0.31 gL^{-1}min^{-1}, which is significantly higher than the 0.17 gL^{-1}min^{-1} value observed for β -CD. The same trend was observed for the immobilized CGTase but with a reduced reaction rate. Substrate inhibition was not

observed in both graphs in the substrate concentration range used in this work, although it was reported at concentrations higher than 20 gL^{-1} [151], which were not considered in this work. As shown in the Figure, the production rates of both CDs using the free CGTase were higher than those obtained using the immobilized CGTase at the same protein amounts. As explained earlier, this phenomenon is largely attributed to the diffusion limitations encountered by the substrate when the enzyme was used in the immobilized form. It was also observed that the production rate of α-CD was higher than that of β-CD for both free and immobilized CGTases, as evidenced in the kinetic parameter obtained, using Michaelis Menten (MM) model in Table 8, with V_{max} being 0.64 and 0.42 gL^{-1}min^{-1} for α-CD and β-CD, respectively, using the free CGTase. As mentioned earlier, this result is due to the used pH, which favors the production of α-CD [150].
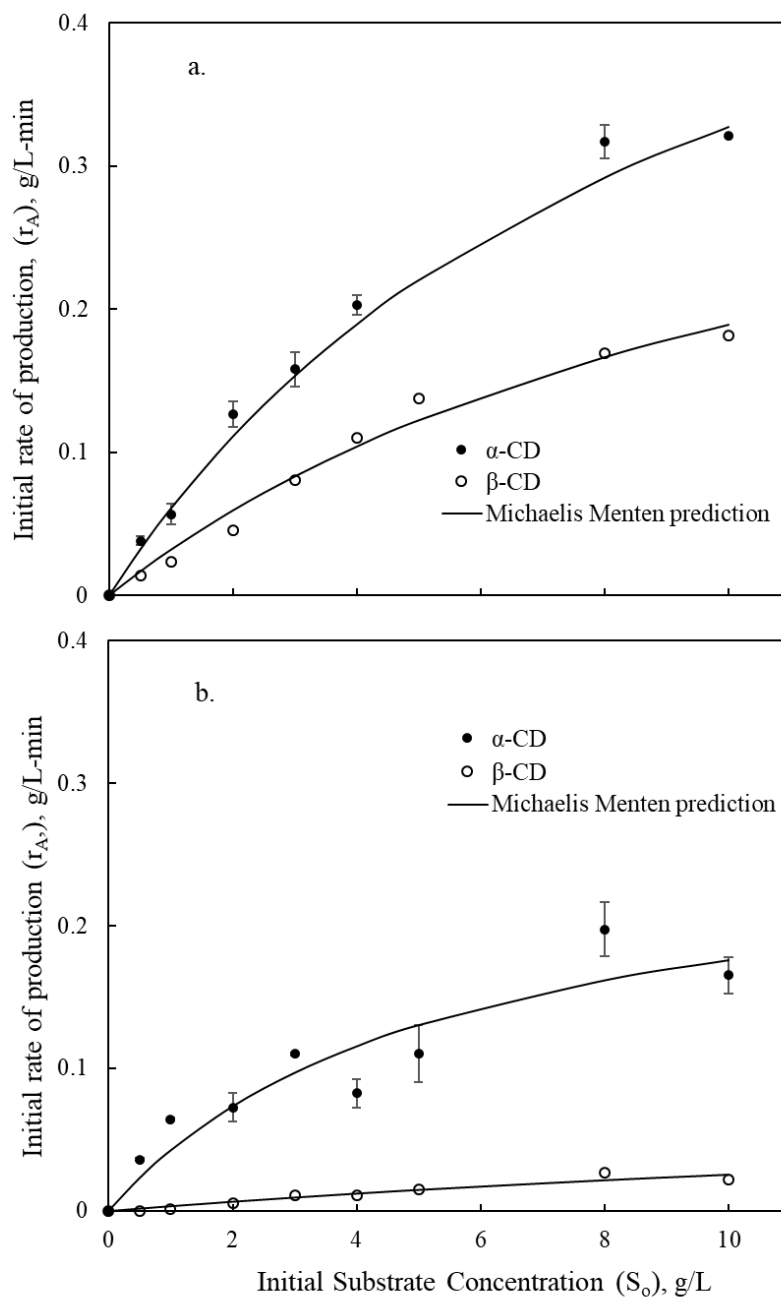
Figure 9: Initial Substrate Concentration Effect on the Initial Rates of α-CD and β-CD
Production at 70°C using (a) Free CGTase and (b) CGTase@MIL-101

Table 8: Michaelis–Menten Kinetics Parameters of CGTase for α-CD and β-CD

Parameter	α-CD	β-CD
V_{max} (g/L · min)	0.64	0.42
K_M (g/L)	9.44	12.00
R^2	0.97	0.98

Figure 10 shows the total yield of CD as the total amount of α-CD and β-CD produced over the initial substrate amount used using both free and immobilized CGTases. The CD yield was higher at a low substrate concentration of up to 2 gL^{-1}, reaching over 90% in 10 min. Then, it gradually decreased at higher concentrations. The drop in the observed yield as the substrate concentration increased should not be understood as substrate inhibition, which was not encountered within the substrate concentration used in this work, as shown in Figure 5. However, this drop was mainly because the produced total CDs did not linearly increase with the substrate concentration. Hence, the yield drop was observed at a higher substrate concentration as the yield was obtained by dividing the produced CD by the initial amount of the used substrate.
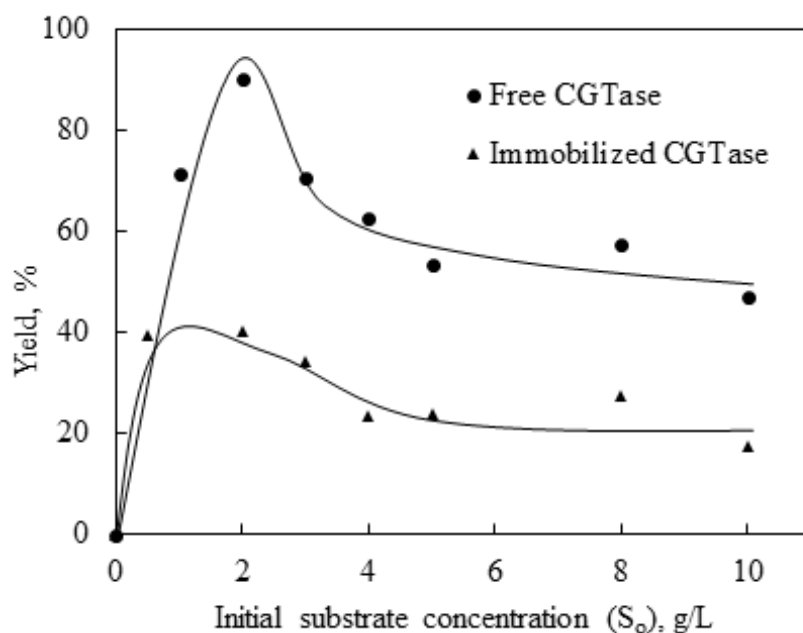
Figure 10: Effect of Initial Substrate Concentration on Total CD Yield after 10 min at pH 7.4 and 70°C

As mentioned earlier, α-CD is almost 10 times more expensive than β-CD [13, 16]. Therefore, the selectivity of α-CD over β-CD is an essential factor for the economic feasibility of the production process. Higher selectivity also simplifies the purification of the designed product. Figure 11 shows the selectivity of α-CD over β-CD using free and immobilized CGTases at various substrate concentrations. With the free enzyme, relatively higher selectivity was observed toward α -CD. Besides the effect of the used pH, the source of CGTase also had an influence on the type of the produced CD. Using the enzyme in the immobilized form, a much higher selectivity was obtained, especially at lower substrate concentrations, which is a very interesting finding as it adds an important advantage to using the enzyme in the immobilized form, besides the other advantages mentioned earlier. This higher selectivity is attributed to the diffusion limitations encountered with the immobilized enzyme, and as α -CD is a smaller molecule, it is expected to diffuse faster. At higher concentrations, the diffusion rate increased. Thus, a selectivity drop was observed. The conformational changes that CGTase underwent after immobilization could also play a part, suggesting that the increase in the β-sheets in the secondary structure of CGTase aided the production of α-CD, a less bulky product, compared with β-CD.
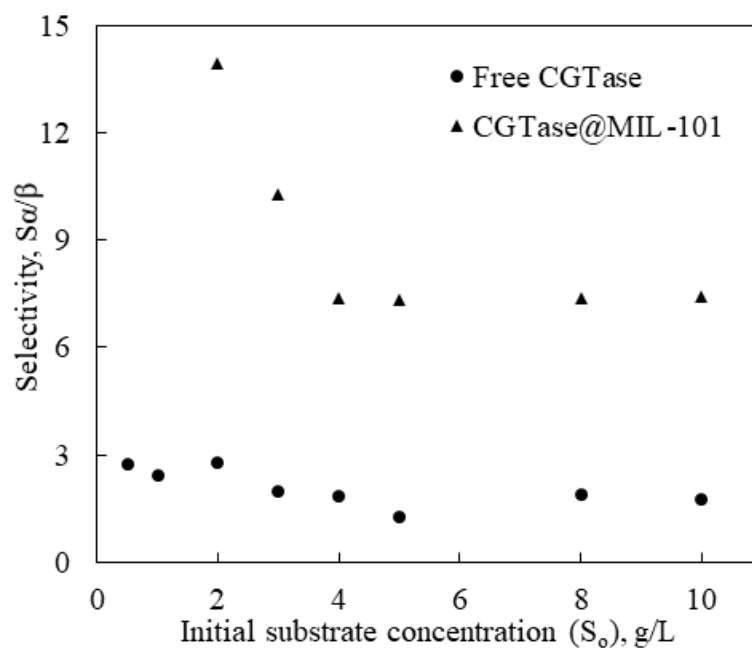
Figure 11: Selectivity of α-CD to β-CD using Free CGTase and Immobilized
CGTase@MIL-101 at Different Substrate Concentrations

4.1.6 Immobilized Enzyme Reusability

As mentioned earlier, one of the main advantages of using enzymes in the immobilized form is their easy separation from reaction mediums, allowing their repeated reuse. However, for this process to be effective, an immobilized enzyme has to maintain its activity. To evaluate the recovery of the immobilized CGTase from the reaction medium, the residual enzyme activity, defined as the activity of the enzyme in a cycle divided by its activity in the first cycle as determined. Figure 19 shows the residual activity after a number of repeated cycles for the immobilized MIL-101. The relative CGTase@MIL-101 activity values in the second cycle were 81% and 88% of the initial activity for α-CD and β-CD, respectively. The relative activity continued to drop from one cycle to the next, until reaching 29% and 14% for the two products, respectively. The reusability of CGTase on MIL-101 found in this work was lower than that reported by Suhaimi et. al [152] for the immobilization of the same enzyme on polyvinylidene difluoride (PVDF) hollow fiber membranes. However, it should be noted that the immobilization protocol was different from the surface attachment method used in this work.
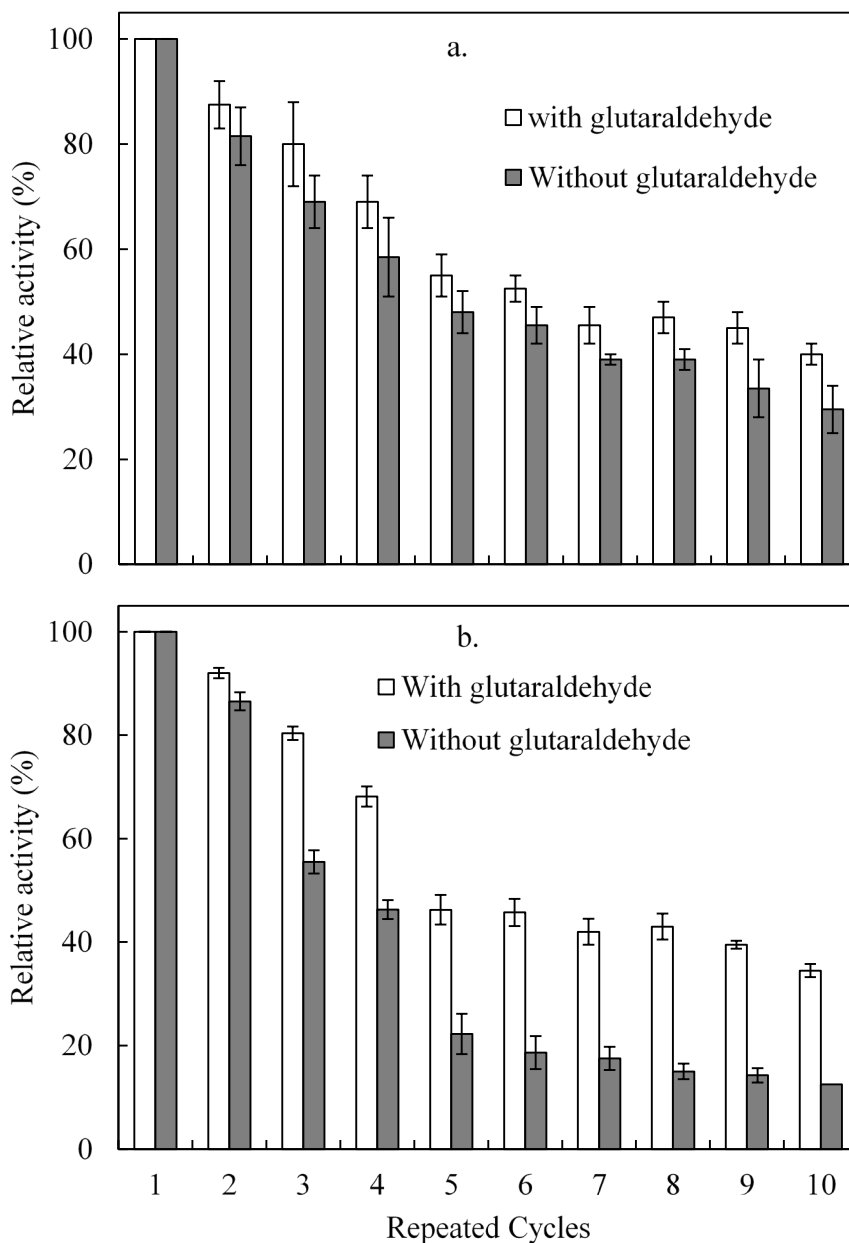
Figure 12: Reusability of the Immobilized CGTase on MIL-101 for the Production of (a) α-CD and (b) β-CD

This study, for the first time, demonstrated the possibility of utilizing MOFs in CGTase immobilization. The loss of CGTase activity observed after 10 cycles of usage could be attributed to the gradual detachment arising from the washing step conducted after each cycle. Therefore, the covalent attachment of CGTase onto MIL-101 was suggested to improve reusability. The attachment of CGTase to MIL-101 via covalent attachment was achieved using 1 mL of glutaraldehyde. The result showed an improvement over that obtained for surface attachment, as shown in Figure 9. However,

the stability of the immobilized enzyme was still not high, and more investigations can be performed to further improve its stability.

4.2 Immobilization of Cyclodextrin glycosyltransferase onto Three Dimensional-Hydrophobic and Two Dimensional- Hydrophilic Supports: A Comparative Study (Paper II)

In this work, CGTase from *Thermoanaerobacter sp.* was immobilized by adsorption on Graphene Nanoplatelets (GNP), as a 3D model and calcium-based 2D MOF, both with different surface properties. The effect of CGTase immobilization using different surfaces on the enzyme's secondary structures, uptake, specific activity and operational stability of CGTase were analyzed. To the best of our knowledge, this is the first study of its type on the use of 2-D support, in comparison to 3D materials used by previous studies. The results obtained in this study will open the door to further works on enzymatic production of CDs using a more efficient bio-catalyst.

4.2.1 Summary of Main Findings

Cyclodextrin glycosyltransferase (CGTase) degrades starch into cyclodextrin via enzymatic activity. In this study, CGTase from *Thermoanaerobacter* sp. was immobilized on two supports, namely Graphene Nanoplatelets (GNP) consisting of short stacks of graphene nanoparticles and a calcium-based two-dimensional metal organic framework (Ca-TMA). The uptakes of CGTase on GNP and Ca-TMA reached 40 and 21 mg/g respectively, but immobilized CGTase on Ca-TMA showed a higher specific activity (38 U/mg) than that on GNP (28 U/mg). Analysis of secondary structures of CGTase, shows that immobilization reduces the proportion of β-sheets in CGTase from 56% in the free to 49% and 51.3% for GNP and Ca-TMA respectively, α-helix from 38.5% to 18.1 and 37.5%, but led to increased β-turns from 5.5 to 40% and 11.2% for GNP and Ca-TMA, respectively. Lower levels of conformational changes were observed over the more hydrophilic Ca-TMA compared to hydrophobic GNP, resulting in its better activity. Increased β-turns were found to correlate with lower β-CD production, while more β-sheets and α-helix favored more β-CD. Reusability studies revealed that GNP retains up to 74% of initial CGTase activity, while Ca-TMA dropped to 33% after eight consecutive uses. The results obtained in this work provide insight on the effect of support's surface properties on CGTase performance and can assist in developing robust CGTase-based

50

biocatalysts for industrial application.

4.2.2 Secondary Structure Analysis

For an in-depth examination of the effect of immobilization on protein structure, FTIR was employed to study possible conformational alterations in the secondary structures of CGTase resulting from immobilization. The amide I region (1600–1700 cm^{-1}) was subjected to peak deconvolution to reveal the numerous overlapping peaks (Figure 13) as it provides information on the changes caused by immobilization to CGTase secondary structures, and the results are shown in Table 9. The stretching vibrations of carbonyl groups (C=O) in proteins are responsible for the amide I, and each deconvoluted peak stores data about α-helix, β-sheets, and β-turns [153-156].
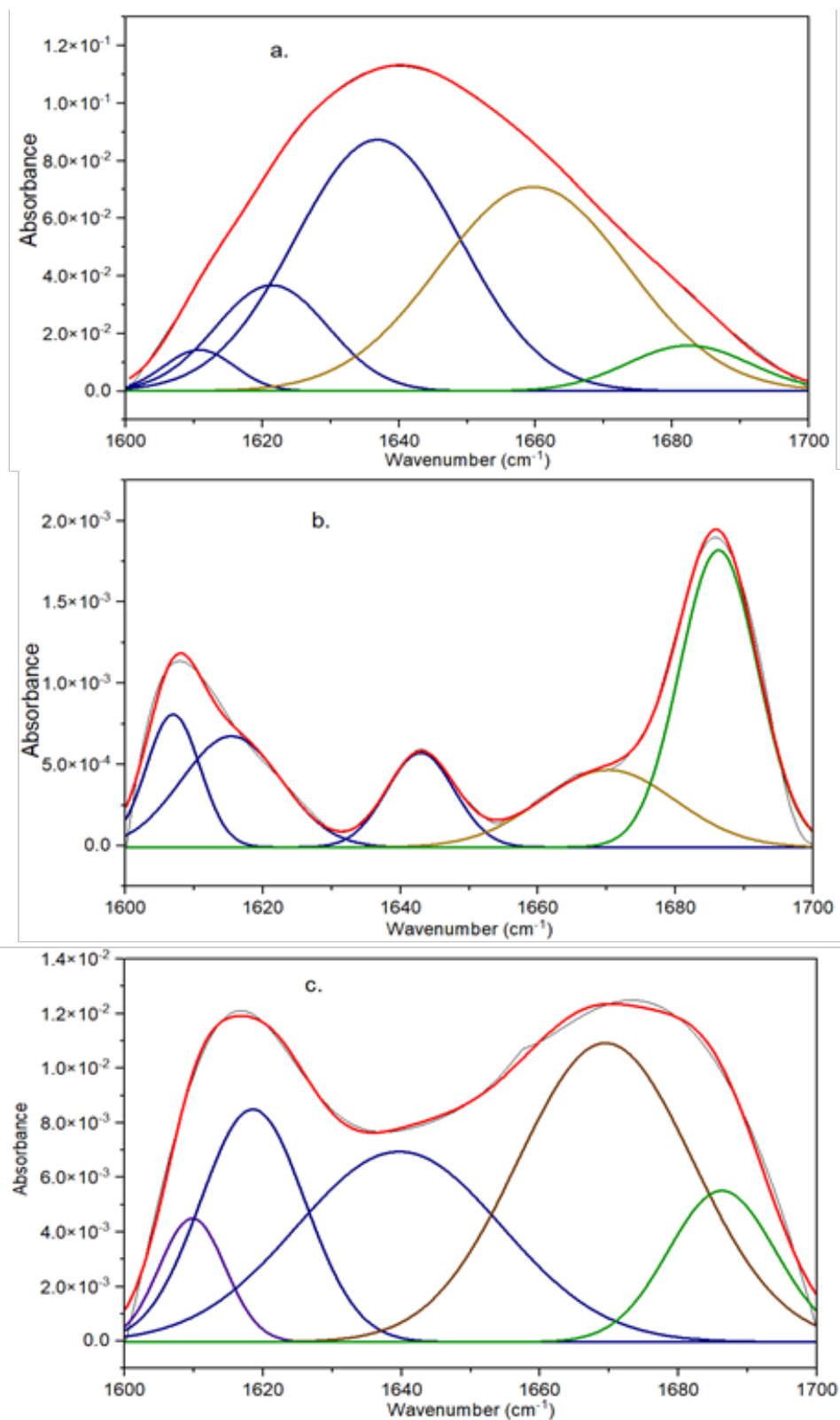
Figure 13: Deconvoluted FTIR Spectra for CGTase (a) Free and Immobilized on (b) GNP and (c) Ca-TMA

Table 9: Results of Peak Deconvolution of Amide I Band

	Percentage (%)		
	β-sheets	α-helix	β-turns
CGTase	56.0	38.5	5.5
CGTase@graphene	41.9	18.1	40.0
CGTase@Ca-TMA	51.3	37.5	11.2

After deconvolution, free CGTase (Figure 13a) showed five peaks assigned to β-sheets (1610, 1621, 1636 cm^{-1}, indicated in dark blue), α-helix (1659 cm^{-1}, in brown) and β-turns (1682 cm^{-1}, in green) with each of the secondary structure accounting for 56, 38.5, and 5.5% respectively. Thus, β-sheets and the α-helix are the major structural components of CGTase. β-turns are found at locations of directional change on a polypeptide chain and make up around one-fourth of the residues in proteins, forming the smallest secondary structure. Nevertheless, these turns could have a significant effect on enzyme stability [157-159].

The amide I spectrum of immobilized CGTase on GNP is shown in Figure 13b. Deconvolution reveals five peaks, similar to free CGTase at 1610, 1621, 1643, 1663, and 1685 cm^{-1}, with a reduction in the β-sheets (41.9%) and α-helix (18.1%), but enhanced β-turns (40.0%). Ca-TMA (Figure 13c) also showed a similar trend to that of GNP, with peaks at 1610, 1618, 1640, 1669, and 1686 cm^{-1} and β-sheets, α-helix and β-turns contents of 51.3, 37.5, and 11.2%, respectively. Changes in β-sheets and the α-helix are usually attributed to the distortion of hydrogen bonds present in an enzyme [158], and in this case, it appeared that GNP showed more loss of both β-sheets and α-helix structures and a higher increment in β-turns, compared to Ca-TMA.

The two key factors that affect the enzymes' secondary structures during adsorption are the operating conditions (such as temperature, pH, surface polarity [i.e., hydrophilic or hydrophobic], and others) and the amino acid sequence [160]. Apart from the surface polarity of the supports, all other factors were the same. As shown in Table 12, GNP, which is the support with higher hydrophobicity, displayed larger changes in the CGTase secondary structure, compared to Ca-TMA, which is more hydrophilic. This was expected, as hydrophobic surfaces usually cause loss of the protein ordered structure [160]. Thus, secondary structure of CGTase could be preserved by using a hydrophilic support.

4.2.3 CGTase Immobilization

The CGTase used in this study is very stable at the immobilization conditions up to 24 h, maintaining good stability up to 36 h, other authors have also reported similar findings about Toruzyme's (the source of CGTase used in this work) stability during use for over 24 h. It was reported that the activity of the CGTase used was unaffected after 24 h even up to 70°C [51, 161]. The specific activity of the free CGTase used was 167 U/mg protein, and upon immobilization on GNP and Ca-TMA, the specific activity was 28 and 38 U/mg protein, resulting in activity yields of 16.8 and 22.8% for the two supports respectively. Ca-TMA displayed better residual activity when used as the support, due to lesser loss of protein ordered structure as discussed in Section 4.2.2. These results also confirms that immobilization affects the activity of CGTase as already reported [162].

Figure 14 shows the equilibrium relationship between CGTase concentration and the quantity of CGTase adsorbed per gram of GNP and Ca-TMA. To confirm the reproducibility of the results, the analysis was performed in triplicate, and the presented results denote the average values. The uptake on GNP increased to around 40 mg/g, whereas on Ca-TMA, it increased to about 21.1 mg/g at CGTase concentration of 0.12 mg/mL, before showing a form of curvature. As shown in Figure 28, GNP offered better adsorption for CGTase than Ca-TMA owing to better hydrophobic interactions, as Ca-TMA contains more hydrophilic functional groups, as confirmed by the hydrophobicity measurement [163]. This is similar to the result obtained for bovine serum albumin (BSA) adsorption on supports with different hydrophobicities. It was shown that increase in surface hydrophobicity led to higher adsorbed protein [160, 164] due to a decreased effect of competitive interactions with water molecules [165].
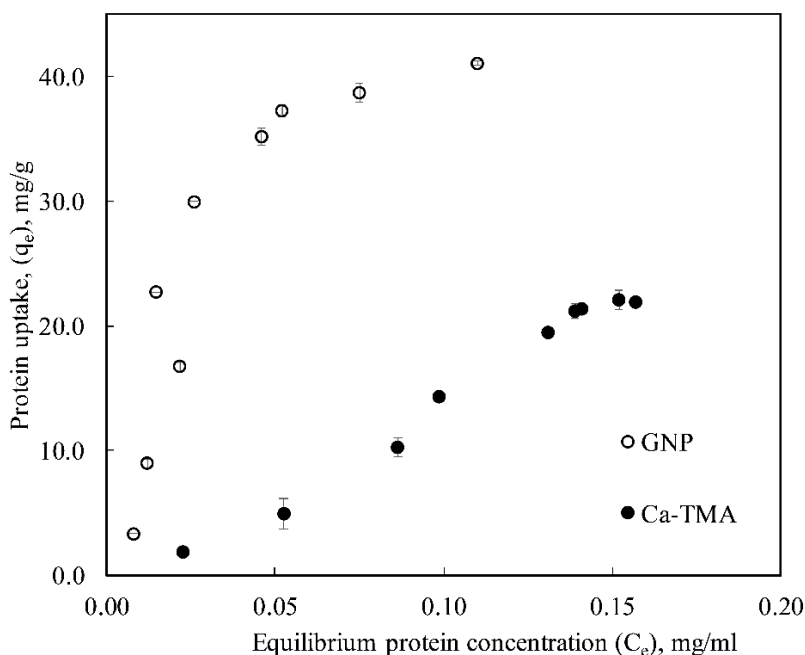
Figure 14: Equilibrium Relationship between CGTase Uptake vs. Concentration at 25ºC

Although, GNP had better uptake of CGTase, its lower residual activity compared to Ca-TMA could be attributed to the larger changes in secondary structures, as discussed in Section 4.2.2. Also, it is possible that some of the CGTase could be attached within the stacks of graphene layer or its micropores, thus, reducing the active sites available for starch degradation.

Another interesting finding is the steeper slope at lower protein concentration for GNP compared to Ca-TMA, which can be attributed to CGTase binding to the GNP surface, as well as diffusing into the short stacks of graphene sheets found in the used GNP. The amount of CGTase adsorbed in this study was higher than most reported values in the literature. For example, using Eupergit C as the support, 8.1 mg/g was reported using covalent binding of CGTase [51]. Lower capacities of 4.1 and 0.73 mg/g were reported using activated silica X030 [142] and controlled pore silica [166]. In contrast, a higher capacity of 42 mg/g was reported using a melamine–polyethylene glycol composite [141].

4.2.4 Enzymatic Production of CDs

The kinetic test results, carried out to assess the performance of CGTases@GNP on CDs production, are shown in Figure 15. Similar graphs were obtained for free CGTase

and CGTase@Ca-TMA. Only α-CD and β-CD were considered, as minute amount of γ-CD was detected after the reaction, similar to a previous report [150]. No CD was detected in the blank runs using the empty GNP and Ca-TMA, which confirms that the activity was solely owing to the attached enzyme. With time, the amount of CD produced increased up to 10 mins before reaching a plateau. The highest concentration using free CGTase for α-CD and β-CD were 2.3 and 1.5 gL^{-1} respectively after 30 mins, (α: β ratio of 1.5:1), corresponding to yield of 76% using a starch solution of 5 gL^{-1}. For CGTase@GNP, the concentrations of α-CD and β-CD were 1.9 and 0.2 gL^{-1} (α: β ratio of 9.5:1), respectively, which corresponds to 42% yield with total CDs productivity of 18.1 $mg.min^{-1}$ per gram of support. Additionally, for CGTase@Ca-TMA, α-CD and β-CD concentrations were 1.7 and 0.6 gL^{-1} (α: β ratio of 2.8:1), respectively, corresponding to a yield of 46%, with total CDs productivity of 18.0 $mg.min^{-1}$ per gram of support. Because the same amount of attached enzyme was used in the experiment, the amount of Ca-TMA used was higher than that of GNP, due to its lower capacity. However, the higher yield obtained using the CGTase@Ca-TMA therefore resulted in a similar total CDs productivity per gram of support.
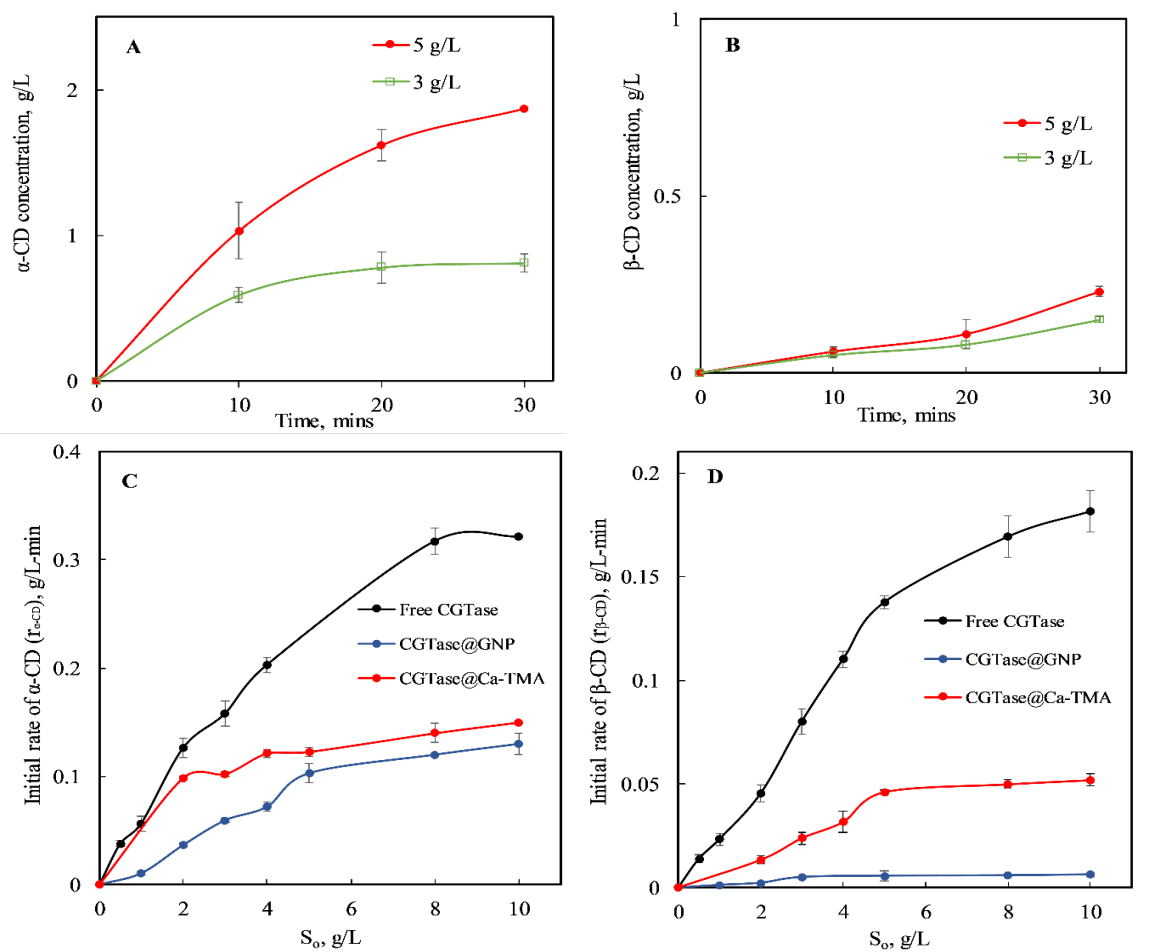
Figure 15: CD Production at Various Substrate Concentration using CGTase@GNP for (A) α-CD (B) β-CD, Reaction Rate with Respect to Substrate Concentration using Free and Immobilized CGTase for (C) α-CD, (D) β-CD, at 70ºC, pH 7.4

The changes in the initial rate of CDs production with respect to starch concentration are shown in Figures 15C, 15D and Figure 16, obtained from the slope at time zero of concentration vs. time graphs of the free and immobilized CGTase at different starch concentrations (1– 10 gL^{-1}). As the substrate concentration increases, there is a gradual rise in the initial CDs production rate. The increase in the CDs production rate as the starch concentration increases could be attributed to the increase in amylopectin availability, a highly branched structure with more α-1,4-glycosidic bonds, which are cleaved by CGTase to form CDs [167]. The effect of increasing starch concentration is reduced at higher concentrations, when the active site on CGTase becomes saturated with the starch molecules [168]. The total CDs production rate using CGTase@Ca-TMA was higher than that of CGTase@GNP, which could be due to the combined effect of enzyme

clustering that might be present on GNP (high protein uptake), thus, negatively affecting its activity and planar 2-D shape of Ca-TMA compared to GNP, leading to less diffusional limitations and easier access of substrate molecules on CGTase@Ca-TMA [169]. These results support the hypothesis that 2-D structures would be more favorable supports for this type of reaction provided it possesses high external surface area. The difference in the enzyme conformational changes on the two supports could likewise have an effect. Relating the observed trend in CD production to the secondary structures analyzed in Section 4.2.2, the higher number of β-turns observed for CGTase@GNP therefore suggests less activity towards β-CD production.
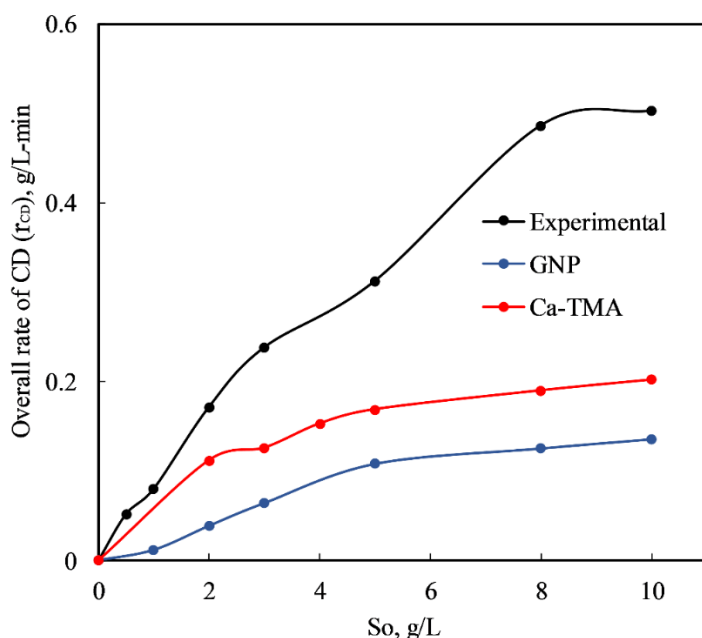
Figure 16: Overall Initial CD Production Rate for Various Substrate Concentration at 70ºC, pH 7.4

Comparing the results in the current work to those reported in literature using CGTase immobilized on other supports, for example, using covalently immobilized CGTase (from *Thermoanaerobacter* sp.) on both amine- and thiol-functionalized silica (Si-NH and Si-SH), protein uptake of 9.7 and 8.5 mg/g was achieved respectively, leading to starch conversion of 14% and 22% at 60ºC after 200 h of reaction in a continuous packed bed reactor, using 4% (w/v) soluble starch solution as substrate. The total CDs productivities per gram of support were 1.22 mg.min^{-1} for Si-SH (α:β:γ ratio 1.4:1.5:1) and 1.56 mg.min^{-1} for Si-NH (α:β:γ ratio 3.3:3:1) [170]. The lower productivity using

immobilized CGTase on 3-D structures is mainly attributed to the mass transfer limitations. In 2-D structures, these limitations are limited to only external mass transfer from the substrate bulk solution to the surface of the support. In contrast, in 3-D structures, additional internal diffusion limitations, that are significantly higher, become more significant. Also, in order to facilitate unrestrained access to the active site on immobilized CGTase, covalent attachment via inclusion of 3-aminopropyltrimethoxysilane (APTMS) as a spacer arm was studied, which led to an activity recovery of 73% [Matte, 2012]. In another study, CDs yield of 40% CD was achieved after 1.2 h retention time, using CGTase from *B. macerans* immobilized on Amberite IRA 900 with 10% (w/w) partially cyclized starch at 50°C [171]. Furthermore, improved yield of CDs (43%) was obtained after 3 h with an α:β:γ mass ratio of 1.5:2:1 at enzyme loading of 5.0 U/g starch, using post-modified CGTase to form crosslinked enzyme aggregates (CLEAs) [63]. Despite achieving a relatively similar yield to the one reported in this study, the time needed to achieve this yield was longer, resulting in a lower productivity of 0.12 and 1.4 mgmin^{-1} per gram of support, using CGTase@Amberite IRA and CLEAs, respectively [63, 171]. These comparisons show that the use of Ca-TMA could provide better support for CGTase in CDs production.

A significant factor that must be considered for the feasible application of immobilized enzymes at the industrial scale is their reusability. This property refers to how rapidly an immobilized enzyme loses its activity with multiple recycling uses. Immobilized CGTase on GNP and Ca-TMA were examined up to eight successive cycles, and the residual activity, relative to the activity of the first cycle, is shown in Figure 17. After eight cycles, CGTase@GNP retained 74% of its activity, while Ca-TMA retained only 33%. The drop in the activity of the immobilized CGTase can be attributed to detachment of CGTase from the support surface during washing. Ca-TMA showed a lower retained activity compared to GNP, which suggests that a higher leaching of the enzyme occurred. This is attributed to its higher hydrophilicity, as it has been reported that enzymes adsorbed on hydrophilic surfaces are easier to remove, as compared to hydrophobic surfaces [164]. This could be further confirmed by studying the adsorption isotherms at different temperature, which yields information of the type of the attachment. The stability of GNP was higher than that reported using melanine epoxy sponge as

support, which dropped to 54% after 10 cycles [141]. Other supports tested resulted in even lower stability; for example, 19.1% retained activity was observed after nine cycles using polydopamine coated Fe_3O_4 [15], and 7.19 and 3.89% retained activity was reported after only five cycles, using controlled pore silica with surface anchoring and covalent bonding, respectively [166]. A higher stability of 91.9% retained activity after 20 cycles was reported using gelatin as support for CGTase obtained from *Bacillus circulans* [162]. Notably, however, the highest total CDs yield, obtained after 36 h reaction time, was smaller (8.7%), compared to the present work. Also, CGTase covalently attached on silica microspheres gave a residual activity of 60% after 15 reuse cycles, but data on total CD produced is not available for effective comparison. The reusability studies showed that GNP could also serve as a good support for CGTase immobilization, but more studies are needed in order to minimize significant conformational changes observed using it.
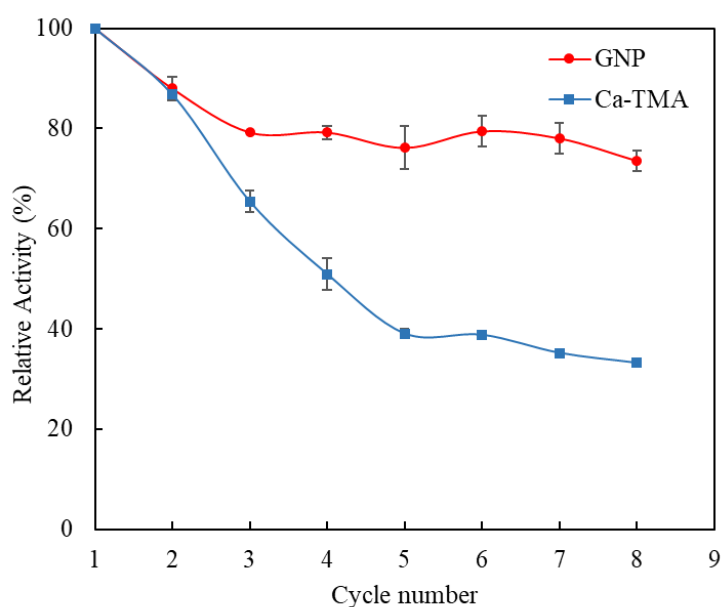
Figure 17: Reusability test for immobilized CGTase on different supports

4.3 Enhanced Performance of Cyclodextrin glycosyltransferase by Immobilization on Amine-Induced Macroporous Metal Organic Framework (Paper III)

In this study, a hierarchical copper-based MOF was synthesized by employing an organic amine to support CGTase immobilization and utilizing the immobilized enzyme in the conversion of corn flour waste without the need for pretreatment. The presence of mesopores and macropores within the MOF framework is expected to enhance enzyme

loading, stability, and accessibility. The outcome of this study could drastically minimize the diffusional limitations previously encountered during starch degradation to CD using immobilized CGTase and open up economic benefits that can be derived from waste products.

4.3.1 Summary of Main Findings

This study examined the effectiveness of a hierarchical copper-based metal–organic framework (H-Cu-BTC) in comparison with its microporous counterpart (Cu-BTC) for the immobilization of cyclodextrin glycosyltransferase (CGTase) for use in cyclodextrin production. The adsorption capacity, conformational changes, and operational stability of the immobilized enzymes were examined. The presence of both macropores and micropores in the proposed H-Cu-BTC resulted in an enhanced maximum adsorption capacity of 49.5 mg/g for CGTase as compared to 30.6 mg/g for Cu-BTC, which contains only micropores. The presence of macropores in H-Cu-BTC was also shown to more favorably affect the secondary structure of the immobilized enzyme. Using H-Cu-BTC, the proportion of β-sheets, which form the major structure in the protein and are responsible for the enzyme's stability, was shown to increase from 56% in free CGTase to 76.1% after immobilization. However, when using the microporous Cu-BTC, the proportion of β-sheets decreased to 44.1%. The favorable surface attachment of CGTase to H-Cu-BTC reflected its better reusability, wherein the activity was preserved up to 87% of the original CGTase activity after ten repeated cycles of reuse, compared to only 70% using Cu-BTC. The successful immobilization of CGTase on H-Cu-BTC demonstrated that it could be used as a robust biocatalyst for the conversion of starchy waste into cyclodextrins.

4.3.2 Characterization

Figure 18A shows the XRD patterns of the MOF samples compared with the simulated patterns. The diffraction peaks of the synthesized samples are located at $2\theta = 6.8°, 9.6°, 11.7°, 13.5°,$ and $16.6°$, corresponding to (200), (220), (222), (400), and (333) crystal planes, respectively, which are typical for the Cu-BTC cubic crystal structure [172]. They also agreed well with those of the simulated patterns obtained from the Crystallography Open Database CIF file 2300380 [173], indicating that the samples were

well-crystalized Cu-BTC MOFs. MOF formation under ambient conditions is aided by organic amines via deprotonation of the organic ligands [128]. Both Cu-BTC and H-Cu-BTC exhibited identical patterns, indicating that the prepared MOFs had similar frameworks.

The FTIR spectra of Cu-BTC and H-Cu-BTC are shown in Figure 18B. The Cu-BTC spectrum agreed well with that of H-Cu-BTC, and both matched the reported patterns in the literature [108, 174]. Key peaks were observed at 1443 and 1378 cm^{-1}, belonging to the symmetric vibrations of the carboxylate group, 1638 and 1569 cm^{-1}, owing to asymmetric stretching vibrations, and 1715 cm^{-1}, due to the presence of at least one partially deprotonated carboxylic acid group on the trimesic acid [175]. The peak at 1715 cm^{-1} for H-Cu-BTC was less intense than that for Cu-BTC because of better deprotonation of the carboxylic group. Figure 18B shows the FTIR spectra of both supports containing the immobilized enzyme. After enzyme immobilization, the peak within the amide I region (1600–1690 cm^{-1}) for the supports became more intense, confirming the presence of CGTase.

The pore size distributions and surface areas of the studied supports, Cu-BTC and H-Cu-BTC, were determined using N_2 adsorption–desorption isotherms, displayed in Figure 18C and 18D. The Cu-BTC curve shows a typical Type I isotherm with an H1 hysteresis loop, which is typical of microporous structures. However, H-Cu-BTC exhibited a Type IV isotherm, with strong uptake at low relative pressures ($P/P_o < 0.02$) and hysteresis loops at high relative pressures ($P/P_o > 0.45$), indicating the presence of mesopores [176]. Indeed, Figure 1D shows that H-Cu-BTC had mesopores (pore sizes of 2–50 nm) and macropores (pore sizes > 50 nm), which were not present in Cu-BTC, in addition to inherent micropores. This gave rise to the observed higher surface area of H-Cu-BTC compared to Cu-BTC, as shown in Table 10. These findings confirmed that the

organic amine used as a template introduced a hierarchical porous structure within the Cu-BTC framework.
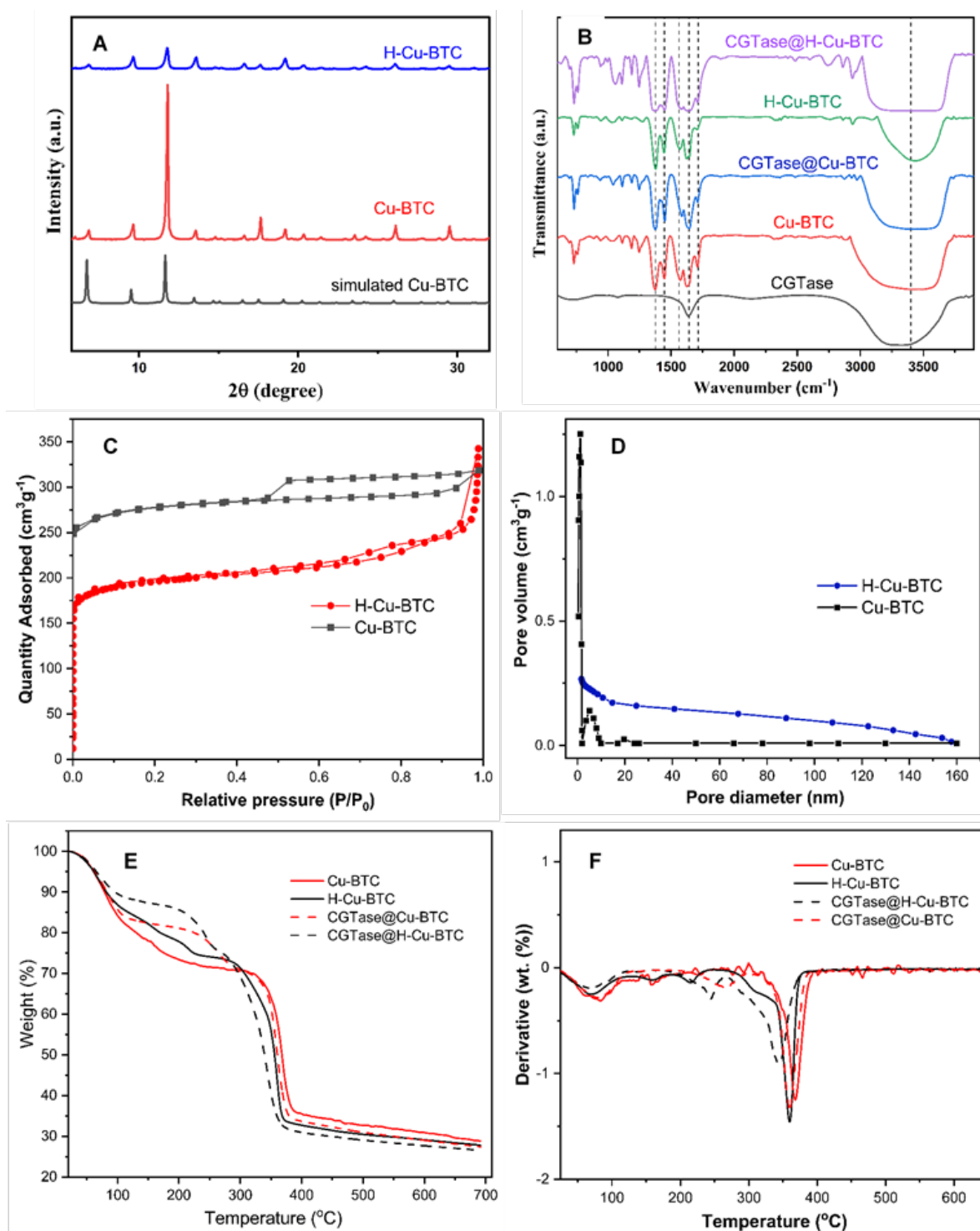

Figure 18: Characterization Results of the Supports. (A) XRD, (B) FTIR, (C) N_2 Adsorption–Desorption Isotherm, (D) Pore Size Distribution, (E) TGA, and (F) DTG curve

Table 10: N_2 Adsorption–Desorption Measurements for Samples

Sample	BET surface area (m^2/g)	Pore volume (cm^3/g)	Average pore width[a] (nm)
Cu-BTC	58.0	0.17	1.2
H-Cu-BTC	622.7	0.67	10.8

[a]Average pore width calculated from the adsorption branch of the N_2 isotherm with P/P^o = 0.99.

The TGA and derivative temperature gradient (DTG) curves of the Cu-BTC and H-Cu-BTC supports with and without enzyme immobilization are shown in Figure 18E and 18F, respectively. Three regions of weight loss can be observed for the empty and CGTase immobilized supports between 30–100°C, 100–200°C, and 200–360°C. The weight loss for each support is presented in Table 11. The first region could be attributed to the loss of water from the support surface, the second was due to the loss of trapped solvent molecules, such as water, methanol, or amine, and the third was related to the breakdown of the Cu-BTC structures [128]. The temperatures at which the structures of the Cu-BTC and H-Cu-BTC crystals collapsed were very similar (Figure 18F), indicating that the introduction of hierarchical pores did not affect their thermal stability. The difference in organic weight loss between each empty sample and its immobilized counterpart was used to calculate the amount of CGTase present within the sample. H-Cu-BTC had over three times the amount of CGTase on microporous Cu-BTC, which can be attributed to its higher surface area.

Table 11: Weight Loss Analysis and Estimate of Organic Content

Sample	Weight loss (%)		Total organic mass lost (g/g sample)[1]	CGTase amount/g of sample
	<200°C	200–360°C		
Cu-BTC	29.8	33.9	3.5	-
CGTase@Cu-BTC	28.6	33.7	3.8	4.2 μmol CGTase
H-Cu-BTC	27.5	38.7	3.3	-
CGTase@H-Cu-BTC	14	55.7	4.3	14.2 μmol CGTase

[1] Determined from the TGA result from 200–360°C

4.3.3 CGTase Immobilization

CGTase immobilization was conducted for up to 24 h to attain equilibrium, as the enzyme maintained good stability [177]. The specific activity of the free CGTase was 167 U/mg of protein. Upon immobilization on Cu-BTC and H-Cu-BTC, the residual activity

dropped to 65.2 and 98.5 U/mg protein, respectively. This decrease was mainly due to additional diffusional limitations inevitably encountered by the immobilized enzyme. The enzyme immobilized on H-Cu-BTC showed greater residual activity, mainly because of its larger pore size, which resulted in reduced diffusional resistance. The lesser conformational changes experienced by CGTase upon immobilization on H-Cu-BTC compared to microporous Cu-BTC could also contribute to the larger residual activity on the former support.

The results of CGTase adsorption on Cu-BTC and H-Cu-BTC are displayed in Figure 19. Within the tested experimental range, as the CGTase concentration increased, the equilibrium capacities of the supports increased to 25 and 37.3 mg/g for Cu-BTC and H-Cu-BTC, respectively. The data were fitted to the Langmuir and Freundlich models to determine the best fit, as shown in Figure 19, and the results of the fitting are listed in Table 12. Due to its higher R^2 and lower χ_v^2 values, the Langmuir isotherm was selected as the better model for both supports, which agrees with previous results reported for CGTase immobilization on MIL-101 and Ca-MOF [177, 178]. The maximum capacity of H-Cu-BTC was determined to be 49.5 mg/g, which is almost 62% higher than that of microporous Cu-BTC (30.6 mg/g).
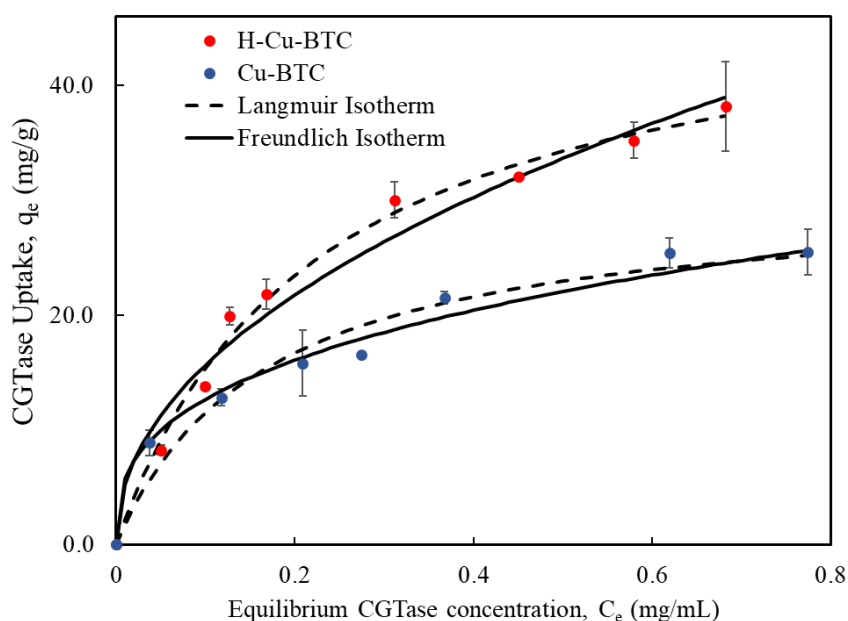

Figure 19: CGTase Uptake at Equilibrium (25°C) vs. Equilibrium Concentration with Isotherm Predictions

Table 12: Adsorption Isotherm Parameters of CGTase on Supports

Support	Langmuir model				Freundlich model			
	q_m (mg/g)	b (mL/mg)	R^2	χ_v^2	K_F (mg/g (mL/mg)^n)	n	R^2	χ_v^2
Cu-BTC	30.6±2.1	6.0±1.4	0.98	0.92	28.0±0.9	2.9±0.2	0.98	1.45
H-Cu-BTC	49.5±2.2	4.5±0.5	0.99	1.46	46.8±2.3	2.1±0.2	0.98	4.64

The observed higher CGTase uptake by H-Cu-BTC indicates that the presence of mesopores and macropores promotes the uptake of CGTase by offering a greater surface area for immobilization. However, with microporous Cu-BTC, only the external surface area and limited available mesopores were utilized, as the CGTase molecule size was larger than that of the micropores. This explanation is supported by the pore size distribution shown in Figure 18D, with most pore sizes in Cu-BTC being less than 3.6 nm (the size of CGTase). Thus, most of the CGTase was expected to be on the external surface, and the introduction of macropores into the structure of the MOFs led to enhanced CGTase immobilization. In addition, the uptake observed for H-Cu-BTC was higher than that reported in the literature for other supports, as shown in Table 13.

Table 13: Comparison of Reported CGTase Uptake on Different Supports

Support	Method of Immobilization	Maximum CGTase uptake, q_m (mg/g)	Surface area (m^2/g)	Average pore size	Ref.
MIL-101	Surface attachment	37.5	1428	3.4 nm	[178]
Zeolite Y	Surface attachment	6.1	-	0.8 nm	[178]
Melamine-epoxy resin	Cross-linking	42	46	100 μm	[141]
Eupergit C	Covalent attachment	8.1	-	-	[51]
Activated silica	Covalent attachment	4.1	50	60 nm	[142]
Hierarchical Cu-BTC	Physical adsorption	49.5	622.7	10.8 nm	This work

4.3.4 Secondary Structure Analysis

The electrostatic attraction between the charged amino acids on the enzyme and the support surface, which drives the forces involved in enzyme adsorption on the surfaces during immobilization, may cause structural deformation or changes in the secondary structure of the polypeptide chain. The amide bands in the FTIR spectra were used to identify the structure. Because of the correlation between its vibrational frequencies and secondary structure elements, the amide I band (1600–1700 cm^{-1}), which arises primarily from the C=O stretching vibration of the amide group (80%), coupled with in-plane NH bending (contributes less than 20%), is widely used and accepted as a predictor for the quantitation of protein secondary structures among several amide bands [179]. Peaks located between 1620–1641 cm^{-1} (1600–1620 cm^{-1} in some proteins) are often attributed to β-sheets, whereas peaks located at 1648–1660 and 1665–1688 cm^{-1} are attributed to α-helices and β-turns, respectively [144].

After baseline correction and the removal of the support FTIR spectrum from that of the immobilized enzyme, the FTIR deconvolution of the amide I band in the free CGTase, CGTase@Cu-BTC, and CGTase@H-Cu-BTC was carried out using the peak deconvolution program in Origin® 2021 in order to ascertain the changes in the secondary structures, and the result is displayed in Figure 20. Table 14 displays the secondary structure assignments, which were calculated as percentages of the total area of the amide I band based on the matching areas. When comparing the amide I band intensity of all immobilized CGTases with that of free CGTase, a reduction was observed, suggesting that immobilization affected the secondary structure. The results indicate that free CGTase exhibited a β-sheet signature both before and after immobilization, with a maximal amide I vibration centered at 1626–1644 cm^{-1}, as shown in Figure 20A. After immobilization, the percentage of β-sheets decreased from 56% to 44.1% on Cu-BTC but increased to 76.1% on H-Cu-BTC. In most proteins, β-sheets perform a stabilizing cross-link via hydrogen bonding or van der Waals interactions; thus, the increase in β-sheets observed following immobilization over H-Cu-BTC could suggest a better stability as compared to Cu-BTC [180]. Compared to the free form of CGTase, there was no discernible peak for the β-turns after immobilization on H-Cu-BTC. The α-helices also decreased post-immobilization from 38.5% in free form to 26.5% and 23.9% on Cu-BTC and H-Cu-BTC,

respectively. The deformation of the α-helix plays a key role in protein function, as it maintains the protein's tertiary structure and affects its stability and folding. The abundance of β-sheets and α-helices, generally considered as "ordered" secondary structures, over H-Cu-BTC and the presence of significant β-turns, considered as "unordered" secondary structures, over Cu-BTC indicated that the introduction of hierarchical structures led to reduced conformational changes in the immobilized CGTase [181].
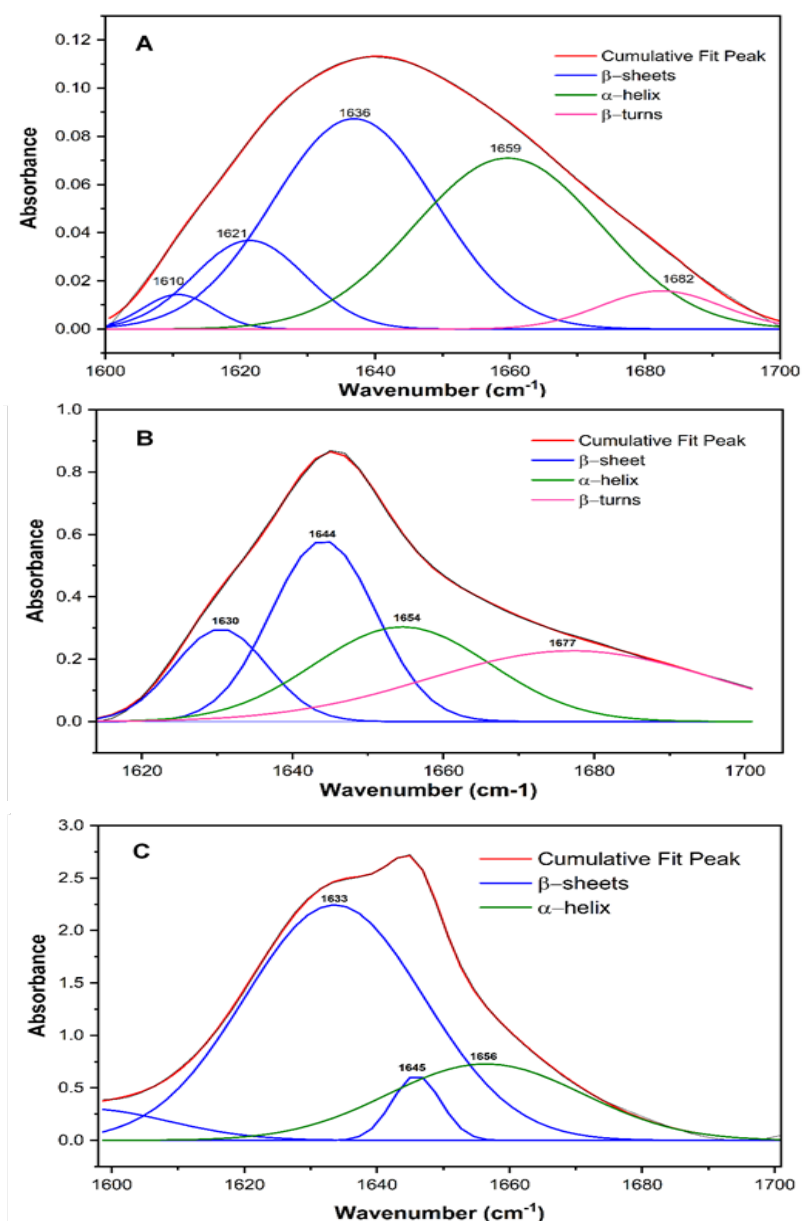

Figure 20: Peak Deconvolution of FTIR Spectra for (a) Free CGTase, (b) CGTase@Cu-BTC, and (c) CGTase@H-Cu-BTC

Table 14: Deconvolution of the Amide I Band in the FTIR Spectrum for Secondary Structure Analysis

	Wavenumber range[1] (cm^{-1})	Percentage (%)		
		Free CGTase	CGTase@Cu-BTC	CGTase@H-Cu-BTC
β-sheets	1620–1644	56.0	44.1	76.1
α-helices	1648–1660	38.5	26.5	23.9
β-turns	1660–1688	5.5	29.7	-

[1][144]

4.3.5 Catalytic Performance of Immobilized CGTase

The effect of the initial substrate concentration on the initial rate of the CD reaction at different substrate concentrations is shown in Figure 21. The initial reaction rate slowly increased with an increase in the substrate concentration for free CGTase up to 10 gL^{-1}, with α-CD production reaching a value of 0.31 gL^{-1}min^{-1}. The enzyme was more selective towards α-CD, with a production rate almost double that found for β-CD, which was 0.17 gL^{-1}min^{-1}. Only trace amount of γ-CD was observed in the products and it wasn't considered in this study. The Michaelis–Menten model was used to study the enzymatic kinetics of free CGTase, based on the main product, α-CD. The K_M and V_{max} of the free CGTase CGTase were calculated to be 9.44 gL^{-1} and 0.64 gL^{-1}min^{-1}, respectively.
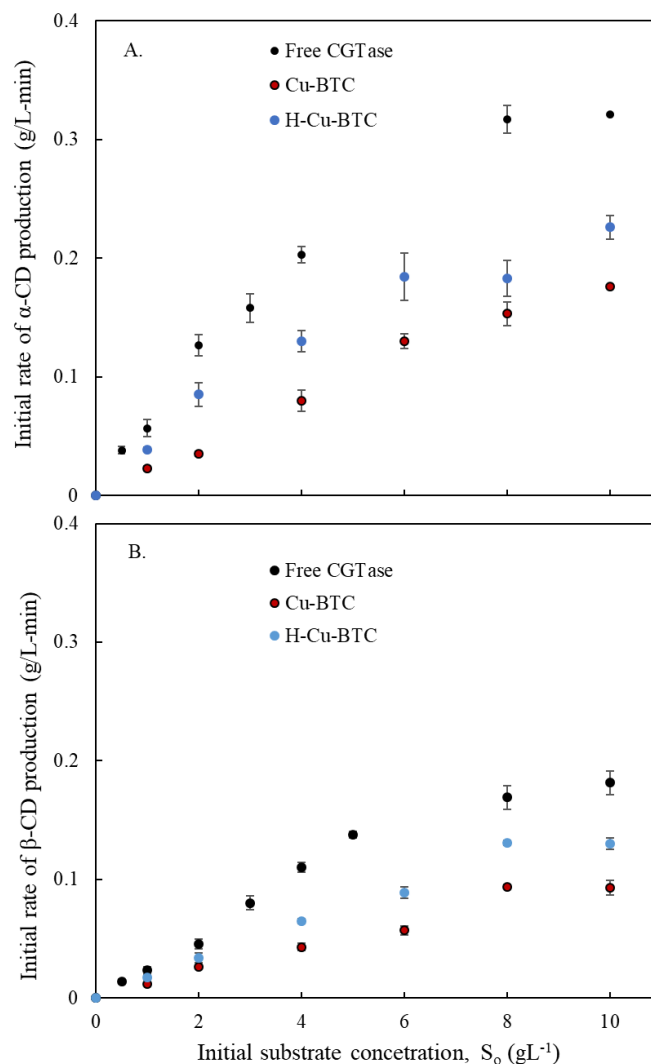
Figure 21: Initial rate of CD Production vs. Concentration at 70°C and pH 7.4 for
(A) α-CD and (B) β-CD

Immobilized enzymes exhibit catalytic activities that differ from those of unbound enzymes. One of the complexities introduced by immobilization is that substrate molecules must first diffuse through the surrounding layers to reach the catalytic sites, which serve as a form of resistance before reactions can occur and must be addressed alongside enzyme kinetics. Furthermore, the immobilization process and surface features of the supports may cause conformational changes in the enzymes, which may also affect enzyme activity.

The immobilized CGTase showed a lower rate compared to the free enzyme, with CGTase@H-Cu-BTC showing better performance than CGTase@Cu-BTC. This was attributed to the lower diffusion resistance of H-Cu-BTC. To confirm this explanation, the

mass transfer coefficient (k_L) over each support was estimated using the initial slope from the plot of dimensionless activity (v/V_{max}) against dimensionless bulk substrate concentration β_o (S_0/K_M), as shown in Figure 22. The microenvironment substrate concentration was determined at the points of intersection (denoted by × on the graph) where lines with negative values of k_L (-k_L) as slope intersected various lines drawn from the bulk concentration along the x-axis, corresponding to the horizontally drawn experimental reaction rate. The mass transfer coefficient, k_L, for Cu-BTC was 0.68 min^{-1}, which is comparable to another microporous MOF, MIL-101 (0.68 min^{-1}), which was utilized in our previous studies [178]. When H-Cu-BTC was used, k_L increased to 0.89 min^{-1}. This confirms that the hierarchical nature of H-Cu-BTC enhances the mass transfer of the substrate, providing bulky starch molecules with better access to the active sites of the enzyme and easy diffusion of the product. This result supports the hypotheses of this study.
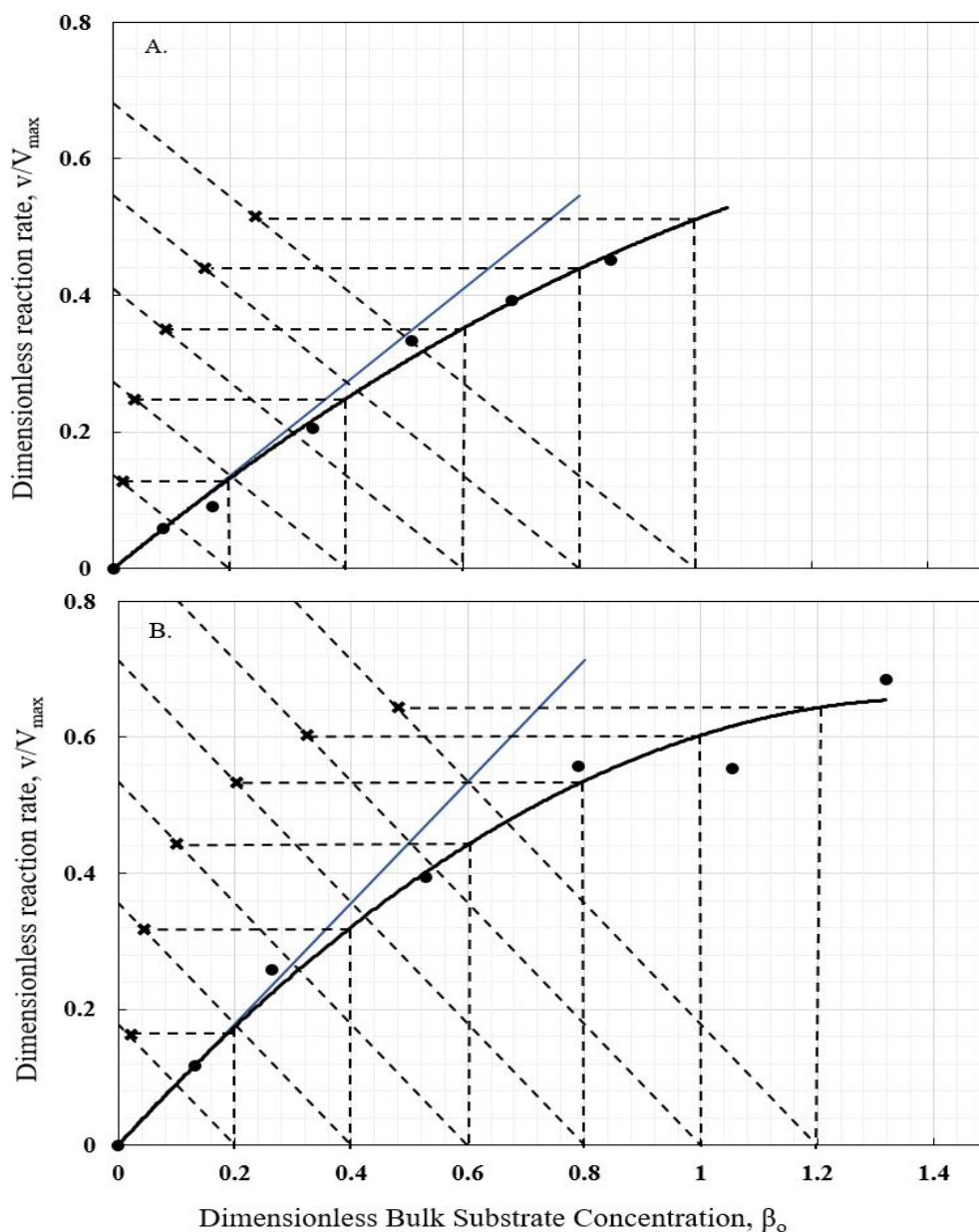
Figure 22: Plot of Dimensionless Activity vs. Dimensionless Substrate Concentration for (A) Cu-BTC and (B) H-Cu-BTC

Operational stability of biocatalysts is an important feature that must be considered for the practical use of immobilized enzymes on an industrial scale. Reusability is the rate at which an immobilized enzyme loses its activity after being recycled several times. Figure 23 illustrates the relative activity of the biocatalyst after each cycle, which shows that after ten cycles, CGTase@H-Cu-BTC maintained a higher stability with a residual activity of 87%. The stability of CGTase@Cu-BTC was low, with 70% residual activity. The decrease in immobilized CGTase activity can be attributed to the loss of CGTase after

each cycle. Hierarchical Cu-BTC showed a higher relative activity compared to other reported systems, including CGTase over graphene nanoplatelets, melanine epoxy sponges, and polydopamine-coated Fe_3O_4, which retained 74% activity after eight successive cycles [177], 54% after ten cycles [141], and 19.1% after nine cycles [15], respectively. Using controlled pore silica, a lower stability of 7.19 and 3.89% retained activity after only five cycles were observed with surface anchoring and covalent bonding, respectively [166]. On the other hand, a higher stability of 91.9% retained activity was achieved after 20 cycles using gelatin as a support for CGTase derived from *Bacillus circulans* [162]. Nevertheless, the results clearly demonstrated that H-Cu-BTC provided good stability and served as a good support for CGTase immobilization.
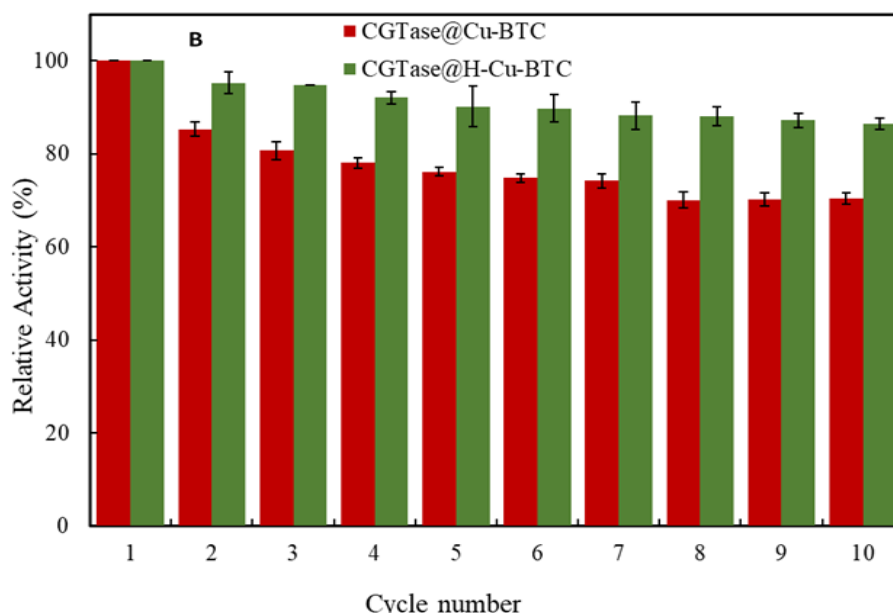
Figure 23: Reusability Studies using a Substrate Concentration of 10 gL^{-1}

To validate the use of immobilized CGTase for starchy waste materials, corn flour waste that had been used to produce 'pap', a custard-like delicacy common in West Africa, was tested as a substrate. The total amount of CD produced using this food waste material is shown in Figure 24 and is compared with that produced using commercial soluble starch. The relative amount of CD produced using raw corn flour was lower than that produced using commercially available soluble starch. This is mainly attributed to the low purity and presence of impurities in the waste material. In addition, a significant portion of the starch component had been extracted from the corn flour to produce pap, leaving the corn

flour waste with only a fraction of the original starch. Nevertheless, the feasibility of obtaining CD directly from corn flour waste without any pretreatment, which otherwise would have been discarded, could drastically reduce the costs associated with CD production.

Figure 24: Total CD Production at Various Substrate Concentrations at 70°C and 10 min

Chapter 5: General Discussion

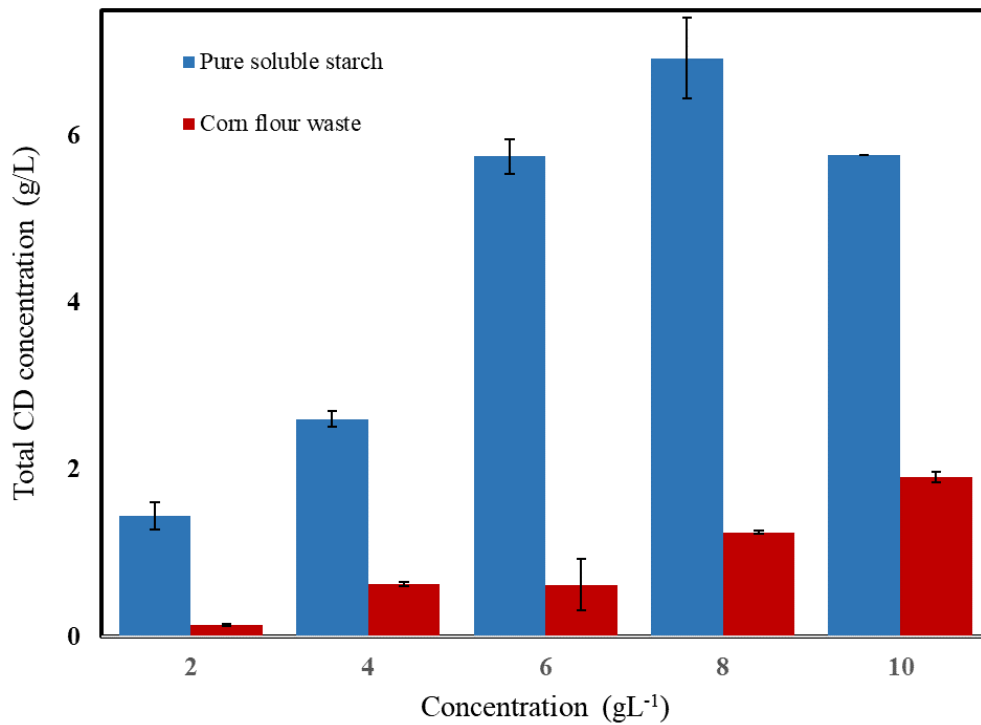This dissertation seeks to present MOFs as a viable alternative to other materials as supports in CGTase immobilization for cyclodextrin production. Six different supports with varying properties were utilized in this dissertation in order to understand how the properties of the support, which were studied using various characterization techniques, could impact the uptake of CGTase, secondary structures of the enzyme, diffusional restraints and kinetics.

The supports used in this dissertation were two microporous materials, zeolite-Y and MIL-101, three-dimensional GNP with higher external surface area compared to internal area, two-dimensional Ca-TMA, and both microporous and hierarchical counterpart of Cu-BTC/H-Cu-BTC. Zeolite-Y was used as a representative of conventional supports and it was compared to microporous MIL-101. It was expected that CGTase immobilization on both support will be primarily on the external surface, as the size of CGTase (3.6 nm) is bigger than the pore size of zeolite-Y (~0.8 nm) and closer to that of MIL-101 (2 -3 nm), although thermal vibrations within the structure of MIL-101 could still allow some of the CGTase to be trapped within the pores. MIL-101 showed an optimum CGTase uptake of 37.5 mg/g, six-fold higher than the uptake over zeolite-Y. This result can be attributed to the combined effect of the larger surface area and more enzyme-compatible functional groups, mainly the –COOH groups offered by MIL-101 compared with zeolite Y. CGTase uptake was improved upon with the use of GNP to 40 mg/g, as the support provides more external area, coupled with better hydrophobic interactions it offered CGTase. Ca-TMA, a non-porous MOF could have resulted in higher CGTase uptake except for its low specific surface area and presence of more hydrophilic functional groups. The optimum CGTase uptake was further improved using hierarchical MOFs which allows for complete usage of both internal and external surface area of the support. H-Cu-BTC gave an optimum uptake of 49.5 mg/g compared to 30.6 mg/g using Cu-BTC. The uptake observed over H-Cu-BTC was higher than that reported in the literature for other supports. Immobilization of CGTase on the supports was modelled using the Langmuir and Freundlich models, with R^2 and χ_v^2 used as validation parameters. Langmuir isotherm was selected as the better model for MIL-101, zeolite-Y, Cu-BTC and

H-Cu-BTC supports, which agrees with previous results reported for CGTase immobilization. The Langmuir isotherm is predicated on the homogeneous adsorption of CGTase with monolayer coverage on the support surface.

Peptide bonds hold strands of amino acids together, forming proteins. The rotation of the main chain about the two torsion angles allows for a wide range of conformations for this chain. Deconvolution of the amide I band was used to study conformational changes that occur to CGTase after immobilization on the supports. Free CGTase showed a composition of 56% β-sheets, 38.5% α-helices and 5.5% β-turns. Post-immobilization, the composition varied for all the supports studied; MIL-101 (84.1% β-sheets, no α-helices and 15.9% β-turns), GNP (41.9% β-sheets, 18.1% α-helices and 40% β-turns), Ca-TMA (51.3% β-sheets, 37.5% α-helices and 40% β-turns), Cu-BTC (44.1% β-sheets, 26.5% α-helices and 29.7% β-turns) and H-Cu-BTC (76.1% β-sheets, 23.9% α-helices and no β-turns). Protein function is significantly impacted by the β-sheets and α-helix's deformation, which preserves the protein's tertiary structure and influences folding and stability as they are considered as "ordered" secondary structures. Hence, increase in their proportion could signify that the enzyme's overall catalytic performance might not be negatively affected. β-turns are classified to be "unordered" secondary structures. GNP and Cu-BTC showed reduced β-sheets compared to free CGTase while MIL-101, Ca-TMA and H-Cu-BTC gave better β-sheets. Increment in β-sheets after immobilization suggests that CGTase could have form aggregates on the support surfaces, resulting in protein–protein interactions [148]. All supports except H-Cu-BTC showed increased β-turns suggesting that the introduction of hierarchical pores reduced conformational changes in the immobilized CGTase [181].

Kinetic studies were used to study the performance of free and immobilized CGTases, Analysis of the product showed a very minute quantity of γ-CD; hence, it was not considered in this dissertation. Based on α-CD, the maximum initial reaction rate for free CGTase, CGTase@MIL-101, CGTase@GNP, CGTase@Ca-TMA, CGTase@Cu-BTC and CGTase@H-Cu-BTC were 0.31. 0.19, 0.11, 0.12, 0.19 and 0.21 gL^{-1}min^{-1}, respectively. Since equivalent protein amounts were used for the free and immobilized CGTases, the lower production using the immobilized CGTase could be attributed to the combination of substrate diffusion limitation and conformational changes in the CGTase

secondary structure. Due to the bulkiness of starch molecules, their diffusion into the pores of the MOF matrix was expected to be limited except with MOFs with macroporous structure. The external mass transfer coefficient from the bulk fluid to the MOF surface (k_L) was evaluated to be 0.68 min^{-1} for all macroporous MOFs studied (MIL-101, Cu-BTC) while H-Cu-BTC, which was the only macroporous MOF showed an improvement, with a value of 0.89 min^{-1}, thus, confirming the hypotheses made in this dissertation that introduction of mesopores/macropores enhance the mass transfer of starch molecules.

Operational stability of the biocatalysts is an important feature that was evaluated using the residual activity of CGTase after repeated use in the reaction. MIL-101 gave a 29% residual activity based on α-CD production after 10 cycles, which was improved to 40% by introduction of glutaraldehyde before CGTase immobilization (covalent immobilization). CGTase@GNP and CGTase@Ca-TMA showed 74 and 33% residual activity after eight reaction cycles respectively. In comparison between Cu-BTC and H-Cu-BTC, a residual activity of 87% was observed on the more stable H-Cu-BTC, higher than 70% obtained for Cu-BTC. Detachment of CGTase from the supports during washing contributed to the drop in activity of the immobilized enzyme. Also, it has been reported that enzyme leaching occurs more on surfaces with higher hydrophilicity compared to hydrophobic surfaces [164].

Chapter 6: Conclusion, Future Perspectives and Limitations

6.1 Conclusions

This dissertation aimed at immobilizing CGTase on MOFs for enhanced performance in terms of protein uptake, specific activity, secondary structures, CD production and reusability, with comparison to conventional supports that have been reported in the literature. The following conclusions could be derived from the studies:

- The results indicate that presence of high surface area, enzyme compatible groups and macroporous structure in the support contribute to better CGTase uptake. In the comparison between microporous MOFs and zeolite, MIL-101 showed a maximum CGTase uptake of 37.5 mg/g compared with the value obtained for zeolite (6.1 mg/g). GNP and Ca-TMA yielded CGTase uptakes up to 40 and 21 mg/g respectively with GNP possessing higher external surface area. The uptake reached 49.5 mg/g over H-Cu-BTC with macropores, which was significantly higher than previously reported values.

- Using CGTase in the immobilized form, a much higher α-CD selectivity could be obtained, especially at lower substrate concentrations, which is a very interesting finding as it could simplify the purification of the product when α -CD is much more desired.

- Investigation into the secondary structures of the immobilized CGTase showed that transition from α-helix to β-sheets occurred after immobilization, thus, affecting the specific activity observed over each support. H-Cu-BTC, Cu-BTC and Ca-TMA showed the best specific activity of 98.5, 65.2 and 38 U/mg, depicting an interplay between the proportions of ordered to unordered secondary structures.

- Reusability studies showed that 87% of the CGTase initial activity can be retained after ten successive reaction cycles using H-Cu-BTC and the immobilized CGTase can be used to convert waste materials containing starch into cyclodextrin without any form of pre-treatment.

6.2 Future Perspectives and Limitations

Based on the results obtained in this dissertation, further studies will need to be conducted on H-Cu-BTC, which was identified as a better support for CGTase immobilization in terms of CGTase uptake, CD production and operational stability. The performance of H-Cu-BTC needs to be subjected to optimization studies using temperature, pH, agitation rate, to mention a few, as parameters. After identifying the optimum conditions, the support can be utilized in continuous CD production.

The diversification of the feedstock used for CD production also needs to be investigated further. Studies should highlight the factors that led to lesser production of CD and how it can be improved.

6.3 Research Implications

This dissertation opens up intriguing possibilities for the development of efficient and sustainable biocatalyst for cyclodextrin synthesis utilizing cyclodextrin glycosyltransferase immobilized in metal organic frameworks (MOFs). In addition to improving the enzyme's stability and reusability, the effective immobilization of cyclodextrin glycosyltransferase within MOFs offers a framework for definite control over reaction conditions and substrate specificity. This accomplishment has substantial implications for a number of industrial uses, such as food processing, medicines, and environmental cleanup.

The dissertation also highlights the potential of MOFs as adaptable hosts for enzyme immobilization, adding to the increasing body of research on utilizing these materials' special qualities for biocatalysis. Thus, this study paves way for more research into improving the efficiency, selectivity, and scalability of MOF-based biocatalytic systems in cyclodextrin production. The studies embarked on in this dissertation will improve the utilization of CGTase during CD production while ensuring that it can withstand industrial conditions. This dissertation opens up a pathway for waste materials containing starch to be processed into cyclodextrin without any form of pre-treatment. Nevertheless, further research is necessary to evaluate the performance of immobilized enzymes in waste valorization under various conditions and to optimize the process before scaling up.

References

[1]   N. Szerman, I. Schroh, A. L. Rossi, A. M. Rosso, N. Krymkiewicz, and S. A. Ferrarotti, "Cyclodextrin production by Cyclodextrin glycosyltransferase from Bacillus circulans DF 9R," *Bioresour. Technol.*, vol. 98, no. 15, pp. 2886-2891, Nov. 2007, doi: https://doi.org/10.1016/j.biortech.2006.09.056.

[2]   X. Duan, S. Chen, J. Chen, and J. Wu, "Enhancing the cyclodextrin production by synchronous utilization of isoamylase and α-CGTase," *Appl. Microbiol. Biotechnol.*, vol. 97, no. 8, pp. 3467-3474, Apr. 2013, doi: 10.1007/s00253-012-4292-9.

[3]   Z. Zhou and M. Hartmann, "Progress in enzyme immobilization in ordered mesoporous materials and related applications," *Chem. Soc. Rev.*, vol. 42, no. 9, pp. 3894-3912, 2013, doi: 10.1039/C3CS60059A.

[4]   H. R. Luckarift, J. C. Spain, R. R. Naik, and M. O. Stone, "Enzyme immobilization in a biomimetic silica support," *Nat. Biotechnol.*, vol. 22, no. 2, pp. 211-213, Feb. 2004, doi: 10.1038/nbt931.

[5]   I. Gill and A. Ballesteros, "Encapsulation of biologicals within silicate, siloxane, and hybrid sol−gel polymers: An efficient and generic approach," *J. Am. Chem. Soc.*, vol. 120, no. 34, pp. 8587-8598, Sep. 1998, doi: 10.1021/ja9814568.

[6]   R. A. Sheldon, "Enzyme immobilization: The quest for optimum performance," *Adv. Synth. Catal.*, vol. 349, no. 8-9, pp. 1289-1307, 2007, doi: 10.1002/adsc.200700082.

[7]   M. Hartmann and D. Jung, "Biocatalysis with enzymes immobilized on mesoporous hosts: the status quo and future trends," *J. Mater. Chem.*, 10.1039/B907869J vol. 20, no. 5, pp. 844-857, 2010, doi: 10.1039/B907869J.

[8]   Z. Wang and S. M. Cohen, "Postsynthetic modification of metal–organic frameworks," *Chem. Soc. Rev.*, vol. 38, no. 5, pp. 1315-1329, 2009, doi: 10.1039/B802258P.

[9]   N. A. Nikitenko and V. S. Prassolov, "Non-viral delivery and therapeutic application of small interfering RNAs," *Acta Naturae*, vol. 5, no. 3, pp. 35-53, Sep. 2013, doi: 10.32607/20758251-2013-5-3-35-53.

[10]   J. K. Poppe, C. Garcia-Galan, C. R. Matte, R. Fernandez-Lafuente, R. C. Rodrigues, and M. A. Z. Ayub, "Optimization of synthesis of fatty acid methyl esters catalyzed by lipase B from Candida antarctica immobilized on hydrophobic supports," *J. Mol. Catal. B: Enzym.*, vol. 94, pp. 51-56, Oct. 2013, doi: https://doi.org/10.1016/j.molcatb.2013.05.010.

[11]   T. Tan, J. Lu, K. Nie, L. Deng, and F. Wang, "Biodiesel production with immobilized lipase: A review," *Biotechnol. Adv.*, vol. 28, no. 5, pp. 628-634, Sep. 2010, doi: https://doi.org/10.1016/j.biotechadv.2010.05.012.

[12] X. Jia, X. Ye, J. Chen, X. Lin, L. Vasseur, and M. You, "Purification and biochemical characterization of a Cyclodextrin glycosyltransferase from Geobacillus thermoglucosidans CHB1," *Starch - Stärke*, vol. 70, no. 1-2, p. 1700016, Jan. 2018, doi: 10.1002/star.201700016.

[13] A. Biwer, G. Antranikian, and E. Heinzle, "Enzymatic production of cyclodextrins," *Appl. Microbiol. Biotechnol.*, vol. 59, no. 6, pp. 609-617, 2002.

[14] Z. Li, M. Wang, F. Wang, Z. Gu, G. Du, J. Wu, and J. Chen, "γ-Cyclodextrin: a review on enzymatic production and applications," *Appl. Microbiol. Biotechnol.*, vol. 77, no. 2, pp. 245-255, 2007, doi: 10.1007/s00253-007-1166-7.

[15] J. Zhang, H. Mao, M. Li, and E. Su, "Cyclodextrin glucosyltransferase immobilization on polydopamine-coated Fe_3O_4 nanoparticles in the presence of polyethyleneimine for efficient β-cyclodextrin production," *Biochem. Eng. J.*, vol. 150, p. 107264, Oct. 2019, doi: https://doi.org/10.1016/j.bej.2019.107264.

[16] N. Jamil, R. C. Man, S. M. Shaarani, S. Z. Sulaiman, S. K. A. Mudalip, and Z. I. M. Arshad, "Characterization of α-Cyclodextrin glucanotransferase from Bacillus licheniformis," *Indian J. Sci. Technol.*, vol. 10, pp. 1-5, Feb. 2017.

[17] M. M. M. Mora, K. H. Sánchez, R. V. Santana, A. P. Rojas, H. L. Ramírez, and J. J. Torres-Labandeira, "Partial purification and properties of Cyclodextrin glycosiltransferase (CGTase) from alkalophilic Bacillus species," *SpringerPlus*, vol. 1, no. 61, pp. 1-6, 2012.

[18] R. F. Martins and R. Hatti-Kaul, "A new cyclodextrin glycosyltransferase from an alkaliphilic Bacillus agaradhaerens isolate: Purification and characterisation," *Enzyme Microb. Technol.*, vol. 30, no. 1, pp. 116-124, Jan. 2002, doi: https://doi.org/10.1016/S0141-0229(01)00461-6.

[19] I. Pishtiyski, V. Popova, and B. Zhekova, "Characterization of cyclodextrin glucanotransferase produced by Bacillus megaterium," *Appl. Biochem. Biotechnol.*, vol. 144, no. 3, p. 263, Aug. 2007, doi: 10.1007/s12010-007-8009-y.

[20] T. Kato and K. Horikoshi, "A new γ-cyclodextrin forming enzyme produced by Bacillus subtilis no. 313," *J. Jpn. Soc. Starch Sci.*, vol. 33, no. 2, pp. 137-143, 1986.

[21] A. Ebglbrecht, "Biochemical and genetic characterization of a CGTase from an alkalophilic bacterium forming primary γ-cyclodextrin," *Proc. 5th Int. Symp. Cyclodextrins*, Paris, France, 1990, pp. 25-31.

[22] Z. Li, B. Li, Z. Gu, G. Du, J. Wu, and J. Chen, "Extracellular expression and biochemical characterization of α-Cyclodextrin glycosyltransferase from Paenibacillus macerans," *Carbohydr. Res.*, vol. 345, no. 7, pp. 886-892, 2010.

[23] R. D. Wind, W. Liebl, R. M. Buitelaar, D. Penninga, A. Spreinat, L. Dijkhuizen, and H. Bahl, "Cyclodextrin formation by the thermostable alpha-amylase of Thermoanaerobacterium thermosulfurigenes EM1 and reclassification of the enzyme as a Cyclodextrin glycosyltransferase," *Appl. Environ. Microbiol.*, vol. 61, no. 4, pp. 1257-1265, 1995.

[24] M. H. Kim, C. B. Sohn, and T. K. Oh, "Cloning and sequencing of a Cyclodextrin glycosyltransferase gene from Brevibacillus brevis CD162 and its expression in Escherichia coli," *FEMS Microbiol. Lett.*, vol. 164, no. 2, pp. 411-418, 1998.

[25] F. Wang, G. Du, Y. Li, and J. Chen, "Optimization of cultivation conditions for the production of γ-Cyclodextrin glucanotransferase by Bacillus macorous," *Food Biotechnol.*, vol. 18, no. 2, pp. 251-264, 2004.

[26] S. Mori, S. Hirose, T. Oya, and S. Kitahata, "Purification and properties of Cyclodextrin glucanotransferase from Brevibacterium sp. No. 9605," *Biosci., Biotechnol., Biochem.*, vol. 58, no. 11, pp. 1968-1972, 1994.

[27] J. C. M. Uitdehaag, G.-J. W. M. van Alebeek, B. A. van der Veen, L. Dijkhuizen, and B. W. Dijkstra, "Structures of maltohexaose and maltoheptaose bound at the donor sites of Cyclodextrin glycosyltransferase give insight into the mechanisms of transglycosylation activity and cyclodextrin size specificity," *Biochemistry*, vol. 39, no. 26, pp. 7772-7780, Jul. 2000, doi: 10.1021/bi000340x.

[28] H. P. Erickson, "Size and shape of protein molecules at the nanometer level determined by sedimentation, gel filtration, and electron microscopy," *Biol. Proced. Online*, vol. 11, no. 1, p. 32, May 2009, doi: 10.1007/s12575-009-9008-x.

[29] J.-H. Lee, K.-H. Choi, J.-Y. Choi, Y.-S. Lee, I.-B. Kwon, and J.-H. Yu, "Enzymatic production of α-cyclodextrin with the Cyclomaltodextrin glucanotransferase of Klebsiella oxytoca 19-1," *Enzyme Microb. Technol.*, vol. 14, no. 12, pp. 1017-1020, 1992.

[30] B. N. Gawande and A. Y. Patkar, "Application of factorial designs for optimization of Cyclodextrin glycosyltransferase production from Klebsiella pneumoniae pneumoniae AS-22," *Biotechnol. Bioeng.*, vol. 64, no. 2, pp. 168-173, 1999.

[31] M. K. Mahat M.K. Mahat, R.M. Illias, R.A. Rahman, N.A. Rashid, N.A. Mahmood, O. Hassan, S. Abdul Aziz, and K. Kamaruddin, "Production of Cyclodextrin glucanotransferase (CGTase) from alkalophilic Bacillus sp. TS1-1: media optimization using experimental design," *Enzyme Microb. Technol.*, vol. 35, no. 5, pp. 467-473, Oct. 2004, doi: 10.1016/j.enzmictec.2004.07.008.

[32] A. Avci and S. Dönmez, "A novel thermophilic anaerobic bacteria producing Cyclodextrin glycosyltransferase," *Process Biochem.*, vol. 44, no. 1, pp. 36-42, Jan. 2009, doi: 10.1016/j.procbio.2008.09.006.

[33] Y.-C. Park, C.-S. Kim, C.-I. Kim, K.-H. Choi, and J.-H. Seo, "Fed-batch fermentations of recombinant Escherichia coli to produce Bacillus macerans CGTase," *J. Microbiol. Biotechnol.*, vol. 7, no. 5, pp. 323-328, Oct. 1997.

[34] C. C. Kuo, C. A. Lin, J. Y. Chen, M. T. Lin, and K. J. Duan, "Production of Cyclodextrin glucanotransferase from an alkalophilic Bacillus sp. by pH-stat fed-batch fermentation," *Biotechnol. Lett.*, vol. 31, pp. 1723-1727, Jul. 2009.

[35] B. N. Gawande, A. M. Sonawane, V. V. Jogdand, and A. Y. Patkar, "Optimization of Cyclodextrin glycosyltransferase production from Klebsiellapneumoniae AS-22 in batch, fed-batch, and continuous cultures," *Biotechnol. Progr.*, vol. 19, no. 6, pp. 1697-1702, Sep. 2003.

[36] I. Roy and M. N. Gupta, "Freeze-drying of proteins: some emerging concerns," *Biotechnol. Appl. Biochem.*, vol. 39, no. 2, pp. 165-177, Apr. 2004, doi: 10.1042/BA20030133.

[37] J. M. Bolivar, I. Eisl, and B. Nidetzky, "Advanced characterization of immobilized enzymes as heterogeneous biocatalysts," *Catal. Today*, vol. 259, pp. 66-80, Jan. 2016, doi: 10.1016/j.cattod.2015.05.004.

[38] N. Jamil, R. C. Man, S. Suhaimi, S. M. Shaarani, Z. M Arshad, S. A. Mudalip, and S. Z. Sulaiman, "Effect of enzyme concentration and temperature on the immobilization of Cyclodextrin glucanotransferase (CGTase) on hollow fiber membrane," *Mater. Today: Proc.*, vol. 5, no. 10, Part 2, pp. 22036-22042, Jan. 2018, doi: 10.1016/j.matpr.2018.07.065.

[39] S. Sulaiman, M. N. Mokhtar, M. Z. M. Nor, K. F. M. Yunos, and M. N. Naim, "Mass transfer with reaction kinetics of the biocatalytic membrane reactor using a fouled covalently immobilised enzyme layer (α–CGTase–CNF layer)," *Biochem. Eng. J.*, vol. 152, p. 107374, Dec. 2019, doi: https://doi.org/10.1016/j.bej.2019.107374.

[40] J. Steighardt and R. Kleine, "Production and immobilization of a proteinase-reduced Cyclodextrin glycosyltransferase preparation," *Appl. Microbiol. Biotechnol.*, vol. 39, no. 1, pp. 63-68, Apr. 1993, doi: 10.1007/BF00166850.

[41] M. A. Abdel-Naby, "Immobilization of Paenibacillus macerans NRRL B-3186 Cyclodextrin glucosyltransferase and properties of the immobilized enzyme," *Process Biochem.*, vol. 34, no. 4, pp. 399-405, Jun. 1999.

[42] S. Sakai, N. Yamamoto, S. Yoshida, K. Mikuni, H. Ishigami, and K. Hara, "Continuous production of glucosyl-cyclodextrins using immobilized Cyclomaltodextrin glucanotransferase," *Agric. Biol. Chem.*, vol. 55, no. 1, pp. 45-51, 1991.

[43] J. N. Schöffer, C. R. Matte, D. S. Charqueiro, E. W. Menezes, T. M. Costa, E. V. Benvenutti, R. C. Rodrigues, and P. F. Hertz, "Effects of immobilization, pH and reaction time in the modulation of α-, β- or γ-cyclodextrins production by Cyclodextrin glycosyltransferase: batch and continuous process," *Carbohydr. Polym.*, vol. 169, pp. 41-49, Aug. 2017, doi: 10.1016/j.carbpol.2017.04.005.

[44] P. W. Tardioli, G. M. Zanin, and F. F. de Moraes, "Characterization of Thermoanaerobacter cyclomaltodextrin glucanotransferase immobilized on glyoxyl-agarose," *Enzyme Microb. Technol.* , vol. 39, no. 6, pp. 1270-1278, Oct. 2006, doi: 10.1016/j.enzmictec.2006.03.011.

[45] A. S. S. Ibrahim, A. A. Al-Salamah, A. M. El-Toni, M. A. El-Tayeb, and Y. B. Elbadawi, "Cyclodextrin glucanotransferase immobilization onto functionalized magnetic double mesoporous core–shell silica nanospheres," *Electronic Journal of Biotechnology*, vol. 17, no. 2, pp. 55-64, Mar. 2014, doi: https://doi.org/10.1016/j.ejbt.2014.01.001.

[46] S. K. Arya and S. K. Srivastava, "Kinetics of immobilized Cyclodextrin gluconotransferase produced by Bacillus macerans ATCC 8244," *Enzyme Microb. Technol.* , vol. 39, no. 3, pp. 507-510, Jul. 2006, doi: https://doi.org/10.1016/j.enzmictec.2005.12.019.

[47] D. R. Zusfahair, D. Kartika, M. Kurniasih, R. Nofiani, and A. Fatoni, "Improved reuse and affinity of enzyme using immobilized amylase on alginate matrix," *Journal of Physics: Conference Series*, 2020, vol. 1494, p. 012028.

[48] S. Sulaiman, N. L. Cieh, M. N. Mokhtar, M. N. Naim, and S. M. M. Kamal, "Covalent immobilization of Cyclodextrin glucanotransferase on kenaf cellulose nanofiber and its application in ultrafiltration membrane system," *Process Biochem.*, vol. 55, pp. 85-95, Apr. 2017, doi: 10.1016/j.procbio.2017.01.025.

[49] H. Lee, J. Rho, and P. B. Messersmith, "Facile conjugation of biomolecules onto surfaces via mussel adhesive protein inspired coatings," *Adv. Mater.*, vol. 21, no. 4, pp. 431-434, 2009.

[50] J. Liebscher, R. Mrówczyński, H. A. Scheidt, C. Filip, N. D. Hădade, R. Turcu, A. Bende, and S. Becket, "Structure of polydopamine: a never-ending story?," *Langmuir*, vol. 29, no. 33, pp. 10539-10548, Jul. 2013.

[51] M. T. Martín, F. J. Plou, M. Alcalde, and A. Ballesteros, "Immobilization on Eupergit C of Cyclodextrin glucosyltransferase (CGTase) and properties of the immobilized biocatalyst," *J. Mol. Catal. B: Enzym.*, vol. 21, no. 4, pp. 299-308, Feb. 2003, doi: https://doi.org/10.1016/S1381-1177(02)00264-3.

[52] T. Boller, C. Meier, and S. Menzler, "Eupergit oxirane acrylic beads: How to make enzymes fit for biocatalysis," *Org. Process Res. Dev.*, vol. 6, no. 4, pp. 509-519, Jul. 2002, doi: 10.1021/op015506w.

[53] C. Mateo, G. Fernández-Lorente, O. Abian, R. Fernández-Lafuente, and J. M. Guisán, "Multifunctional epoxy supports: a new tool to improve the covalent immobilization of proteins. The promotion of physical adsorptions of proteins on the supports before their covalent linkage," *Biomacromolecules*, vol. 1, no. 4, pp. 739-745, 2000.

[54] K. G. Tina, R. Bhadra, and N. Srinivasan, "PIC: protein interactions calculator," *Nucleic Acids Res.*, vol. 35, no. 2, pp. W473-W476, 2007.

[55] R. M. Kelly, L. Dijkhuizen, and H. Leemhuis, "The evolution of Cyclodextrin glucanotransferase product specificity," *Appl. Microbiol. Biotechnol.*, vol. 84, no. 1, pp. 119-133, 2009.

[56] K. A. Joshi, J. Tang, R. Haddon, J. Wang, W. Chen, and A. Mulchandani, "A disposable biosensor for organophosphorus nerve agents based on carbon nanotubes modified thick film strip electrode," *Electroanalysis*, vol. 17, no. 1, pp. 54-58, 2005.

[57] K. A. Joshi, M. Prouza, M. Kum, J. Wang, J. Tang, R. Haddon, W. Chen, and A. Mulchandani, "V-type nerve agent detection using a carbon nanotube-based amperometric enzyme electrode," *Anal. Chem.*, vol. 78, no. 1, pp. 331-336, 2006.

[58] N. End and K.-U. Schöning, "Immobilized biocatalysts in industrial research and production," in *Immobilized Catalysts*, Berlin, Germany: Springer, 2004, pp. 273-317.

[59] K. Won, S. Kim, K.-J. Kim, H. W. Park, and S.-J. Moon, "Optimization of lipase entrapment in Ca-alginate gel beads," *Process Biochem.*, vol. 40, no. 6, pp. 2149-2154, 2005.

[60] E. Górecka and M. Jastrzębska, "Immobilization techniques and biopolymer carriers," *Biotechnol. Food Sci.*, vol. 75, no. 1, pp. 65-86, 2011.

[61] D. Häring and P. Schreier, "Cross-linked enzyme crystals," *Curr. Opin. Chem. Biol.*, vol. 3, no. 1, pp. 35-38, 1999.

[62] U. Hanefeld, L. Gardossi, and E. Magner, "Understanding enzyme immobilisation," *Chem. Soc. Rev.*, vol. 38, no. 2, pp. 453-468, 2009.

[63] J. M. Rojas, M. Amaral-Fonseca, M. G. Zanin, R. Fernandez-Lafuente, D. R. Giordano, and W. P. Tardioli, "Preparation of crosslinked enzyme aggregates of a thermostable Cyclodextrin glucosyltransferase from Thermoanaerobacter sp. critical effect of the crosslinking agent," *Catalysts*, vol. 9, no. 2, 2019, doi: 10.3390/catal9020120.

[64] B. Brena, P. González-Pombo, and F. Batista-Viera, "Immobilization of enzymes: a literature survey," in *Immobilization of Enzymes and Cells,* New Jersey, USA: Springer, 2013, pp. 15-31.

[65] T. Jesionowski, J. Zdarta, and B. Krajewska, "Enzyme immobilization by adsorption: A review," *Adsorption*, vol. 20, no. 5-6, pp. 801-821, 2014.

[66] X. Wang, T. A. Makal, and H.-C. Zhou, "Protein immobilization in metal–organic frameworks by covalent binding," *Aust. J. Chem.*, vol. 67, no. 11, pp. 1629-1631, 2014.

[67] A. Subramanian, S. J. Kennel, P. I. Oden, K. B. Jacobson, J. Woodward, and M. J. Doktycz, "Comparison of techniques for enzyme immobilization on silicon supports," *Enzyme Microb. Technol.* , vol. 24, no. 1, pp. 26-34, Jan. 1999, doi: https://doi.org/10.1016/S0141-0229(98)00084-2.

[68] S. Nisha, S. A. Karthick, and N. Gobi, "A review on methods, application and properties of immobilized enzyme," *Chem. Sci. Rev. Lett.*, vol. 1, no. 3, pp. 148-155, 2012.

[69] R. A. Sheldon, R. Schoevaart, and L. M. Van Langen, "Cross-linked enzyme aggregates (CLEAs): A novel and versatile method for enzyme immobilization (a review)," *Biocatal. Biotransform.*, vol. 23, no. 3-4, pp. 141-147, 2005.

[70] S. Velasco-Lozano, F. López-Gallego, J. C. Mateos-Díaz, and E. Favela-Torres, "Cross-linked enzyme aggregates (CLEA) in enzyme improvement–a review," *Biocatalysis*, vol. 1, no. open-issue, pp. 166-177, 2016.

[71] L. MacGillivray, R., and C. M. L. (Eds.), *Metal-organic framework materials*. Hoboken, NJ, USA: John Wiley & Sons, 2014, pp. 34-42.

[72] H. Deng, S. Grunder, K. Cordova, C. Valente, H. Furukawa, M. Hmadeh, F. Gándara, A. Whalley, Z. Liu, S. Asahina, H. Kazumori, M. O'Keeffe, O. Terasaki, J. Stoddart, and O. M. Yaghi, "Large-pore apertures in a series of metal-organic frameworks," *Science*, vol. 336, no. 6084, pp. 1018-1023, 2012.

[73] H. He, R. Li, Z. Yang, L. Chai, L. Jin, S. I. Alhassan, L. Ren, H. Wang, and L. Huang, "Preparation of MOFs and MOFs derived materials and their catalytic application in air pollution: A review," *Catal. Today*, Feb. 2020, doi: 10.1016/j.cattod.2020.02.033.

[74] F. G. Cirujano, A. Corma, and F. X. Llabrés i Xamena, "Zirconium-containing metal organic frameworks as solid acid catalysts for the esterification of free fatty acids: Synthesis of biodiesel and other compounds of interest," *Catal. Today*, vol. 257, pp. 213-220, Nov. 2015, doi: 10.1016/j.cattod.2014.08.015.

[75] B. J. Burnett, P. M. Barron, and W. Choe, "Recent advances in porphyrinic metal–organic frameworks: materials design, synthetic strategies, and emerging applications," *Cryst. Eng. Comm.*, vol. 14, no. 11, pp. 3839-3846, Jan. 2012, doi: 10.1039/C2CE06692K.

[76] E. Gkaniatsou, C. Sicard, R. Ricoux, J.-P. Mahy, N. Steunou, and C. Serre, "Metal–organic frameworks: a novel host platform for enzymatic catalysis and detection," *Mater. Horiz.*, vol. 4, no. 1, pp. 55-63, 2017, doi: 10.1039/C6MH00312E.

[77] Y. Chen, S. Han, X. Li, Z. Zhang, and S. Ma, "Why does enzyme not leach from Metal–Organic Frameworks (MOFs)? Unveiling the interactions between an enzyme molecule and a MOF," *Inorg. Chem.*, vol. 53, no. 19, pp. 10006-10008, Oct. 2014, doi: 10.1021/ic501062r.

[78] S. M. Hawxwell, G. M. Espallargas, D. Bradshaw, M. J. Rosseinsky, T. J. Prior, A. J. Florence, J. Streeke and L. Brammer, "Ligand flexibility and framework rearrangement in a new family of porous metal–organic frameworks," *Chem. Commun.*, no. 15, pp. 1532-1534, 2007.

[79] Z. J. Lin, J. Lü, M. Hong, and R. Cao, "Metal–organic frameworks based on flexible ligands (FL-MOFs): structures and applications," *Chem. Soc. Rev.*, vol. 43, no. 16, pp. 5867-5895, 2014, doi: 10.1039/C3CS60483G.

[80]   C. Janiak and J. K. Vieth, "MOFs, MILs and more: Concepts, properties and applications for porous coordination networks (PCNs)," *New J. Chem.*, vol. 34, no. 11, pp. 2366-2388, 2010, doi: 10.1039/C0NJ00275E.

[81]   F. X. Llabrés i Xamena, A. Abad, A. Corma, and H. Garcia, "MOFs as catalysts: Activity, reusability and shape-selectivity of a Pd-containing MOF," *J. Catal.*, vol. 250, no. 2, pp. 294-298, Sep. 2007, doi: 10.1016/j.jcat.2007.06.004.

[82]   A. C. McKinlay, R. E. Morris, P. Horcajada, G. Férey, R. Gref, P. Couvreur, and C. Serre, "BioMOFs: Metal–organic frameworks for biological and medical applications," *Angew. Chem. Int. Ed.*, vol. 49, no. 36, pp. 6260-6266, Aug. 2010, doi: https://doi.org/10.1002/anie.201000048.

[83]   H. Cai, Y.-L. Huang, and D. Li, "Biological metal–organic frameworks: Structures, host–guest chemistry and bio-applications," *Coord. Chem. Rev.*, vol. 378, pp. 207-221, Jan. 2019, doi: 10.1016/j.ccr.2017.12.003.

[84]   S. W. Jaros, P. Smoleński, M. Silva, M. Florek, J. Król, Z. Staroniewicz, A. Pombeiro, and A. M. Kirillov, "New silver BioMOFs driven by 1,3,5-triaza-7-phosphaadamantane-7-sulfide (PTAS): Synthesis, topological analysis and antimicrobial activity," *Cryst. Eng. Comm.*, Issue 40, pp. 8060-8064, Aug. 2013, doi: 10.1039/C3CE40913A.

[85]   D. Ruiz-Molina, F. Novio, and C. Roscini, "MOFs in pharmaceutical technology" in *Bio-and Bioinspired Nanomaterials,* Heidelberg, Germany: Wiley, 2014, pp. 83-112.

[86]   L. Wang, S. Guan, J. Bai, Y. Jiang, Y. Song, X. Zheng, and J. Gao, "Enzyme immobilized in BioMOFs: Facile synthesis and improved catalytic performance," *Int. J. Biol. Macromol.*, vol. 144, pp. 19-28, Feb. 2020, doi: https://doi.org/10.1016/j.ijbiomac.2019.12.054.

[87]   S. W. Jaros, M. F. C. G. d. Silva, M. Florek, P. Smoleński, A. J. L. Pombeiro, and A. M. Kirillov, "Silver(I) 1,3,5-triaza-7-phosphaadamantane coordination polymers driven by substituted glutarate and malonate building blocks: Self-assembly synthesis, structural features, and antimicrobial properties," *Inorg. Chem.*, vol. 55, pp. 5886-5894, May 2016, doi: 10.1021/acs.inorgchem.6b00186.

[88]   Y. Zhang, X. Bo, A. Nsabimana, C. Han, M. Li, and L. Guo, "Electrocatalytically active cobalt-based metal–organic framework with incorporated macroporous carbon composite for electrochemical applications," *J. Mater. Chem. A*, vol. 3, no. 2, pp. 732-738, 2015, doi: 10.1039/C4TA04411H.

[89]   N. A. Khan and S. H. Jhung, "Synthesis of Metal-Organic Frameworks (MOFs) with microwave or ultrasound: Rapid reaction, phase-selectivity, and size reduction," *Coord. Chem. Rev.*, vol. 285, pp. 11-23, Feb. 2015, doi: https://doi.org/10.1016/j.ccr.2014.10.008.

[90]   W. J. Son, J. Kim, J. Kim, and W. S. Ahn, "Sonochemical synthesis of MOF-5," *Chem. Commun.*, no. 47, pp. 6336-6338, Oct. 2008.

[91] M. Y. Masoomi, A. Morsali, and P. C. Junk, "Rapid mechanochemical synthesis of two new Cd(ii)-based metal–organic frameworks with high removal efficiency of Congo red," *Cryst. Eng. Comm.*, vol. 17, no. 3, pp. 686-692, 2015, doi: 10.1039/C4CE01783H.

[92] U. Mueller, M. Schubert, F. Teich, H. Puetter, K. Schierle-Arndt, and J. Pastre, "Metal–organic frameworks—prospective industrial applications," *J. Mater. Chem.*, vol. 16, no. 7, pp. 626-636, 2006.

[93] M. Hartmann, S. Kunz, D. Himsl, O. Tangermann, S. Ernst, and A. Wagener, "Adsorptive separation of isobutene and isobutane on Cu_3 (BTC) $_2$," *Langmuir*, vol. 24, no. 16, pp. 8634-8642, 2008.

[94] J. Y. Wu, T. C. Chao, and M. S. Zhong, "Influence of counteranions on the structural modulation of silver–di(3-pyridylmethyl)amine coordination polymers," *Cryst. Growth Des.*, vol. 13, no. 7, pp. 2953-2964, Jul. 2013, doi: 10.1021/cg400363e.

[95] S. T. Meek, J. A. Greathouse, and M. D. Allendorf, "Metal-organic frameworks: A rapidly growing class of versatile nanoporous materials," *Adv. Mater.*, vol. 23, no. 2, pp. 249-267, Jan. 2011, doi: 10.1002/adma.201002854.

[96] C. Dey, T. Kundu, B. P. Biswal, A. Mallick, and R. Banerjee, "Crystalline Metal-Organic Frameworks (MOFs): Synthesis, structure and function," *Acta Crystallogr. B*, vol. 70, no. 1, pp. 3-10, Feb. 2014, doi: 10.1107/S2052520613029557.

[97] X. Ma, Y. Li, and A. Huang, "Synthesis of nano-sheets seeds for secondary growth of highly hydrogen permselective ZIF-95 membranes," *J. Membr. Sci.*, vol. 597, p. 117629, Mar. 2020, doi: 10.1016/j.memsci.2019.117629.

[98] Y. Ban, Y. Li, X. Liu, Y. Peng, and W. Yang, "Solvothermal synthesis of mixed-ligand metal–organic framework ZIF-78 with controllable size and morphology," *Microporous Mesoporous Mater.*, vol. 173, pp. 29-36, Jun. 2013, doi: https://doi.org/10.1016/j.micromeso.2013.01.031.

[99] S. H. Jhung, J. Lee, and J. Chang, "Microwave synthesis of a nanoporous hybrid material, chromium trimesate," *Bull. Korean Chem. Soc.*, vol. 26, no. 6, pp. 880-881, 2005.

[100] Z. Ni and R. I. Masel, "Rapid production of metal−organic frameworks via microwave-assisted solvothermal synthesis," *J. Am. Chem. Soc.*, vol. 128, no. 38, pp. 12394-12395, Sep. 2006, doi: 10.1021/ja0635231.

[101] Y. Thi Dang et al., "Microwave-assisted synthesis of nano Hf- and Zr-based metal-organic frameworks for enhancement of curcumin adsorption," *Microporous Mesoporous Mater.*, vol. 298, p. 110064, May 2020, doi: https://doi.org/10.1016/j.micromeso.2020.110064.

[102] L. Esrafili, M. Gharib, A. Morsali, and P. Retailleau, "Rational morphology control of nano-scale amide decorated metal-organic frameworks by ultrasonic method: Capability to selective and sensitive detection of nitro explosives," *Ultrason. Sonochem.*, p. 105110, Mar. 2020, doi: 10.1016/j.ultsonch.2020.105110.

[103] A. Pichon, A. Lazuen-Garay, and S. L. James, "Solvent-free synthesis of a microporous metal–organic framework," *Cryst. Eng. Comm.*, vol. 8, no. 3, pp. 211-214, 2006.

[104] W. Yuan, A. L. Garay, A.Pichon, R. Clowes, C. D. Wood, A. I. Cooper and S. L. James, "Study of the mechanochemical formation and resulting properties of an archetypal MOF: Cu3 (BTC) 2 (BTC= 1, 3, 5-benzenetricarboxylate)," *Cryst. Eng. Comm.*, vol. 12, no. 12, pp. 4063-4065, Sep. 2010.

[105] T. Zhang, J. Wei, X. Sun, X. Zhao, H. Tang, H. Yan, and F. Zhang, "Rapid synthesis of UiO-66 by means of electrochemical cathode method with electrochemical detection of 2,4,6-TCP," *Inorg. Chem. Communications*, vol. 111, p. 107671, Jan. 2020, doi: https://doi.org/10.1016/j.inoche.2019.107671.

[106] K. Pirzadeh, A. A. Ghoreyshi, M. Rahimnejad, and M. Mohammadi, "Optimization of electrochemically synthesized Cu3(BTC)2 by Taguchi method for CO$_2$/N$_2$ separation and data validation through artificial neural network modeling," *Front. Chem. Sci. Eng.*, vol. 14, no. 2, pp. 233-247, Apr. 2020, doi: 10.1007/s11705-019-1893-1.

[107] H. Li, C. E. Davis, T. L. Groy, D. G. Kelley, and O. M. Yaghi, "Coordinatively unsaturated metal centers in the extended porous framework of Zn3(BDC)3·6CH3OH (BDC = 1,4-Benzenedicarboxylate)," *J. Am. Chem. Soc.*, vol. 120, no. 9, pp. 2186-2187, Mar. 1998, doi: 10.1021/ja974172g.

[108] R. Seetharaj, P. V. Vandana, P. Arya, and S. Mathew, "Dependence of solvents, pH, molar ratio and temperature in tuning metal organic framework architecture," *Arab. J. Chem.*, vol. 12, no. 3, pp. 295-315, Mar. 2019, doi: https://doi.org/10.1016/j.arabjc.2016.01.003.

[109] K. Byrappa and M. Yoshimura, "Hydrothermal technology—principles and applications," in *Handbook of Hydrothermal Technology*, K. Byrappa and M. Yoshimura Eds. Norwich, NY: William Andrew Publishing, 2001, ch. 1, pp. 1-52.

[110] J. Gu, M. Wen, X. Liang, Z. Shi, M. Kirillova, and A. Kirillov, "Multifunctional aromatic carboxylic acids as versatile building blocks for hydrothermal design of coordination polymers," *Crystals*, vol. 8, no. 83, 2018, doi: https://doi.org/10.3390/cryst8020083.

[111] J. Gu, X. Liang, Y. Cai, J. Wu, Z. Shi, and A. Kirillov, "Hydrothermal assembly, structures, topologies, luminescence, and magnetism of a novel series of coordination polymers driven by a trifunctional nicotinic acid building block," *Dalton Trans.*, vol. 46, no. 33, pp. 10908-25, 2017.

[112] O. M. Yaghi, Li, and H. Li, "Hydrothermal synthesis of a metal-organic framework containing large rectangular channels," *J. Am. Chem. Soc.*, vol. 117, no. 41, pp. 10401-10402, 1995.

[113] R. Vakili, S. Xu, N. Al-Janabi, P. Gorgojo, S. M. Holmes, and X. Fan, "Microwave-assisted synthesis of zirconium-based Metal Organic Frameworks (MOFs): Optimization and gas adsorption," *Microporous Mesoporous Mater.*, vol. 260, pp. 45-53, Apr. 2018, doi: 10.1016/j.micromeso.2017.10.028.

[114] C. Gabriel, S. Gabriel, E. H. Grant, B. S. J. Halstead, and D. M. P. Mingos, "Dielectric parameters relevant to microwave dielectric heating," *Chem. Soc. Rev.*, vol. 27, no. 3, pp. 213-224, 1998, doi: 10.1039/A827213Z.

[115] K. S. Suslick, D. A. Hammerton, and R. E. Cline, "Sonochemical hot spot," *J. Am. Chem. Soc.*, vol. 108, no. 18, pp. 5641-5642, 1986.

[116] A. Gedanken, "Using sonochemistry for the fabrication of nanomaterials," *Ultrason. Sonochem.*, vol. 11, no. 2, pp. 47-55, 2004.

[117] C. Vaitsis, G. Sourkouni, and C. Argirusis, "Metal Organic Frameworks (MOFs) and ultrasound: A review," *Ultrason. Sonochem.*, vol. 52, pp. 106-119, Apr. 2019, doi: 10.1016/j.ultsonch.2018.11.004.

[118] N. Stock and S. Biswas, "Synthesis of Metal-Organic Frameworks (MOFs): routes to various MOF topologies, morphologies, and composites," *Chem. Rev.*, vol. 112, no. 2, pp. 933-969, Feb. 2012, doi: 10.1021/cr200304e.

[119] S. Zhang, X. Liu, Q. Yang, Q. Wei, G. Xie, and S. Chen, "Mixed-Metal–Organic Frameworks (M′ MOFs) from 1D to 3D based on the "organic" connectivity and the inorganic connectivity: Syntheses, structures and magnetic properties," *Cryst. Eng. Comm.*, vol. 17, no. 17, pp. 3312-3324, 2015.

[120] N. A. Khan, E. Haque, and S. H. Jhung, "Rapid syntheses of a metal–organic framework material Cu 3 (BTC) 2 (H 2 O) 3 under microwave: A quantitative analysis of accelerated syntheses," *Phys. Chem. Chem. Phys.*, vol. 12, no. 11, pp. 2625-2631, 2010.

[121] E. Haque, N. A. Khan, J. H. Park, and S. H. Jhung, "Synthesis of a metal–organic framework material, iron terephthalate, by ultrasound, microwave, and conventional electric heating: a kinetic study," *Chem. Eur. J*, vol. 16, no. 3, pp. 1046-1052, 2010.

[122] J. S. Choi, W. J. Son, J. Kim, and W. S. Ahn, "Metal–organic framework MOF-5 prepared by microwave heating: Factors to be considered," *Microporous Mesoporous Mater.*, vol. 116, no. 1, pp. 727-731, Dec. 2008, doi: https://doi.org/10.1016/j.micromeso.2008.04.033.

[123] M. Majewski, A. Howarth, M. Wasielewski, J. Hupp, and O. Farha, "Enzyme encapsulation in metal–organic frameworks for applications in catalysis," *Cryst. Eng. Comm.*, vol. 19, pp. 4082-4091, Jan. 2017, doi: 10.1039/C7CE00022G.

[124] J. E. Mondloch, W. Bury, D. Jimenez, S. Kwon, E. J. DeMarco, M. H. Weston, A. A. Sarjeant, S. T. Nguyen, P. C. Stair, R. Q. Snurr, O. K. Farha, and J. T. Hupp, "Vapor-phase metalation by atomic layer deposition in a metal–organic framework," *J. Am. Chem. Soc.*, vol. 135, no. 28, pp. 10294-10297, Jul. 2013, doi: 10.1021/ja4050828.

[125] Y. Luo, M. Ahmad, A. Schug, and M. Tsotsalas, "Rising up: Hierarchical metal–organic frameworks in experiments and simulations," *Adv. Mater.*, vol. 31, no. 26, p. 1901744, Jun. 2019, doi: 10.1002/adma.201901744.

[126] U. Lee, A. H. Valekar, Y. K. Hwang, and J. Chang, " Granulation and shaping of metal–organic frameworks," in *The Chemistry of Metal-Organic Frameworks*, S. Kaskel, Ed. Weinheim, Germany: Wiley, 2016, ch. 18, pp. 551-565.

[127] L. Bromberg, Y. Diao, H. Wu, S. A. Speakman, and T. A. Hatton, "Chromium (III) terephthalate metal organic framework (MIL-101): HF-free synthesis, structure, polyoxometalate composites, and catalytic properties," *Chem. Mater.*, vol. 24, no. 9, pp. 1664-1675, 2012.

[128] C. Duan, F. Li, S. Luo, J. Xiao, L. Li, and H. Xi, "Facile synthesis of hierarchical porous metal-organic frameworks with enhanced catalytic activity," *Chem. Eng. J.*, vol. 334, pp. 1477-1483, 2018.

[129] S. S. Y. Chui, S. M. F. Lo, J. P. H. Charmant, A. G. Orpen, and I. D. Williams, "A chemically functionalizable nanoporous material [Cu3 (TMA) 2 (H2O) 3] n," *Science*, vol. 283, no. 5405, pp. 1148-1150, 1999.

[130] C. L. Kielkopf, W. Bauer, and I. L. Urbatsch, "Bradford assay for determining protein concentration," *Cold Spring Harb. Protoc.*, vol. 2020, no. 4, pp. 102269-102269, 2020.

[131] L. F. de Sousa Lima, C. R. Coelho, G. H. M. Gomes, and N. D. S. Mohallem, "Nb_2O_5/SiO_2 mesoporous monoliths synthetized by sol–gel process using ammonium niobate oxalate hydrate as porogenic agent," *J. Solgel Sci. Technol.*, vol. 93, no. 1, pp. 168-174, Oct. 2020.

[132] A. P. Terzyk, S. Furmaniak, P. A. Gauden, P. J. F. Harris, and P. Kowalczyk, "Virtual porous carbons," in *Novel Carbon Adsorbents*, J. M. D. Tascón Ed. Amsterdam, Netherlands: Elsevier, 2012, ch. 3, pp. 61-104.

[133] T. K. Dalsgaard, D. Otzen, J. H. Nielsen, and L. B. Larsen, "Changes in structures of milk proteins upon photo-oxidation," *J. Agric. Food Chem.*, vol. 55, no. 26, pp. 10968-10976, Dec. 2007, doi: 10.1021/jf071948g.

[134] U. P. Andley, P. Sutherland, J. N. Liang, and B. Chakrabarti, "Changes in tertiary structure of calf-lens α-crystallin by near-UV irradiation: role of hydrogen peroxide," *Photochem. Photobiol.*, vol. 40, no. 3, pp. 343-349, 1984.

[135] N. Ayawei, A. N. Ebelegi, and D. Wankasi, "Modelling and interpretation of adsorption isotherms," *J. Chem.*, vol. 2017, p. 3039817, Sep. 2017, doi: 10.1155/2017/3039817.

[136] D. A. Loris, T. Raoul, A. D. Cyrille, K. Idris-Hermann, D. Giscard, T. D. Clovis, A. S. Gabche, and N. Jean, "Kinetic and isotherm studies of the adsorption phenacetin onto two copper porous coordination compounds: Nonlinear regression analysis," *J. Chem.*, vol. 2022, p. 2828860, Aug. 2022, doi: 10.1155/2022/2828860.

[137] A. A. Ichou, R. Benhiti, M. Abali, A. Dabagh, G. Carja, A. Soudani, M. Chiban, M. Zerbet, and F. Sinanet, "Characterization and sorption study of Zn2[FeAl]-CO3 layered double hydroxide for Cu(II) and Pb(II) removal," *J. Solid State Chem.*, vol. 320, p. 123869, Apr. 2023, doi: 10.1016/j.jssc.2023.123869.

[138] M. Vikmon, "Rapid and simple spectrophotometric method for determination of micro-amounts of cyclodextrins," in *Proc. 1st Int. Symp. Cyclodextrins*, J. Szejtli, Ed., Dordrecht, Netherlands, 1982, pp. 69-74, doi: 10.1007/978-94-009-7855-3_7.

[139] H. N. Tran, S. J. You, A. Hosseini-Bandegharaei, and H.-P. Chao, "Mistakes and inconsistencies regarding adsorption of contaminants from aqueous solutions: A critical review," *Water Res.*, vol. 120, pp. 88-116, Sep. 2017, doi: https://doi.org/10.1016/j.watres.2017.04.014.

[140] R. Li, S. Liu, X. Zhou, H. Liu, H. Zhou, C. Wang, Y. Liu, X. Zhang, "Efficient immobilization of catalase on mesoporous MIL-101 (Cr) and its catalytic activity assay," *Enzyme Microb. Technol.*, vol. 156, p. 110005, May 2022, doi: 10.1016/j.enzmictec.2022.110005.

[141] S. W. Zhao, Q. Zhou, N. B. Long, and R. F. Zhang, "Preparation and characterization of a novel 3D polymer support for the immobilization of cyclodextrin glucanotransferase and efficient biocatalytic synthesis of α-arbutin," *Biochem. Eng. J.*, vol. 185, p. 108519, Jul. 2022, doi: 10.1016/j.bej.2022.108519.

[142] M. T. Martín, M. Alcalde, F. J. Plou, and A. Ballesteros, "Covalent immobilization of Cyclodextrin glucosyltransferase (CGTase) in activated silica and sepharose," *Indian J. Biochem. Biophys.*, vol. 39, no. 4, pp. 229-234, Aug. 2002.

[143] R. Datta, S. Anand, A. Moulick, D. Baraniya, S. I. Pathan, K. Rejsek, V. Vranova, M. Sharma, D. Sharma, A. Kelkar, and P. Formanek, "How enzymes are adsorbed on soil solid phase and factors limiting its activity: A review," *Int. Agrophys.*, vol. 31, no. 2, pp. 287-302, 2017, doi: 10.1515/intag-2016-0049.

[144] H. Yang, S. Yang, J. Kong, A. Dong, and S. Yu, "Obtaining information about protein secondary structures in aqueous solution using Fourier transform IR spectroscopy," *Nat. Protoc.*, vol. 10, no. 3, pp. 382-396, 2015.

[145] S. Vonhoff, J. Condliffe, and H. Schiffter, "Implementation of an FTIR calibration curve for fast and objective determination of changes in protein secondary structure during formulation development," *J. Pharm. Biomed. Anal.*, vol. 51, no. 1, pp. 39-45, Jan. 2010, doi: 10.1016/j.jpba.2009.07.031.

[146] P. I. Haris and F. Severcan, "FTIR spectroscopic characterization of protein structure in aqueous and non-aqueous media," *J. Mol. Catal. B: Enzym.*, vol. 7, no. 1, pp. 207-221, Sep. 1999, doi: 10.1016/S1381-1177(99)00030-2.

[147] P. Yu, "Protein secondary structures (α-helix and β-sheet) at a cellular level and protein fractions in relation to rumen degradation behaviours of protein: a new approach," *Br. J. Nutr.*, vol. 94, no. 5, pp. 655-665, 2005.

[148] K. Fu, K. Griebenow, L. Hsieh, A. M. Klibanov, and L. Robert, "FTIR characterization of the secondary structure of proteins encapsulated within PLGA microspheres," *J. Control. Release*, vol. 58, no. 3, pp. 357-366, Apr. 1999, doi: 10.1016/S0168-3659(98)00192-8.

[149] F. Ding, J. M. Borreguero, S. V. Buldyrev, H. E. Stanley, and N. V. Dokholyan, "Mechanism for the α-helix to β-hairpin transition," *Proteins*, vol. 53, no. 2, pp. 220-228, Nov. 2003, doi: 10.1002/prot.10468.

[150] K. Kamaruddin, R. M. Illias, S. A. Aziz, M. Said, and O. Hassan, "Effects of buffer properties on Cyclodextrin glucanotransferase reactions and cyclodextrin production from raw sago (Cycas revoluta) starch," *Biotechnol. Appl. Biochem.*, vol. 41, no. 2, pp. 117-125, 2005.

[151] G. Matioli, G. M. Zanin, and F. F. De Moraes, "Influence of substrate and product concentrations on the production of cyclodextrins by CGTase of Bacillus firmus, strain no. 37," in *Biotechnology for Fuels and Chemicals, M. Finkelstein,* J. D. McMillan, B. H. Davison, Eds. Totowa, NJ, USA: Humana Press, 2002, pp. 947-961.

[152] S. Suhaimi, R. C. Man, N. Jamil, Z. Arshad, S. Shaarani, S. K. Mudalip, S. Z. Sulaiman, and A. N. Ramli, "Stability and reusability of Cyclodextrin glucanotransferase immobilized on hollow fiber membrane," *IOP Conf. Ser.: Earth Environ. Sci.*, Hangzhou, China, Aug. 2018, pp. 1-7012002, doi: 10.1088/1755-1315/185/1/012002.

[153] J. Yong, K. Hakobyan, J. Xu, A. S. Mellick, J. Whitelock, and K. Liang, "Comparison of protein quantification methods for protein encapsulation with ZIF-8 metal-organic frameworks," *Biotechnol. J.*, vol. 18, no. 11, p. 2300015, Nov. 2023, doi: 10.1002/biot.202300015.

[154] J. Bandekar, "Amide modes and protein conformation," *Biochim. Biophys. Acta Mol. Enzymol.*, vol. 1120, no. 2, pp. 123-143, 1992.

[155] M. Carbonaro and A. Nucara, "Secondary structure of food proteins by Fourier transform spectroscopy in the mid-infrared region," *Amino Acids*, vol. 38, no. 3, pp. 679-690, 2010.

[156] M. Mangiagalli, D. Ami, M. Divitiis, S. Brocca, T. Catelani, A. Natalello, and M. Lotti, "Short-chain alcohols inactivate an immobilized industrial lipase through two different mechanisms," *Biotechnol. J.*, vol. 17, no. 6, p. 2100712, Jun. 2022, doi: 10.1002/biot.202100712.

[157] H. T. Wright, H. X. Qian, and R. Huber, "Crystal structure of plakalbumin, a proteolytically nicked form of ovalbumin: Its relationship to the structure of cleaved α-1-proteinase inhibitor," *J. Mol. Biol.*, vol. 213, no. 3, pp. 513-528, 1990.

[158] K. Kavitha and L. Palaniappan, "FTIR study of synthesized ovalbumin nanoparticles," *Anal. Biochem.*, vol. 636, p. 114456, Jan. 2022, doi: https://doi.org/10.1016/j.ab.2021.114456.

[159] H. Fu, G. R. Grimsley, A. Razvi, J. M. Scholtz, and C. N. Pace, "Increasing protein stability by improving beta-turns," *Proteins*, vol. 77, no. 3, pp. 491-498, Nov. 2009, doi: 10.1002/prot.22509.

[160] H. Wu, Y. Fan, J. Sheng, and S.-F. Sui, "Induction of changes in the secondary structure of globular proteins by a hydrophobic surface," *Eur. Biophys. J.*, vol. 22, no. 3, pp. 201-205, Aug. 1993, doi: 10.1007/BF00185781.

[161] D. Svensson and P. Adlercreutz, "Immobilisation of CGTase for continuous production of long-carbohydrate-chain alkyl glycosides: Control of product distribution by flow rate adjustment," *J. Mol. Catal. B: Enzym.*, vol. 69, no. 3, pp. 147-153, May 2011, doi: 10.1016/j.molcatb.2011.01.009.

[162] S. Chen, Z. Li, Z. Gu, X. Ban, Y. Hong, L. Cheng, and C. Li, "Immobilization of β-Cyclodextrin glycosyltransferase on gelatin enhances β-cyclodextrin production," *Process Biochem.*, vol. 113, pp. 216-223, Feb. 2022, doi: 10.1016/j.procbio.2022.01.005.

[163] S. S. Ashok Kumar, S. Bashir, K. Ramesh, and S. Ramesh, "A comprehensive review: Super hydrophobic graphene nanocomposite coatings for underwater and wet applications to enhance corrosion resistance," *FlatChem*, vol. 31, p. 100326, Jan. 2022, doi: 10.1016/j.flatc.2021.100326.

[164] S. H. Lee and E. Ruckenstein, "Adsorption of proteins onto polymeric surfaces of different hydrophilicities—a case study with bovine serum albumin," *J. Colloid Interface Sci.*, vol. 125, no. 2, pp. 365-379, Oct. 1988, doi: 10.1016/0021-9797(88)90001-X.

[165] B. Huang, "Current molecular dynamics opinions on interactions between bone morphogenetic protein-2 and inorganic materials," *Mater. Today Communications*, vol. 34, p. 105307, Mar. 2023, doi: 10.1016/j.mtcomm.2022.105307.

[166] G. G. Gimenez, R. M. Silva, C. P. Francisco, F. Rando, J. H. Dantas, H. M. de Souza, and G. Matioli, "Immobilization of commercial Cyclomaltodextrin glucanotransferase into controlled pore silica by the anchorage method and covalent bonding," *Process Biochem.*, vol. 85, pp. 68-77, Oct. 2019, doi: 10.1016/j.procbio.2019.07.002.

[167] H. K. Jeong, D. Lee, H. P. Kim, and S.-H. Baek, "Structure analysis and antioxidant activities of an amylopectin-type polysaccharide isolated from dried fruits of Terminalia chebula," *Carbohydr. Polym.*, vol. 211, pp. 100-108, 2019.

[168] A. M. M. Sakinah, A. F. Ismail, R. M. Illias, A. W. Zularisam, O. Hassan, and T. Matsuura, "Effect of substrate and enzyme concentration on cyclodextrin production in a hollow fibre membrane reactor system," *Sep. Purif. Technol.*, vol. 124, pp. 61-67, 2014.

[169] N. Miletić, A. Nastasović, and K. Loos, "Immobilization of biocatalysts for enzymatic polymerizations: Possibilities, advantages, applications," *Bioresour. Technol.*, vol. 115, pp. 126-135, Jul. 2012, doi: 10.1016/j.biortech.2011.11.054.

[170] J. Schöffer, C. Matte, D. Charqueiro, E. de Menezes, T. Costa, E. Benvenutti, R. Rodrigues, and P. Hertz, "Directed immobilization of CGTase: The effect of the enzyme orientation on the enzyme activity and its use in packed-bed reactor for continuous production of cyclodextrins," *Process Biochem.*, vol. 58, pp. 120-127, 2017.

[171] Y. H. Lee and S. H. Lee, "Performance of column type bioreactor packed with immobilized Cyclodextrin glucanotransferase for cyclodextrin production," *J. Microbiol. Biotechnol.*, vol. 1, no. 1, pp. 63-69, 1991.

[172] S. Hao, L. Yuling, and J. Yang, "Construction of Cu-BTC by carboxylic acid organic ligand and its application in low temperature SCR denitration," *Sci. Total Env.*, vol. 820, p. 152984, May 2022, doi: 10.1016/j.scitotenv.2022.152984.

[173] A. A. Yakovenko, J. H. Reibenspies, N. Bhuvanesh, and H. C. Zhou, "Generation and applications of structure envelopes for porous metal–organic frameworks," *J. Appl. Crystallogr.*, vol. 46, no. 2, pp. 346-353, 2013.

[174] Y. Li, J. Miao, X. Sun, J. Xiao, Y. Li, H. Wang, Q. Xia, and Z. Li, "Mechanochemical synthesis of Cu-BTC@GO with enhanced water stability and toluene adsorption capacity," *Chem. Eng. J.*, vol. 298, pp. 191-197, Aug. 2016, doi: https://doi.org/10.1016/j.cej.2016.03.141.

[175] S. Hao, L. Yuling, and J. Yang, "Synthesis of Cu-BTC by room temperature hydrothermal and its low temperature SCR denitration," *J. Mol. Struct.*, vol. 1251, p. 132046, Mar. 2022, doi: 10.1016/j.molstruc.2021.132046.

[176] M. Ş. A. Eren, H. Arslanoğlu, and H. Çiftçi, "Production of microporous Cu-doped BTC (Cu-BTC) metal-organic framework composite materials, superior adsorbents for the removal of methylene blue (Basic Blue 9)," *J. Environ. Chem. Eng.*, vol. 8, no. 5, p. 104247, Jan. 2020, doi: https://doi.org/10.1016/j.jece.2020.104247.

[177] B. A. Ogunbadejo, K. A. Aljahoushi, A. Alzamly, Y. E. Greish, and S. Al-Zuhair, "Immobilization of Cyclodextrin glycosyltransferase onto 3D-hydrophobic and 2D-hydrophilic supports: A comparative study," *Biotechnol. J.*, p. 2300195, 2023.

[178] B. A. Ogunbadejo and S. Al-Zuhair, "Bioconversion of starch to cyclodextrin using Cyclodextrin glycosyltransferase immobilized on metal organic framework," *Biocatal. Agric. Biotechnol.*, vol. 53, p. 102878, Oct. 2023, doi: 10.1016/j.bcab.2023.102878.

[179] J. Kong and S. Yu, "Fourier transform infrared spectroscopic analysis of protein secondary structures," *Acta Biochim. Biophys. Sin.*, vol. 39, no. 8, pp. 549-559, Aug. 2007, doi: 10.1111/j.1745-7270.2007.00320.x.

[180] K. Numata, P. Cebe, and D. L. Kaplan, "Mechanism of enzymatic degradation of beta-sheet crystals," *Biomaterials*, vol. 31, no. 10, pp. 2926-2933, 2010.

[181] A. Sadat and I. J. Joye, "Peak fitting applied to Fourier transform infrared and Raman spectroscopic analysis of proteins," *Appl. Sci.*, vol. 10, no. 17, 2020, doi: 10.3390/app10175918.

List of Other Publications

1. B. Ogunbadejo and S. Al-Zuhair, "MOFs as potential matrices in Cyclodextrin glycosyltransferase immobilization," *Molecules,* vol. 26, no. 3, p. 680, Jan. 2021. https://doi.org/10.3390/molecules26030680

2. R. Shomal, B. Ogubadejo, T. Shittu, E. Mahmoud, W. Du, and S. Al-Zuhair, "Advances in enzyme and ionic liquid immobilization for enhanced in MOFs for biodiesel production," *Molecules,* vol. 26, no. 12, p. 3512, Jun. 2021. https://doi.org/10.3390/molecules26123512

Appendix

Supplementary Information for Paper II
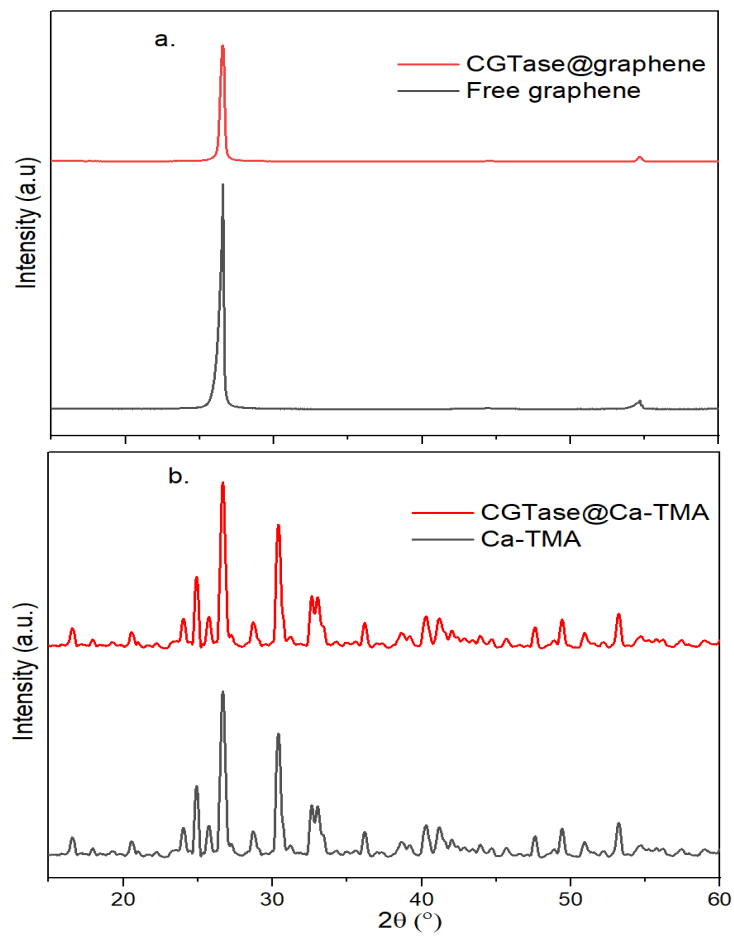
Figure A1: XRD Patterns of (a) GNP (b) Ca-TMA, with and without Enzyme
Immobilization
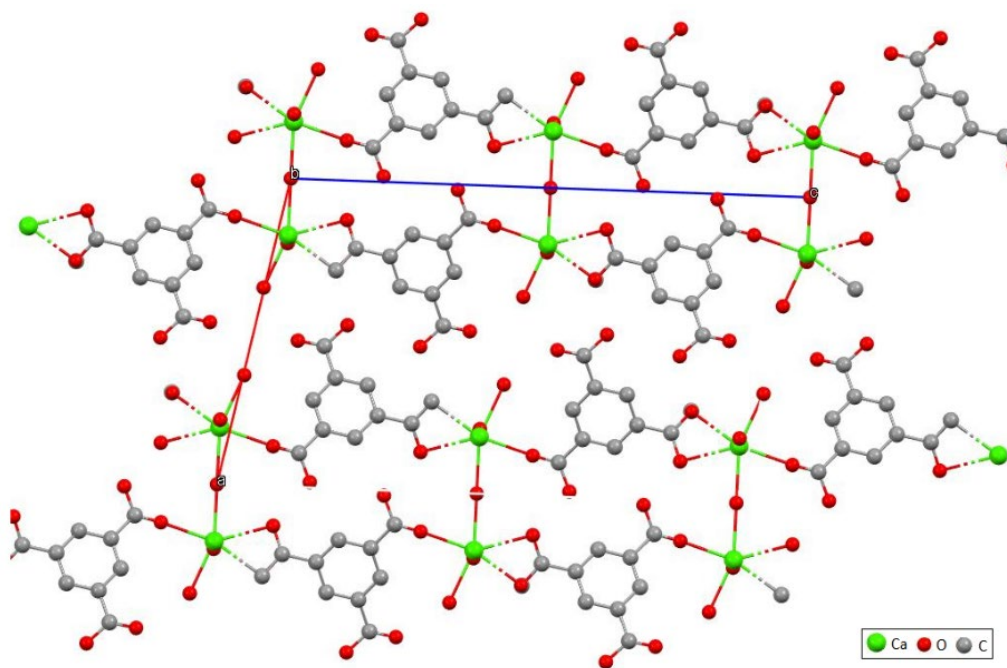
Figure A2: Projection View Showing Extended Packing of Ca-TMA 2D Crystal Structure
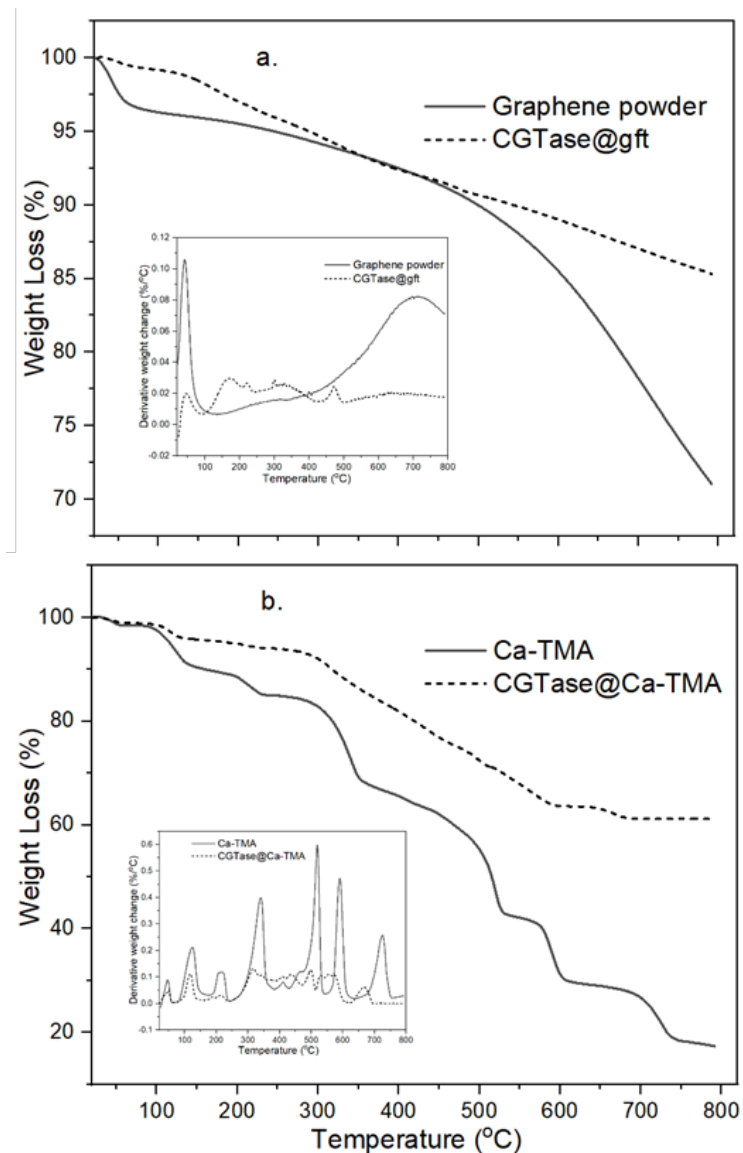
Figure A3: Thermogravimetric Analysis of Free and Immobilized Supports (a) GNP and (b) Ca-TMA
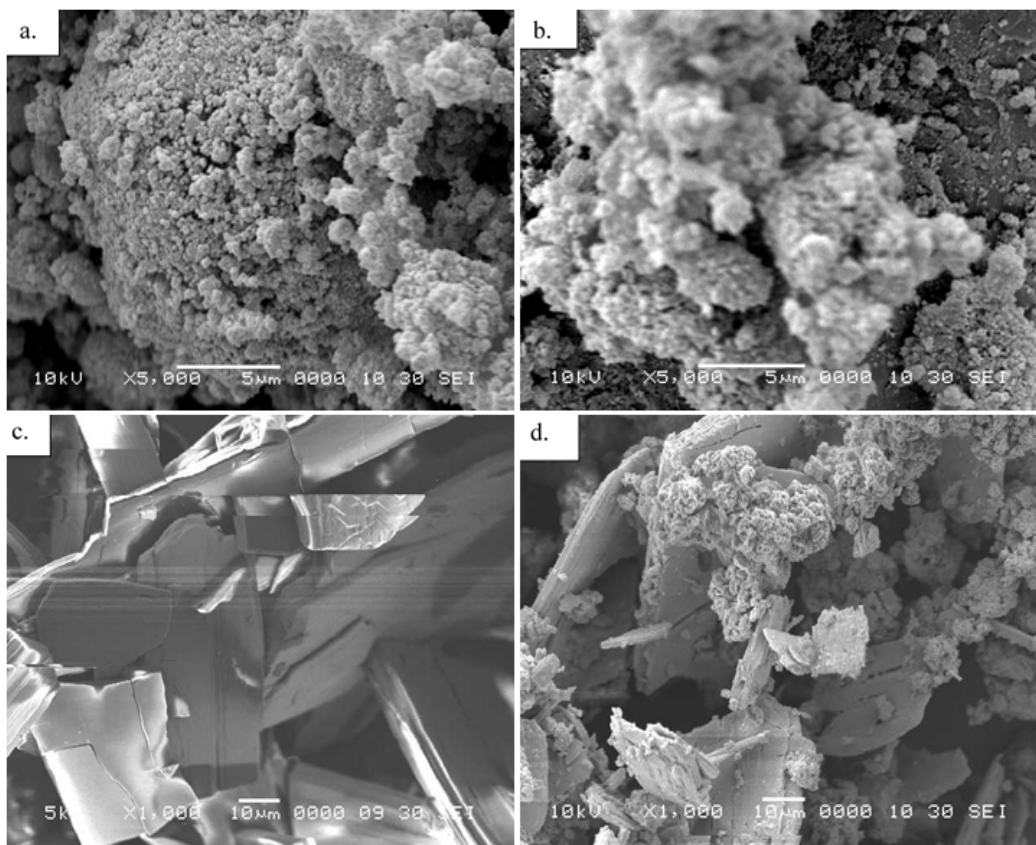
Figure A4: SEM Analysis of (a) GNP, (b) CGTase@GNP, (c) Ca-TMA, and (d) CGTase@Ca-TMA
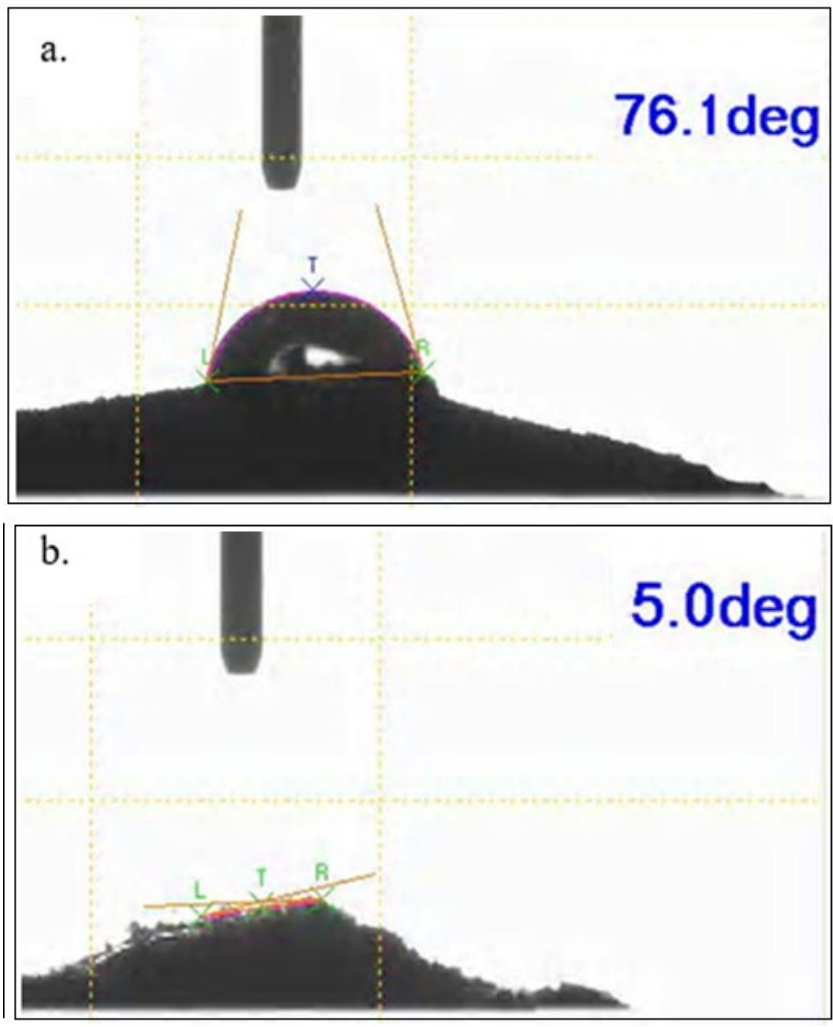
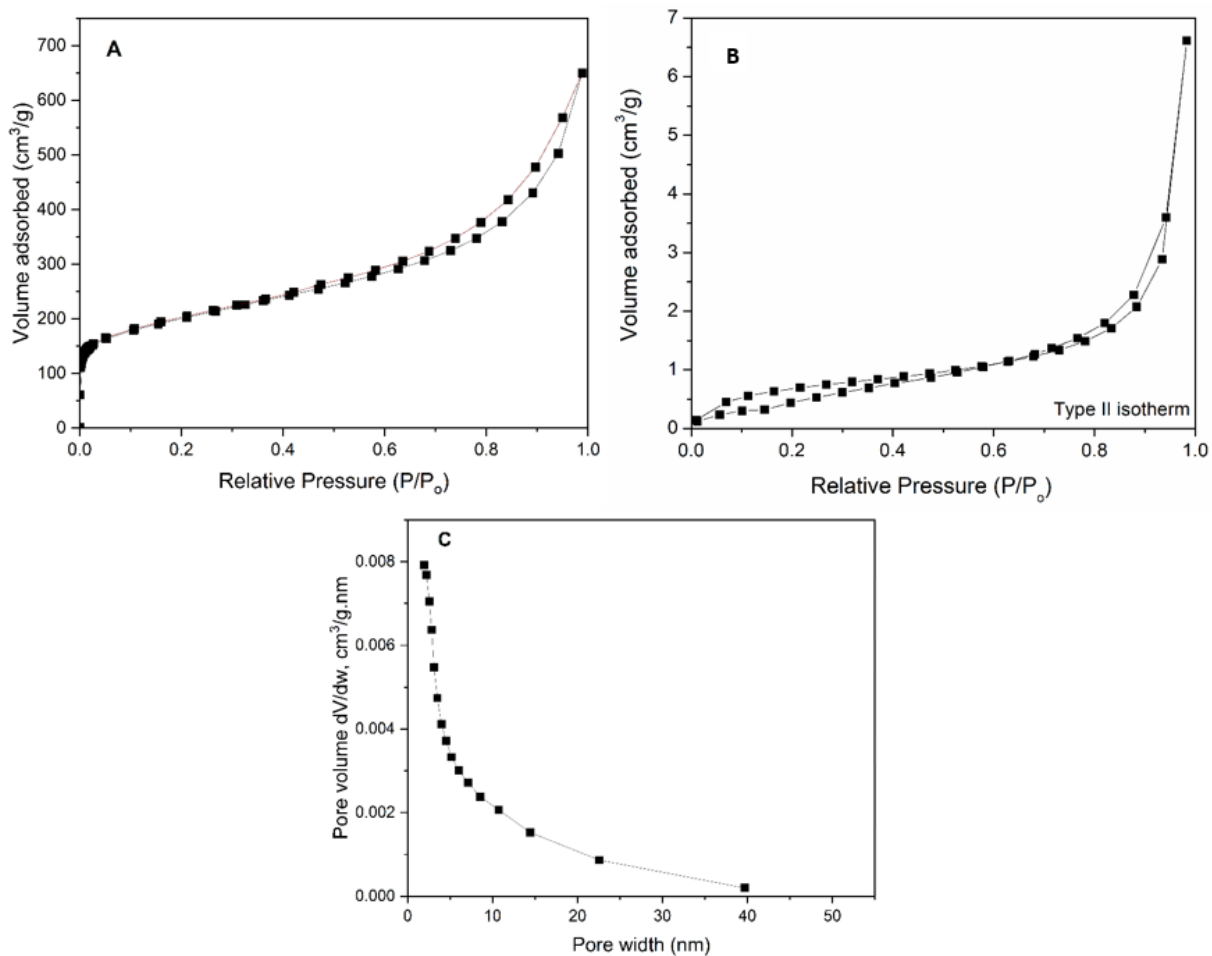Figure A5: Surface Contact Angles of (a) GNP and (b) Ca-TMA

Figure A6: N$_2$ Physisorption Results Showing (A) GNP Isotherm (B) Ca-TMA Isotherm (C) Pore Size Distribution of GNP
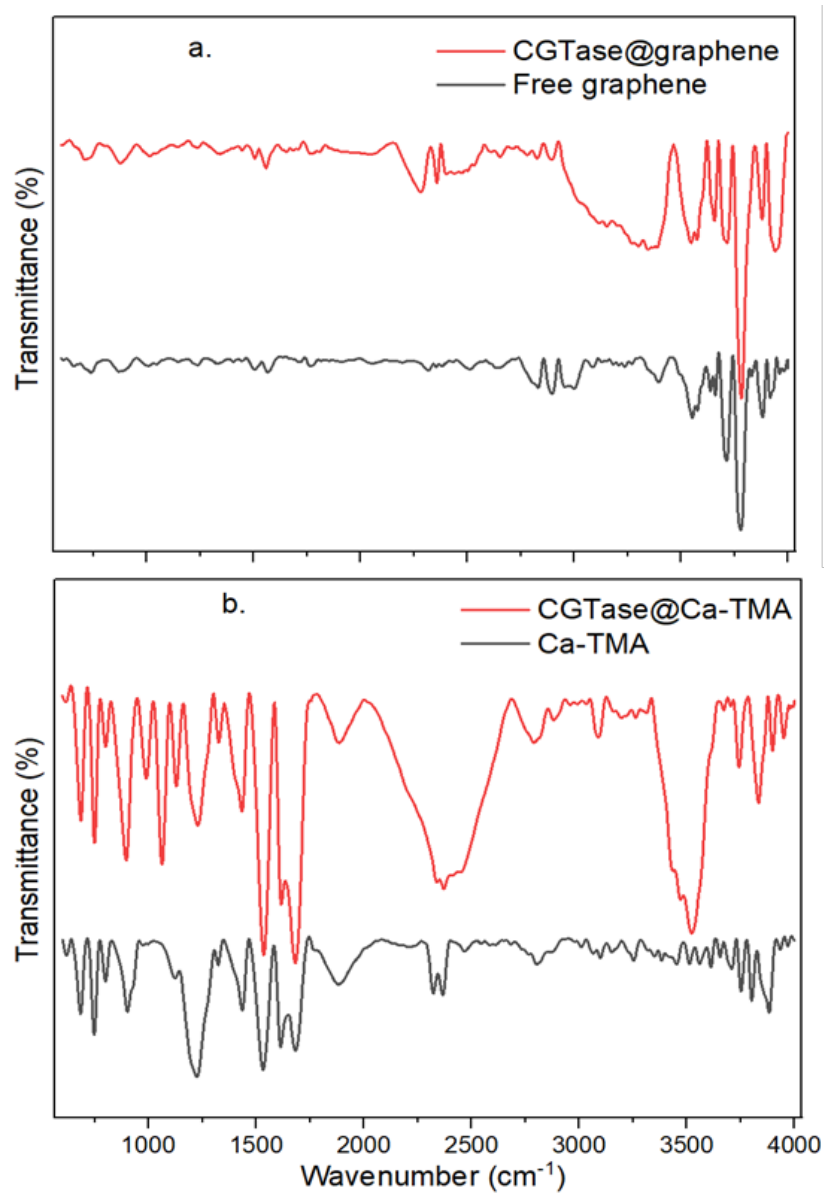
Figure A7: FTIR Analysis of Supports (a) GNP and (b) Ca-TMA, with and without Enzyme Immobilization
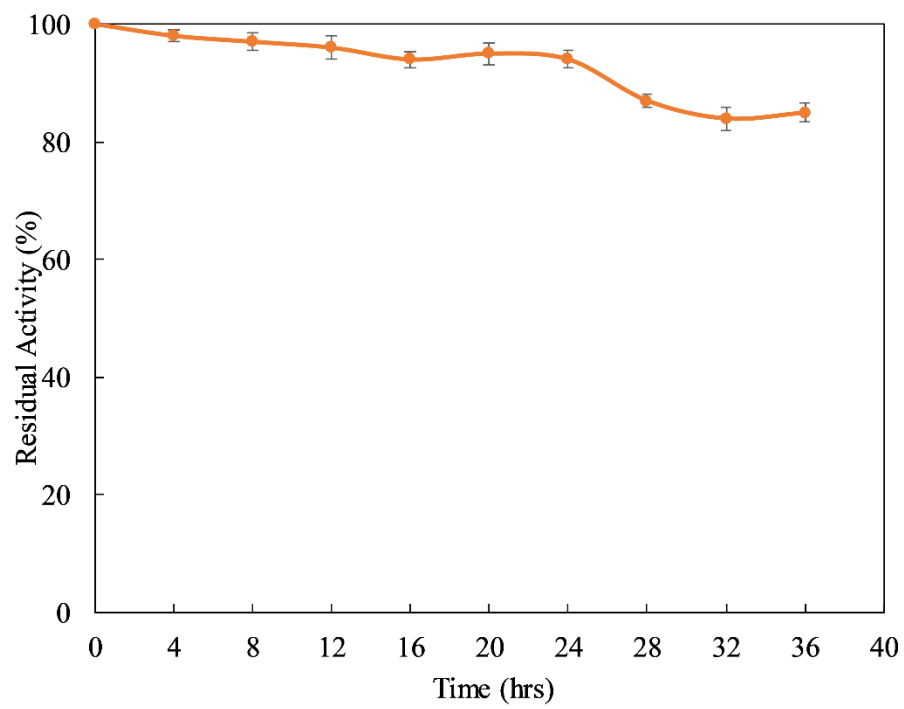
Figure A8: CGTase Stability at pH 7.4, 25°C in Solution at Different Time

This dissertation seeks to utilize metal organic frameworks as support for cyclodextrin glycosyltransferase for use in cyclodextrin production. The results obtained showed that metal organic frameworks performed better when compared to previous supports that have been used. Enzyme uptake was enhanced and diffusional restraint was minimized.

Babatunde Ogunbadejo received his PhD in Chemical Engineering from the Department of Chemical Engineering, College of Engineering at United Arab Emirates University, UAE. He received his Master of Science in Chemical Engineering from the College of Engineering, King Fahd University of Petroleum and Minerals, Saudi Arabia.

www.uaeu.ac.ae

جامعة الإمارات العربية المتحدة
United Arab Emirates University

عمادة المكتبات
Libraries Deanship

قسم الخدمات المكتبية الرقمية - Digital Library Services Section